Catalytic Hydrogenation of Butadiene Copolymers

by

John Scott Parent

A thesis
presented to the University of Waterloo
in fulfilment of the
thesis requirement for the degree of
Doctor of Philosophy
in
Chemical Engineering

Waterloo, Ontario, Canada, 1996

The University of Waterloo requires the signatures of all persons using or photocopying this thesis. Please sign below, and give address and date.

Abstract

Selective hydrogenation of the olefin residing within nitrile butadiene rubber (NBR) yields an elastomer that possesses remarkable thermal and oxidative stability. A new generation of homogeneous catalysts have been identified for the reaction, having the general form $OsHCl(CO)(L)(PCy_3)_2$ (**1a**, L=vacant; **2a**, L=O_2). In the present work, the merits of this new technology have been assessed in comparison to the Rh(I) phosphine catalysts that are currently in use. Comprehensive kinetic and selectivity data have been acquired under reaction conditions that are industrially relevant. These measurements, coupled with fundamental studies of the structure and reactivity of **1a** and **2a**, have improved our understanding of the novel catalytic chemistry of this class of complexes.

The rates of hydrogenation supported by **2a** are superior to those produced by $RhCl(PPh_3)_3$ over the entire range of conditions studied. Unique to the **2a** system is an apparent second order dependence of the reaction rate on the concentration of H_2. At pressures exceeding 60 bar, this reaction order diminishes until the rate is virtually independent of the hydrogen pressure. In contrast, the hydrogenation of substrates lacking nitrile functionality is indifferent to [H_2] at all system pressures. An unconventional catalytic mechanism in which two molecules of H_2 are required to bring about the rate determining step is supported by the kinetic data.

A spectroscopic analysis of HNBR produced using **2a** revealed no evidence for the reduction of the copolymer's nitrile unsaturation to amine. However, the olefin hydrogenation was accompanied by an undesirable crosslinking reaction that was not observed for the rhodium catalysts. Detailed studies of the effect have indicated that elevated pressures and minimized catalyst concentrations suppress, but do not eliminate, the crosslinking process. By monitoring the evolution of the side-reaction product with time, it has been connected to the presence of residual olefin. Various mechanisms by which the cross-linking process could occur have been explored.

An alternative to batch HNBR production has been explored in the form of a continuous, plug-flow reactor configuration. The design considerations underlying the new production strategy have been detailed along with criteria used for its evaluation. To demonstrate the operating principles of the new approach, a bench-scale prototype has been constructed and assessed according to these standards. The breadth and form of the residence time distribution afforded by the unit have been measured and related to its hydrogenation performance. The data suggests that HNBR may be synthesized efficiently by this method.

Acknowledgements

I wish to express my gratitude to the following individuals:

Prof. G.L Rempel for his interest and support of both this project and my development as a researcher.

Dr. N.T. McManus for generously sharing his time, knowledge and experience.

Mr. S.A. Kehl for assistance with the continuous reactor assessments.

Mrs. J. Venne and Prof. W. Power for the patience and advice afforded during the NMR investigations.

Mr. F. Wassmer for assistance with the design and fabrication of physical components required by the project.

Michelle Antoinette Parent for sharing equally in the disappointments and delights experienced over the course of this work.

Financial assistance from the Ontario Centre for Materials Research (OCMR), Petro-Canada and the Ontario Graduate Student Program is greatly appreciated. Project funding from the Natural Sciences and Engineering Research Council (NSERC) is gratefully acknowledged.

To Laura Parent

Table of Contents

List of Figures

List of Tables

Table

Index of Complex Codes

1a,b: $OsHCl(CO)(PR_3)_2$

2a,b: $OsHCl(CO)(O_2)(PR_3)_2$

3a,b: $OsH(H_2)Cl(CO)(PR_3)_2$

4a,b: $OsHCl(CO)(C{=}C)(PR_3)_2$

5a,b: $OsHCl(CO)_2(PR_3)_2$

6a,b: $OsHCl(CO)(R'CN)(PR_3)_2$

7: $RuHCl(CO)(PCy_3)_2$

a, R = Cy
b, R = *i*Pr

Chapter 1

Introduction

In many respects the demand for robust elastomers has extended beyond the limits of traditional diene-based polymers (Watanabe et al., 1989). For example, the development of more efficient automotive powertrains has significantly increased engine compartment temperatures, putting an additional stress on key rubber components such as hoses and timing belts (Klingender and Bradford, 1991). The chemical modification of these materials has satisfied this demand to some extent, creating a new class of specialty polymers with improved mechanical, thermal and chemical properties. Since these second generation materials can not be made by conventional polymerization techniques, the modification of diene-based rubber remains the only synthetic route for their production (McGrath et al., 1995). However, the cost of these processes is reflected by the limited number of applications to which modified materials have found use.

Most modification reactions of commercial interest focus on improving thermal and oxidative stability (Schultz, 1988). Residual carbon-carbon double bonds in the backbone of diene-based materials are sites of degradation when exposed to oxygen, ozone and heat. Prolonged exposure to such conditions may result in a decay in the mechanical integrity of the material and its eventual failure. A selective hydrogenation of the C=C unsaturation can reduce the reactivity of the material, thereby extending its range of application. A leading example is the catalytic hydrogenation of nitrile butadiene rubber (NBR) to yield its more stable counterpart, HNBR (Figure 1.1).

Due to its remarkable oil and solvent resistance, high nitrile NBR is commonly employed in oil and gas production equipment and engine fluid delivery systems (Hertz et al., 1995). However, its performance is compromised by contact with sour gas, oxidized fuel and aggressive solvents, particularly at high temperatures. The hydrogenation of NBR to produce an apparent ethylene-acrylonitrile random copolymer has alleviated this deficiency and developed an expanding specialty market. As this saturated copolymer cannot be

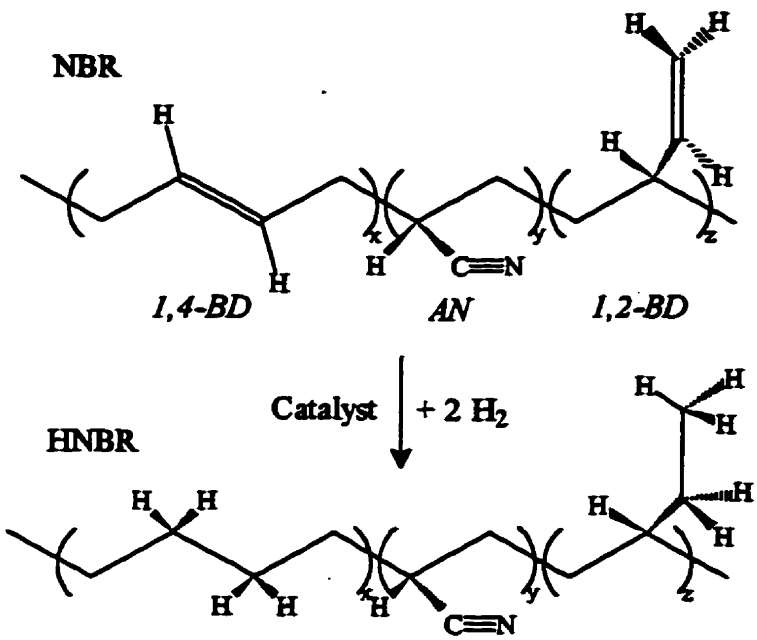

Figure 1.1: General Structure of NBR and HNBR

synthesized by traditional approaches such as free radical or coordinative polymerization, the modification route has been adopted.

1.1 Commercial HNBR Production Technology

In the production of HNBR its is required to selectively hydrogenate olefin in the presence of the copolymer's nitrile unsaturation (Figure 1.1). Significant levels of nitrile reduction to primary amine not only diminishes the apolar solvent resistance for which HNBR is designed, but is thought to facilitate an undesirable crosslinking reaction (McManus and Rempel, 1995). This selectivity criterion prohibits the use of chemical reagents such as hydrazine or $LiAlH_4$. Hydrogen transfer reactions that make use of compounds such as isopropanol are also inapplicable, as NBR is insoluble in systems containing substantial amounts of alcohol. The remaining option is a metal catalyzed process employing molecular hydrogen.

For the modification of polymers, homogeneous complexes or highly dispersed slurries of platinum metals are preferred over heterogeneous systems such as Raney nickel. While the selectivity of solid catalysts is often lacking, these systems also suffer greatly from polymer diffusion limitations. The meagre diffusivity of macromolecules in solution reduces the rate which they interact with a liquid-solid interface. As a result, hydrogenation rates are often dominated by an inefficient mass transfer process. By their nature, homogeneous catalysts associate intimately with the polymeric substrate to produce superior rates of hydrogenation. This advantage offsets the cost of metal recovery.

There exist further complications in adapting a technology that was designed for monomers to macromolecule transformations. Emulsifiers, chain transfer agents and stabilizers used in the synthesis of NBR often remain in undefined amounts. These residual carboxylates, mercaptans and alcohols can adversely affect a catalyst that efficiently hydrogenates purified olefin. Difficulties may also arise from the presence of coordinating functional groups or the variety of olefin isomers within a butadiene-based material. Consequently, a meaningful evaluation of a modification technology must involve studies of the material in question at operating conditions that are relevant to its final application.

As HNBR occupies a small fraction of the elastomers market, semi-batch hydrogenation processes are used throughout the industry. Typically, the polymer is dissolved in a polar solvent (chlorinated aromatics or ketones) and the solution purged of atmospheric gases. The desired reaction temperature and pressure is established and the catalyst charged to the vessel. Pressures in excess of 20 bar and temperatures in the range of 100°C are used to enhance the hydrogenation rate while minimizing the required amount of precious metal. Upon reaching the desired conversion, steps may be taken to recover catalyst residue and the polymer is isolated by precipitation.

Of the innumerable transition metal complexes that are capable of catalyzing olefin hydrogenation, those identified up until this time as having the greatest merit for HNBR have been based upon rhodium, palladium and ruthenium. Of these, most polymer

hydrogenation literature has been devoted to the rhodium(I) phosphine complexes, especially $RhCl(PPh_3)_3$. A patent filed in 1976 by Bayer Rubber Inc. protected its use for HNBR production (Oppelt et al., 1976) and stimulated interest in developing new technology. Polysar (now a division of Bayer Rubber) was granted patent protection for a $RhH(PPh_3)_4$ process 8 years later (Rempel and Azizian, 1984). The examples provided in these rhodium patents suggest operating at pressures near 28 bar, temperatures in the range of 110°C and catalyst loadings of 1 wt% based on polymer.

Reports of the activity and selectivity of the Rh(I) phosphine complexes under commercially relevant conditions are scarce, despite the enormous body of literature dealing with their general catalytic chemistry. Based on available information, it appears that the rhodium systems are entirely selective for olefin hydrogenation (Bhattacharjee et al., 1991). This allows the process to be operated at extreme conditions without concern for the product quality. This is discussed in greater detail in Chapter 6.

A competitive technology based on a palladium metal system is used commercially by Nippon Zeon Co. Ltd. The original catalyst consisted of Pd dispersed on a solid support such as silica-alumina (Kubo and Ohura, 1982). Much better activity has been reported for Pd carboxylate complexes that are soluble in an NBR/ketone solution (Kubo and Kohtaki, 1985). When exposed to H_2 at elevated temperatures, these catalyst precursors are reduced to create a highly dispersed Pd metal colloid. By enhancing the effective surface area of exposed palladium, the liquid/solid mass transfer rates that are required for the polymer to migrate to a catalytic site are improved. As a result, better overall activity is observed.

The patent granted to Nippon Zeon Co. Ltd. for its Pd carboxylate technology recommends operation at 50 bar and 50°C. More severe reaction conditions promote solvent and/or nitrile reduction reactions. As a result, Pd loadings in the range of 500 ppm are required to support reasonable hydrogenation rates. This relatively high catalyst loading offsets the cost advantage of using a Pd rather than a Rh-based system. Both technologies are therefore competitive in the HNBR market.

A surge in the cost of Rh metal to a high of 7000 USD/oz in 1990 motivated a search for a viable ruthenium-based process. Although the price of rhodium has since declined, expenditures on a ruthenium catalyst could be as little as 1/20th of those for a $RhCl(PPh_3)_3$ system. Of all those screened, complexes of the form $RuHCl(CO)(PR_3)_2$ (R=Cy, *i*-Pr) have proven to be best suited for NBR hydrogenation (Rempel et al., 1991). These exhibit exceptional hydrogenation activity in all types of solvents while creating a marginal amount of polymer crosslinking. In their kinetic study of the PCy_3 analogue, Martin et al. (1992) report a first order dependence of the reaction rate on [Ru] and $[H_2]$ and an inverse relationship between activity and nitrile loading.

Only very recently has attention turned from ruthenium to its third row congener, osmium. This oversight is likely due to observations that the 5d metals coordinate too strongly with ligands encountered in catalytic cycles. A stronger association with hydrides, alkenes and phosphine has the potential to limit the overall reactivity of the metal centre (Sanchez-Delgado et al., 1995). It was, therefore, somewhat unexpected that the osmium analogue of $RuHCl(CO)(PR_3)_2$ proved to be extremely active for NBR hydrogenation when screened by Dr. N.T. McManus of our laboratory. Further work revealed the activity of the osmium system to be superior to ruthenium, in contrast to these commonly held assumptions.

The commercial potential of the osmium technology has been recognized by Bayer Rubber Inc. who have sponsored the patent claim of McManus et al. (1996). Given the scarcity of osmium catalytic literature and the commercial demand for a more efficient HNBR process, continued research promises to address the interests of both the academic and industrial community.

1.2 Structure and Reactivity of $OsHCl(CO)(PR_3)_2$ (1a, R=Cy; 1b, R=*i*-Pr)

The synthesis of $OsHCl(CO)(PCy_3)_2$ by refluxing a solution of PCy_3 and K_2OsCl_6 in methoxyethanol was first reported by Moers (1971). Although **1a** and **1b** are coordinatively unsaturated, they are monomeric in both the solid phase and in solution

(Moers, 1971; Esteruelas and Werner, 1986). Their structure is square pyramidal, with the bulky phosphines *trans* disposed within a plane shared by Cl and CO (Figure 1.2). Moers (1984) attests that osmium lies essentially in the basal plane of **1a**, leaving a vacant coordination site *trans* to the hydride which is of considerable dimension. However, the coordination of a third bulky phosphine has not been detected for either **1a** or **1b** (Moers, 1971; Esteruelas and Werner, 1986).

The addition of a host of small molecules to form stable, six coordinate complexes of **1a** and **1b** has been observed. Moers (1971) and Moers et al. (1973, 1974) have demonstrated the coordinative capacity of pyridine, SO_2, CS_2 and CO to **1a**. Esteruelas and Werner (1986) have characterized the analogous CO complex of **1b** as well as an octahedral product of PMe_3 or $P(OMe)_3$ addition. The use of a 2:1 PMe_3 to Os ratio did not result in the displacement of a bulky phosphine to form a bis PMe_3 complex. The addition of larger alkyl phosphines was not observed, due to what is believed to be a steric limitation.

A displacement of the chloride of **1b** by an acetate anion to yield an air-stable, microcrystalline solid has been reported (Esteruelas and Werner, 1986). An IR spectrum indicates that the acetate group is bonded through both oxygen atoms as shown below. This type of reaction has the potential to interfere with the hydrogenation of copolymers that contain significant amounts of the carboxylate salts derived from surfactant.

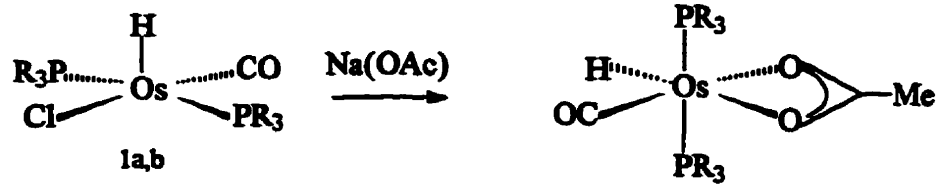

1a,b

Exposed to traces of oxygen (Figure 1.2), the solid form of **1a** and **1b** yield the diamagnetic dioxygen adducts **2a** (Moers et al., 1974b) and **2b** (Esteruelas et al., 1988). The dioxygen ligand is very strongly bound, as indicated by the shift of $\nu_{O\text{-}O}$ in the IR from 1580 cm^{-1} for free O_2 to 820 cm^{-1} and 867 cm^{-1} for **2a** and **2b** respectively. The substantial

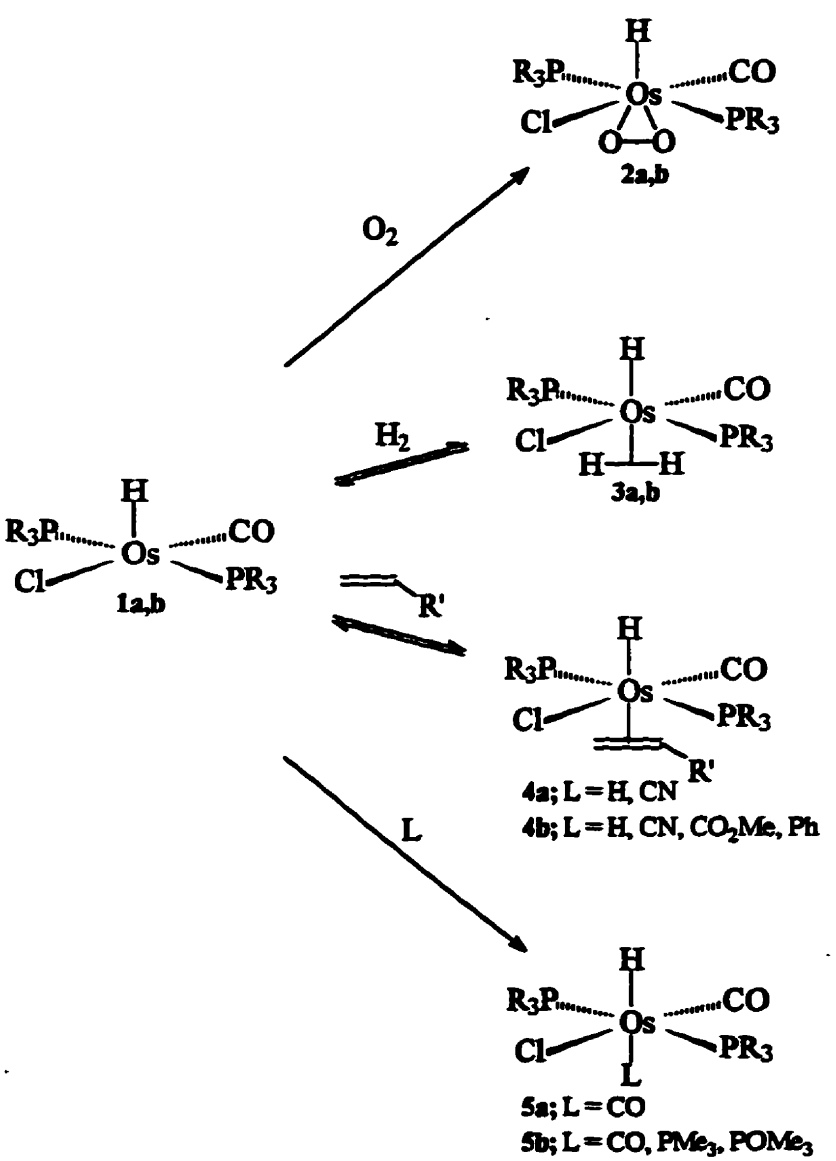

Figure 1.2: Characterized reactions of **1a,b**

single bond character of bound O_2 is characteristic of a η^2-peroxo coordination mode (Esteruelas et al., 1988). In spite of this strong association, a displacement of dioxygen from **2b** was proposed by Andriollo et al. (1989) when employed as a catalyst precursor. Note that over extended periods of time, pure solutions of Os-O_2 complexes are not necessarily stable. Mezzetti et al. (1994) have observed a solution of $[OsCl(O_2)(dcpe)_2]BPh_4$ (dcpe = 1,2-bis(dicyclohexylphosphino)ethane) produce diphosphine oxides during decomposition.

A variety of small olefins have been shown to produce six coordinate complexes of **1a** and **1b** (Figure 1.2). Unactivated olefin such as ethylene must be present in excess to maintain stable adducts (Moers et al., 1974b). However, electron withdrawing substituents such as CN, CO_2Me or CO stabilize the Os-olefin bond enough to produce isolable octahedral complexes (Moers and Langhout, 1977; Esteruelas and Werner, 1986). Esteruelas and Werner (1986) observed no direct evidence for the production of stable metal-alkyls of **1b** that could form by the insertion of olefin into the osmium-hydride bond. However, in a later report they provide convincing evidence to support the insertion of styrene at room temperature according to the scheme presented in Figure 1.3 (Andriollo et al., 1989).

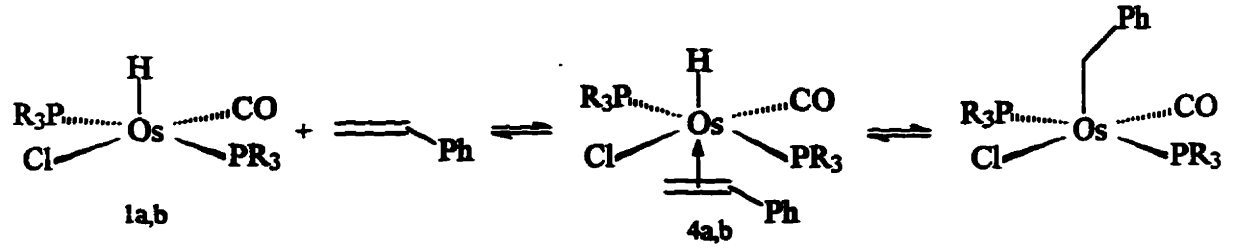

Figure 1.3: Styrene insertion into the Os-H bond of **1b**

In a benzene solution with styrene, the hydride region of a ^1H NMR spectrum of **1b** is reported to undergo significant changes. The hydride triplet of **1b** at -31.9 ppm disappears, to be replaced by a broad resonance at -27.9 ppm. In a separate experiment, the addition of styrene to $OsDCl(CO)(P\textit{i}\text{-}Pr_3)_2$ initiated an H-D exchange as the hydride signal at -27.9 ppm was restored at the expense of the olefin signal. Andriollo et al.

(1989) rationalized these observations as a rapid equilibrium (Figure 1.3) which produced an exchange averaged signal for the hydride of **1b**.

The only other olefin to be scrutinized for Os-alkyl formation is *trans*-PhHC=CHCOMe, or benzylideneacetone (Esteruelas et al., 1992). At room temperature in benzene, four equivalents of substrate failed to produce any changes to the ^{1}H NMR spectrum of **1b**. Under identical conditions, the H-D exchange that had been reported for styrene was not observed. It should be noted that the unsubstituted analogue of benzylideneacteone, H_2C=CHCOMe, forms a very stable π-olefin complex that is unchanged after heating to 70°C in benzene for 24 hours (Esteruelas and Werner, 1986). It would therefore appear that the coordinating ability of an olefin is strongly influenced by the bulk of its substituents.

Complex **1b** has been shown to activate molecular hydrogen by a rather uncommon η^2-coordination mode (Esteruelas et al., 1988). Consistent with other small molecule additions, dihydrogen coordinates *trans* to the hydride to create what is formally an Os(II) complex (Figure 1.4). Removal of an H_2 atmosphere rapidly transforms the dihydrogen adduct back into **1b**. This instability has precluded the isolation of **3b**. It has therefore been characterized by spectroscopic means only.

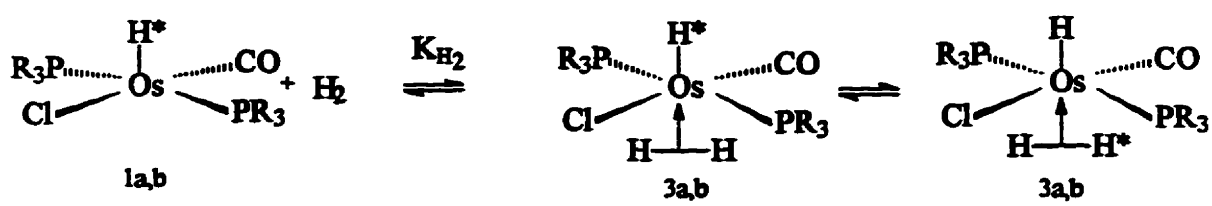

Figure 1.4: Coordination of molecular hydrogen by **1b**

A ^{1}H NMR spectrum of **1b** at 240K under H_2 exhibits a broad resonance at -1.8 ppm (η^2-bonded H_2) and a triplet at -6.5 ppm corresponding to the apical hydride ligand (Bakhmutov et al., 1996). The minimum spin lattice relaxation times (T_{1min}) of these signals are 6.2 ms and 296 ms respectively. Relatively fast relaxation is expected for η^2-

bonded H_2, due to the efficiency of dipole interactions between two protons so close in space. Classical hydrides on the other hand, being located much further from other protons, have a less efficient relaxation mechanism and therefore longer T_1's (Jessop and Morris, 1992).

At 240 K, Bakhmutov et al. (1996) resolved a distinct dihydrogen signal at δ = -1.8 ppm. At higher temperatures an exchange between free and bound H_2 was observed at a rate which varied from slow to fast on the NMR timescale. In the fast exchange domain they have estimated the equilibrium constant, K_{H2}, to range from 2572 M^{-1} at 40°C to 143 M^{-1} at 80°C. Also at 80°C, the rate constant for H_2 loss (k_{-1}) from **3b** was reported to be $7.1*10^5$ s^{-1}. Clearly, the rate of H_2 exchange and the population of dissociated products are favoured by extreme temperatures.

Esteruelas et al. (1992) have noted that the exposure of **1b** to D_2 at room temperature produces $OsD(D_2)Cl(CO)(PiPr_3)_2$ by H-D exchange. The transition state of this Os-H/Os-H_2 exchange process may be relevant to olefin hydrogenation, in that a seven-coordinate trihydride complex may serve as a hydrogenation transition state. To produce such a complex, bound dihydrogen must add oxidatively to the metal centre. Alternatively, Bakhmutov et al. (1996) suggest that η^2-H_2 could migrate from its *trans* position to form a transient *cis* H/H_2, 3-centred, $Os(H_3)$ complex. Given our present state of knowledge, an assignment of either a trihydride or a three-centred $Os(H_3)$ pathway for this exchange may be unjustified.

1.3 Reported Cases of $OsHCl(CO)(PR_3)_2$ Catalyzed Olefin Hydrogenation

Catalytic research on osmium-PR_3 complexes is limited to studies of the $PiPr_3$ and $P(MetBu_2)_3$ systems at mild temperatures and ambient pressures. Esteruelas et al. (1988) first identified the potential of **1b** to catalyze the hydrogenation of styrene, cyclohexene and cyclohexadiene as well as benzylideneacetone. This exploratory work was expanded to study the isomerization of 1,4-cyclohexadiene to the 1,3-position by **1b** under N_2

(Esteruelas et al., 1989). Under an H_2 atmosphere, both isomers of the diene as well as cyclohexene were rapidly hydrogenated.

In a detailed study of the hydrogenation of phenylacetylene, Werner and his coworkers provided twelve measurements of the rate of styrene reduction by $OsHCl(CO)(PMe_tBu_2)_3$ (Andriollo et al., 1989). The experimental conditions were P_{H2}=1 bar, T=23°C, [Os]=0.7-2.5 mM and [styrene]=0.06-0.3 M. The data suggested a first order dependence of the hydrogenation rate on [Os] and [styrene]. Without having determined the influence of H_2 or additional PR_3 on the reaction rate, the coauthors refrained from proposing a reaction mechanism.

The hydrogenation of benzylideneacetone (*trans*-PhHC=CHCOMe) by **1b** has been studied by Esteruelas et al. (1992). Initial rate data, acquired over a narrow range of process conditions ([**1b**]=0.73-2.5 mM, $[C=C]_o$=0.25-0.60 M, P_{H2}=0.71-1.28 bar, T=60°C) established a first order dependence of the reaction rate on [**1b**] and [C=C]. Five rate experiments could resolve no dependence of the reaction rate on P_{H2}. That is, the reaction appeared to be zero order with respect to $[H_2]$. Linn and Halpern (1987) have reported $RuH_4(PPh_3)_3$ to be similarly indifferent to the concentration of H_2 in the bulk.

To rationalize these observations, Esteruelas et al. (1992) proposed the catalytic mechanism illustrated in Figure 1.5. They suggest that **1b** is "activated" by a process involving the initial coordination of H_2, its migration to a position *cis* disposed to the hydride, followed by its subsequent dissociation. This vacated site could then be occupied by olefin whose insertion into the Os-H bond would serve as the rate determining step. A fast elimination of the Os-alkyl ligand by H_2 completes the catalytic cycle.

In accordance with this mechanism, an expression for k' as defined by

$$-\frac{d[C=C]}{dt} = k'\,[C=C]$$

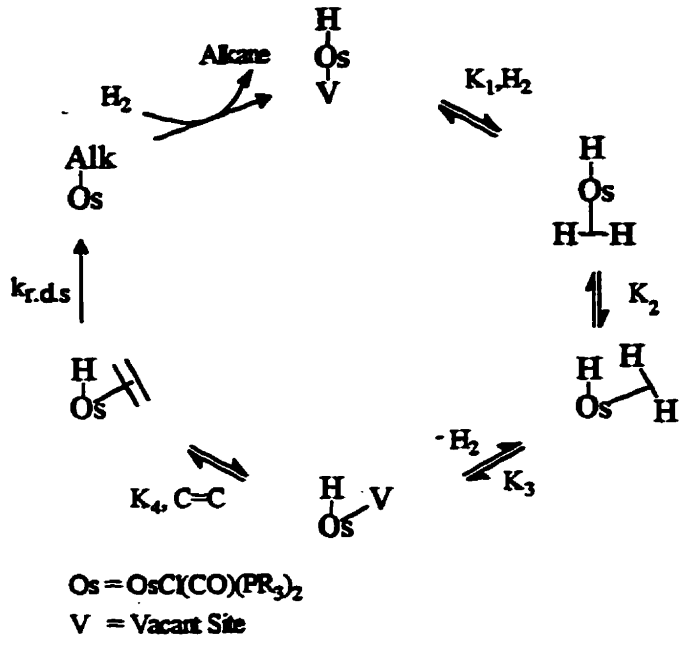

Figure 1.5: Proposed mechanism for benzylideneactone hydrogenation by **1b**

would be (in full and approximate form),

$$k' = \frac{k_{rds}\, K_1 K_2 K_3 [C{=}C][Os]_T}{1 + K_1 K_2 K_3 + K_1[H_2] + K_1 K_2 [H_2] + K_1 K_2 K_3 K_4 [C{=}C]}$$

$$\simeq \frac{K\,[C{=}C][Os]_T}{1 + (K_1 + K_1 K_2)[H_2]} .$$

The proposed mechanism yields a rate expression that is consistent with the experimental data if $K_1[H_2] \ll 1$. Using K_1 = 650 l/mole as provided by Bakhmutov et al. (1996) at 60°C and an H_2 concentration of 0.0035 moles/l at 1 atm (Young, 1981), $K_1[H_2]$ is equal to 2.2. The proposed mechanism therefore predicts an inverse dependence of the reaction rate on $[H_2]$ that is not realized in the experimental data.

1.4 Reactivity and Catalytic Chemistry of $OsHCl(CO)(PPh_3)_3$

The first examples of hydridocarbonyl complexes of Os(II) were prepared by Vaska in 1964. In contrast to the alkyl phosphine systems, the PPh_3 analogues are six coordinate, octahedral complexes. Vaska (1964) noted that the coordinatively saturated system did not add molecular hydrogen and there are no reports of small molecules displacing PPh_3 to form a bis-phosphine complex. However, H-D exchange to form $OsDCl(CO)(PPh_3)_3$ has been observed, suggesting that while not producing a stable complex, molecular hydrogen may be activated by the system.

Excluding a brief reference by Mitchell (1970), the catalytic utility of the PPh_3 system was first recognized by Sanchez-Delgado et al. (1983). They found the system to be an efficient catalyst for C=C bond migration and the hydrogenation of olefin, aldehydes, ketones and unsaturated aldehydes. Under N_2 at 150°C, the complex readily promotes the isomerization of 1-hexene to an equilibrium mixture of *cis* and *trans* 2-hexene. In an H_2 environment, 1-hexene was preferentially hydrogenated relative to the internal olefin. Cyclohexadienes have been efficiently hydrogenated to cyclohexane with little selectivity for the monoolefin (Sanchez-Delgado et al., 1985).

This early research has screened the catalytic potential of mononuclear osmium(II) complexes without proposing reaction mechanisms. A direct comparison of $OsHCl(CO)(PPh_3)_3$ activity to the alkyl-phosphine complexes is not warranted due to widely differing reaction conditions employed in the literature. However, much milder conditions are required for **1b** to achieve the reaction times needed for the PPh_3 analogues to saturate cyclohexene (Esteruelas et al., 1989; Sanchez-Delgado et al., 1983).

1.5 Scope of the Research

The principal objective of this research is to assess the merits of the osmium technology for NBR hydrogenation while furthering our understanding of its underlying chemistry. While not evaluating the commercial viability of an osmium-based process, the study illustrates the advantages and weaknesses of the osmium system relative to the established rhodium(I)

catalysts. By examining the performance of **2a** at conditions that approach those employed industrially, the acquired data is relevant to potential commercial application.

The following two chapters summarize research projects that serve as a foundation to the thesis. A study of the solubility of hydrogen in pure and dilute NBR solutions of chlorobenzene is detailed in Chapter 2. These results simplify the analysis of hydrogenation rate data by rendering the concentration of hydrogen in the condensed phase as a function of process conditions. Chapter 3 relates a kinetic study of the hydrogenation of NBR catalyzed by $RhCl(PPh_3)_3$ and $RhH(PPh_3)_4$ at industrially relevant conditions. This research advances our understanding of the commercial NBR process while establishing a standard to which the new osmium technology may be compared.

The content and objectives of Chapters 4 and 5 are intimately related, the former centering on the structure and reactivity of **1a,b** while the latter focuses on its catalytic chemistry. The high-pressure, nuclear magnetic resonance (NMR) experiments described in Chapter 4 have both revealed and quantified chemical equilibria that are directly related to the hydrogenation mechanism. This fundamental knowledge is applied in Chapter 5, where a comprehensive kinetic analysis of the hydrogenation of NBR by **2a** is detailed along with a mechanistic interpretation of the acquired data.

Having characterized the rhodium and osmium systems from the standpoint of activity, Chapter 6 outlines a series of experiments which sought to evaluate the selectivity of each catalyst. The main body of the thesis is closed with a discussion of a new continuous reactor configuration for HNBR production (Chapter 7). The design features are illustrated along with a preliminary evaluation of a bench-scale prototype.

Chapter 2

Solubility of Hydrogen in Chlorobenzene

Although a variety of polar organic solvents are capable of solvating NBR, chlorobenzene demonstrates superior chemical stability under extreme catalytic conditions. It has therefore been favoured in both industrial and academic investigations. Unfortunately, reliable estimates of the solubility of hydrogen in chlorobenzene at high pressures and temperatures have been unavailable to support these research efforts. The only report on this system is limited to 1.013 bar over a temperature range of 272.3 K to 354.0 K (Horiuti, 1931).

The analysis of hydrogenation rate data is simplified by a knowledge of the concentration of H_2 in the liquid phase under the reaction conditions studied. It is for this reason that the solubility of hydrogen in pure chlorobenzene and dilute NBR solutions has been measured at temperatures ranging from 273.2 K to 443.2 K and total pressures up to 67 bar. These conditions encompass those commonly encountered by catalyst researchers and process designers working in the polymer modification field (McManus and Rempel, 1995).

2.1 Experimental

2.1.1 Materials

All reagents were used as received. Hydrogen gas of 99.99% purity was obtained from Linde-Union Carbide Canada Ltd. Chlorobenzene purchased from Fisher Scientific Ltd had a reported purity of 99%. Decane and 1,3-dimethylbenzene were spectrometric grade products of Aldrich Chemical Company. Samples of NBR (Krynac 38.50) were obtained from Bayer Rubber Inc.

2.1.2 Apparatus and Procedure

An 0.5 litre Autoclave Engineers "Zipperclave", initially charged with 350 cm^3 of chlorobenzene was recharged when no more than 250 cm^3 had been withdrawn for analysis. Each time, the system was degassed using three cycles of charging the autoclave with H_2 to

10 bar, allowing the system to equilibrate, and venting. The total system pressure was measured by a differential pressure transducer that was calibrated to an estimated accuracy of +/- 1% of the range studied, or +/- 65 kPa at 65 bar. An iron-Constantan thermocouple, checked at the ice and steam points, was used to measure the temperature of the condensed phase. Control of the vessel temperature was accomplished to within +/- 0.5K by a PID controller acting on a ceramic insulated heating mantle. Measurements made at 273.2 K were achieved by immersing the autoclave in an ice-water bath.

The analysis technique, based on the work of Lee and Mather (1977), determined the composition of the condensed phase in equilibrium with its vapour at a given pressure and temperature. This equilibrium was established rapidly using an agitation rate of 1200 rpm to intimately mix the two phases. In general, a 30 min equilibration time was sufficient following a change in pressure while at least a 90 min period was required after changing temperatures. The results were unaffected by approaching the experimental pressure from above or below.

Aliquots of chlorobenzene saturated with H_2 were withdrawn from the autoclave through a dip tube attached to a 10 cm length of 1/16" stainless steel tubing. A 125 cm^3 Erlenmeyer flask sealed by an Aldrich Suba-seal rubber stopper was used as a sampling flask. A glass side arm installed on the flask was equipped with a stopcock and a B-14 ground glass joint to interface with a gas burette. In taking a sample a slow, continuous flow of solvent was permitted to purge the dip tube of vapour. Under this flow, the 1/16" tubing was inserted through the stopper in order to inject fluid into the preweighed sample flask. Approximately 15 cm^3 of fluid were required to evolve an amount of H_2 sufficient to be measured accurately. Once collected, the sample was quickly brought to room temperature by immersion in a water bath.

Initially at atmospheric pressure, the sample flask was pressurized by the injection of liquid and the evolution of H_2 dissolved within it. The volumetric expansion required to return the pressure in the sample flask to atmospheric was measured using a gas burette. The

mass of chlorobenzene sampled was then determined gravimetrically. The volume displaced by injecting this amount of chlorobenzene into the sample flask was subtracted from the burette measurement to yield the amount of gas evolved from the sample. A correction for the residual H_2 remaining in the sample liquid was applied using the atmospheric pressure data of Horiuti (1931). Having accounted for the amounts of H_2 and chlorobenzene sampled, the mole fraction of each component was calculated.

In those cases where copolymer solutions were studied, the composition of the liquid was measured by evaporating the solvent and weighing the polymer residue. It was determined that at room temperature, the density of dilute solutions of NBR did not differ from that of pure chlorobenzene.

2.2 Results and Discussion

To verify that the experimental method was capable of yielding results of an accuracy sufficient for research applications, a comparison with published solubility data was made. Two reports, produced by separate laboratories, were selected for comparison over the range of conditions relevant to HNBR production. The first, reported by Sokolov and Polyakov (1977), examined the hydrogen + n-decane system. The second comparison was made with work of Simnick et al. (1979) on the hydrogen + 1,3-dimethylbenzene system. Figure 2.1 illustrates both the literature studies along with the data collected in our laboratory using the procedure described above. In no case did the deviation of the literature data from the values calculated from a linear regression of our results exceed 2%. In a review of the work of Sokolov and Polyakov, Young (1981) assigned an error of +/- 3% to the reported H_2 liquid mole fraction. In light of our comparison to the work, this error estimate is considered to be representative of that associated with the present study.

Having established confidence in the experimental approach, the H_2 + chlorobenzene system was analyzed at (273.2, 296.2, 328.2, 363.2, 403.2 and 443.2)K at pressures up to 67 bar. Figure 2.2 illustrates the liquid phase H_2 mole fraction as a function of the system conditions while numerical values are provided in Table AI, Appendix I. Owing to the

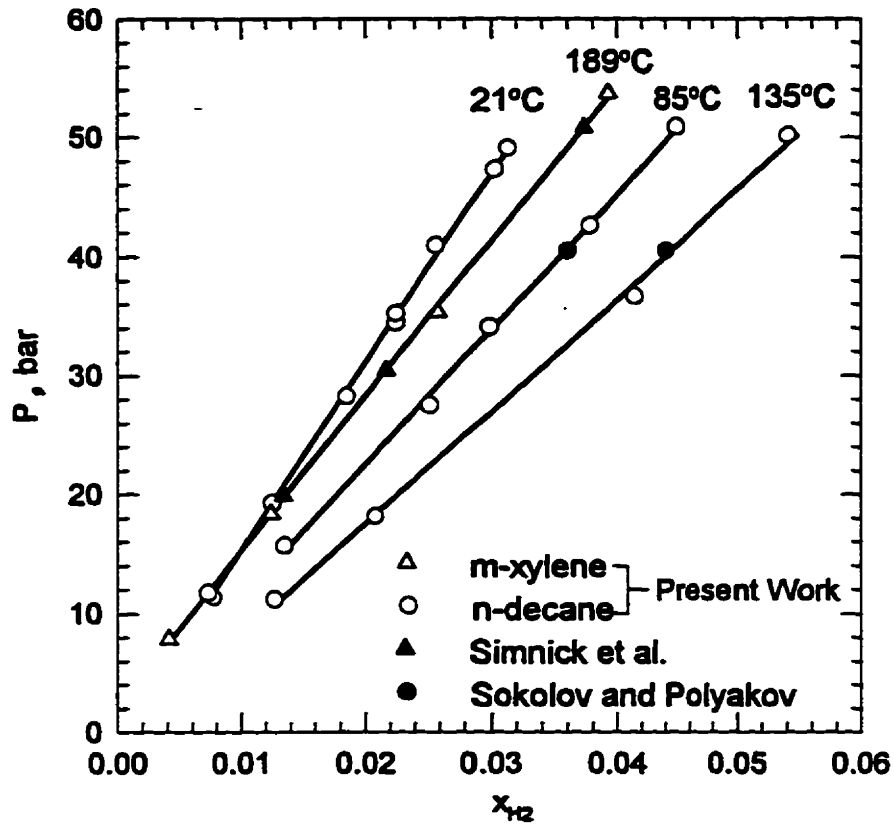

Figure 2.1: Comparison of the developed technique to published work.

lack of vapour phase data, any analysis must be classified as preliminary. Nevertheless, the data appear to be well represented by equation 2.1 over the range of conditions studied.

$$\ln(f_2/x_2) = \ln K_2 + \frac{v_{m,2}}{RT} P_{H_2} \qquad 2.1$$

where, f_2 = fugacity of H_2, bar
x_2 = H_2 liquid mole fraction
K_2 = Henry's constant, bar
$v_{m,2}$ = liquid molar volume of H_2, m^3/mol
T = system temperature, K
P_{H2} = partial pressure of H_2, bar

Defined by the above relation, K_2 (at the saturation pressure of chlorobenzene) is the limiting value of f_2/x_2 as the system approaches infinite dilution.

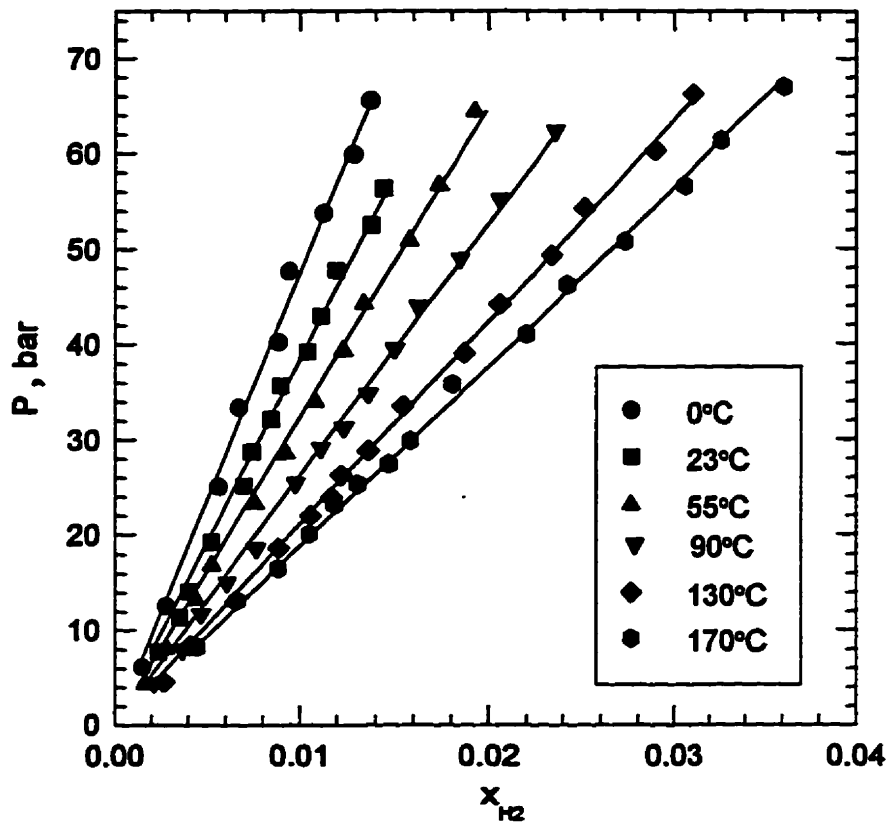

Figure 2.2: Solubility of H_2 in chlorobenzene

Without a knowledge of the vapour phase composition, certain simplifications are required to estimate the fugacity of hydrogen, f_2. The first assumption is that Raoult's law may be applied to estimate the vapour phase hydrogen mole fraction. The second assumes that a binary interaction between H_2 and chlorobenzene may be neglected. This last simplification facilitates an estimate of the vapour phase fugacity coefficient for H_2 from the equation of state of Peng and Robinson (1976). It should be noted that under the conditions studied, the system could well have been represented by an ideal gas approximation. Through these assumptions, the Henry's constant at each temperature has been regressed and plotted in Figure 2.3. The overall temperature dependence of K_2 has been fitted to the expression provided in equation 2.2 using the units specified above.

$$\ln K_2^{P_1^{sat}} = 19.061 + 0.483 / T - 1.915 \ln T \qquad 2.2$$

A comparison of equation 2.2 with the correlation that Fogg and Gerrard (1991) have derived from the data of Horiuti (1931) is favourable. Over the coincident temperature range (273 K to 354 K), the largest deviation between predicted values is 9.1%.

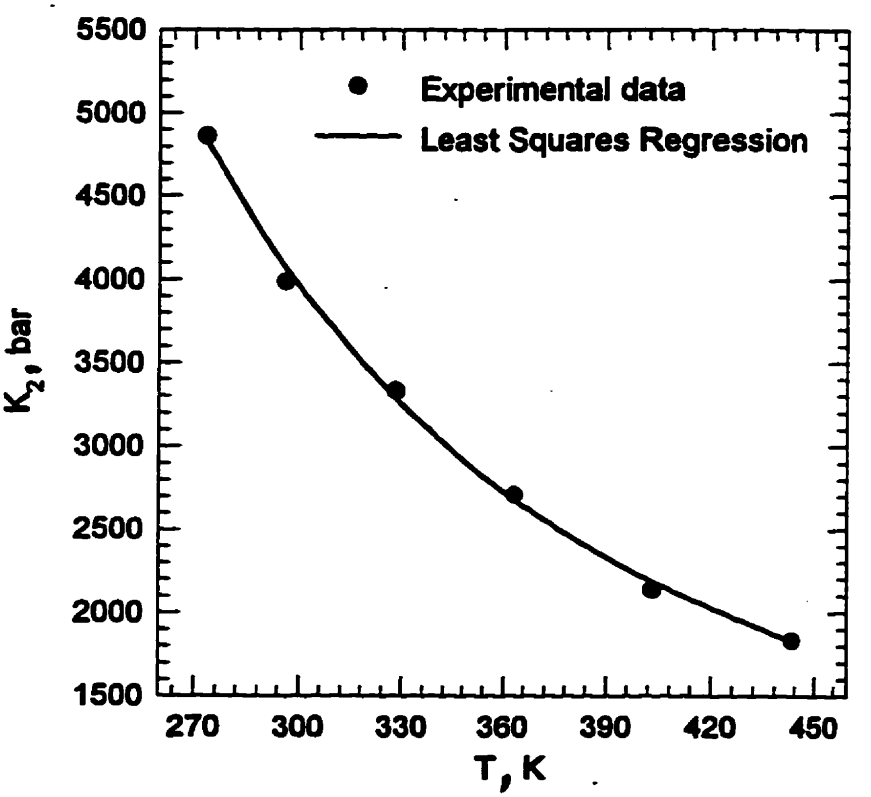

Figure 2.3: H_2 + chlorobenzene: K_2 versus temperature

As the utility of the H_2 + chlorobenzene system lies principally with the hydrogenation of copolymers, a knowledge of the influence of dissolved polymer on the hydrogen solubility is required for many applications. Throughout this research, solutions containing less than 4 wt% of NBR have been studied. Therefore, solutions of 4.09 wt% and 8.08 wt% NBR in chlorobenzene have been analyzed to ensure that pure solvent data may be used with confidence. Figure 2.4 suggests that at these relatively low copolymer loadings, the influence of NBR on H_2 solubility is not significant at 130°C.

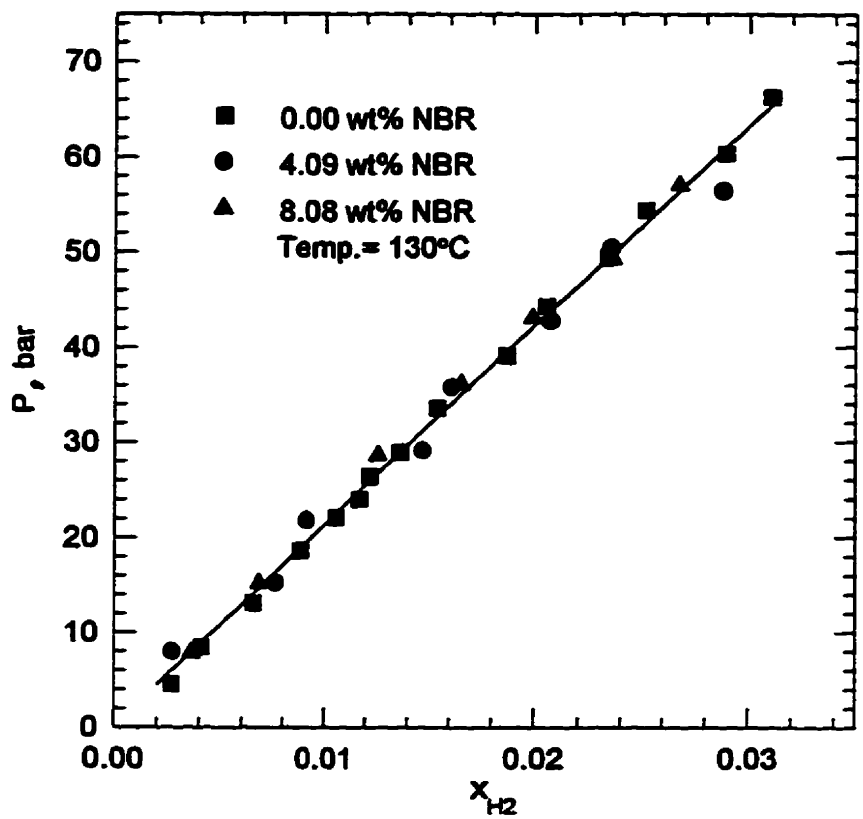

Figure 2.4: Solubility of H_2 in NBR-chlorobenzene solutions, T=403.2 K

Chapter 3

Kinetics of NBR Hydrogenation by $RhCl(PPh_3)_3$ and $RhH(PPh_3)_4$

The catalytic chemistry of Rh(I) phosphine complexes has been researched and reviewed extensively over the last three decades (James, 1973; Jardine, 1981). In so far as they are the only homogeneous systems used commercially for HNBR synthesis (Oppelt et al., 1976; Rempel and Azizan, 1984) they represent the standard to which new generations of catalysts are compared. However, an absence of comprehensive kinetic data on the performance of $RhCl(PPh_3)_3$ and $RhH(PPh_3)_4$ under extreme conditions has precluded direct assessments of these new technologies.

In addition to a brief report by Weinstein (1984), Mohammadi and Rempel (1987) have carried out a mechanistic study of the $RhCl(PPh_3)_3$ / NBR system at the mild reaction conditions of 65°C and pressures near ambient. Bhattacharjee et al. (1991) extended these process conditions to 100°C and 56 bar in an effort to optimize the process and characterize the final product. However, little is known of the kinetic behaviour of $RhCl(PPh_3)_3$ at these elevated conditions and to our knowledge, no reports on the $RhH(PPh_3)_4$/NBR system are present in the open literature.

The research presented in this chapter is an attempt to appreciate the underlying chemistry of both the $RhCl(PPh_3)_3$ and $RhH(PPh_3)_4$ catalyzed hydrogenation of NBR at conditions that are relevant to industrial applications of the technology. Carefully obtained kinetic data is presented within the context of fundamental reaction mechanisms. A likely catalytic pathway is proposed for the $RhCl(PPh_3)_3$ system.

3.1 Experimental

3.1.1 Materials

$RhCl(PPh_3)_3$ and $RhH(PPh_3)_4$ were synthesized according to literature preparations (Osborn et al., 1966; Ahmad et al., 1974) from $RhCl_3*3H_2O$ obtained from Engelhard and recrystallized PPh_3 from Aldrich. Oxygen free hydrogen with a purity of 99.99% was obtained from

Linde-Union Carbide Canada Ltd. All reported kinetic and selectivity experiments employed monochlorobenzene as a solvent. Limited trials with 2-butanone and cyclohexanone were undertaken for comparison to literature reports. In all cases these reagent grade solvents were used as received. The acrylonitrile-butadiene copolymer (NBR) contained 62% butadiene by weight (78% *trans*, 16% *cis*, 6% *vinyl* isomerization) and had a molecular weight of approximately 200,000. This material (Krynac 38.50) was used as received from Bayer Rubber Inc. A styrene-butadiene copolymer (Finaprene 410 from Petrofina) having an 18% styrene content and a molecular weight of 160,000 was used in control experiments that monitored the response of the process to an absence of nitrile functionality.

3.1.2 Apparatus

Raw kinetic data consisted of time-resolved measurements of both the amount of hydrogen consumed by the reaction and the temperature of the rubber solution. The hydrogenation apparatus, a high-pressure variation of that developed by Mohammadi and Rempel (1987), has proven to be capable of monitoring the reaction process in real time. An operational schematic of the equipment is provided in Figure 3.1. Detailed drawings and descriptions of specific components have been reported by Martin (1991).

The apparatus is designed to maintain isothermal and isobaric conditions while monitoring H_2 consumption. A drop in the autoclave pressure relative to the reference bomb RB-1 is detected by the differential pressure transducer PT-1. This error signal serves as the input for the control algorithm residing within a personal computer. Via an i/p converter, the PC actuates the pneumatic control valve to permit H_2 from the supply cell to recharge the autoclave. This control system maintains the autoclave pressure no less than 0.3 psi below its set point.

The amount of H_2 lost from the supply cell during the reaction is an integrated measure of the hydrogenation rate. This is monitored by PT-2, which detects the drop in the supply cell pressure relative to RB-2 created by the transfer of H_2 to the autoclave. Conversion of the signal generated by PT-2 to millimoles of H_2 is accomplished by calibrating its output voltage

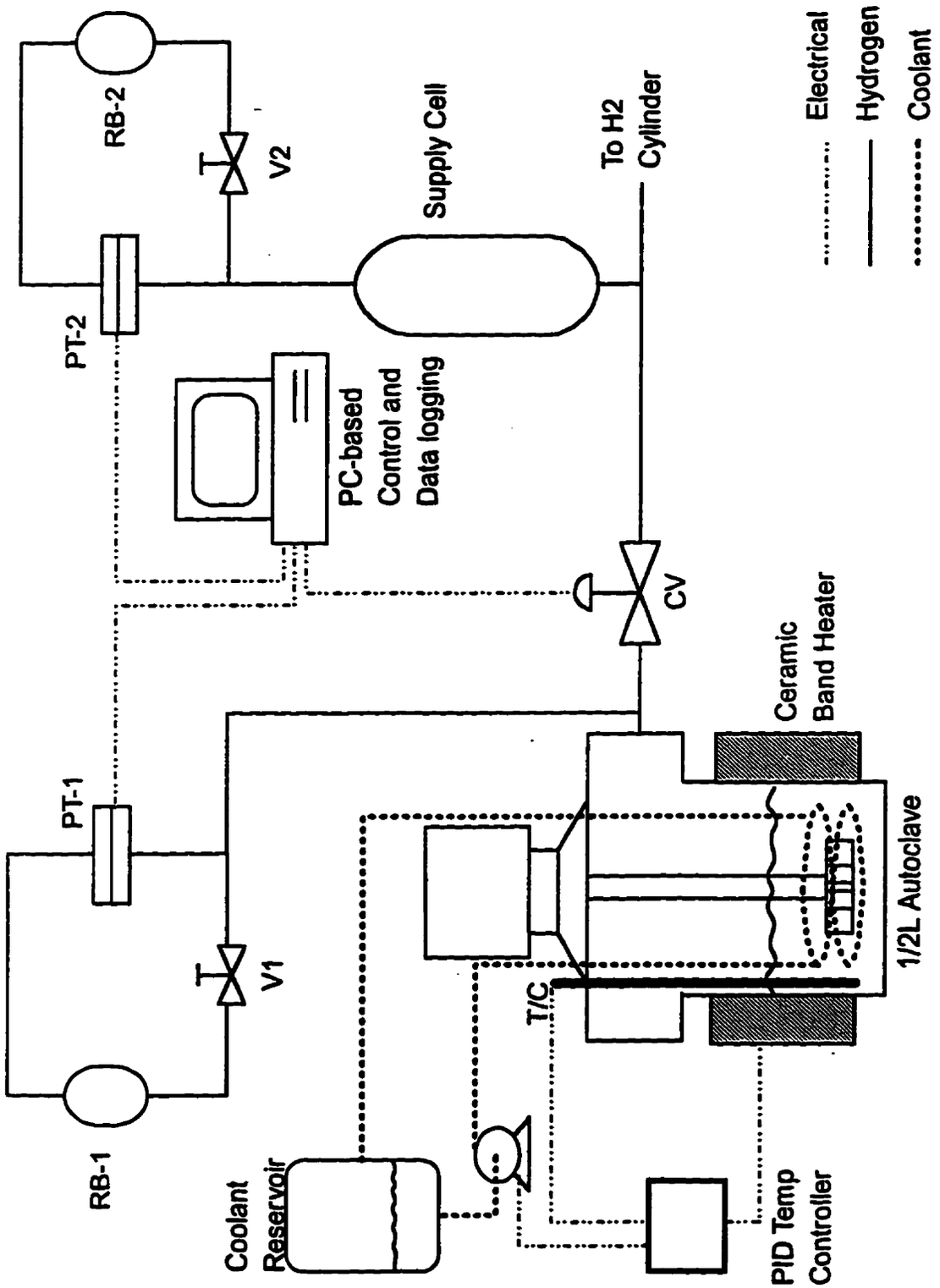

Figure 3.1: Schematic of the hydrogenation apparatus

against the conversion of a known amount of substrate. This technique assumes that a change in pressure is linearly proportional to the H_2 lost from the supply cell. Such ideal gas behaviour holds for H_2 at 1250 psi and 295 K, especially over small changes in pressure.

Although the pressure control algorithm operates with excellent precision, the degree to which the measured gas uptake profile corresponds to the progress of the hydrogenation is dictated by the accuracy of the temperature control. Autoclave temperature fluctuations of $\pm 1°C$ create pressure swings to which the pressure controller responds. The resulting reaction profile may therefore become the sum of the intrinsic reaction rate and artifacts of the temperature control. This is especially problematic at operating pressures above 40 bar where pressure is increasingly sensitive to autoclave temperature variations.

The original apparatus did not include a cooling system and was susceptible to severe reaction exotherms (Martin, 1991). To improve the quality of the kinetic data and facilitate the study of more rapid reactions, a dual output PID controller (Parr model 4842) was installed. Acting upon the ceramic insulated heating mantle and an oil circulating pump (Masterflex model 2020C), the new system controlled the solution temperature to within +/- 1°C of the set point. As a further precaution, the vessel temperature was logged with the H_2 consumption data to provide a means of assessing the controller performance.

3.1.3 Standard Reaction Procedure

Polymer solutions were prepared by dissolving the desired mass of rubber in chlorobenzene within a 100 cm^3 volumetric flask. This took approximately 24 hours, during which the flask was placed under an Argon atmosphere in the dark. This solution was transferred to a glass autoclave liner and the volumetric rinsed with 50 cm^3 of chlorobenzene to make a total solution volume in the liner of 150 cm^3. Any required PPh_3 was added directly to the solution just prior to assembling the autoclave.

The required mass of catalyst precursor was weighed by difference into a dry, glass bucket to an accuracy of +/- 0.0001g. This bucket was then loaded into a catalyst chamber that

was designed to suspend it above the polymer solution during the degassing and heating processes. The autoclave, having been charged with both the glass liner and the catalyst bucket, was assembled according to the manufacturer's instructions.

Beyond the time of weighing the catalyst, all kinetic experiments were performed with the rigorous exclusion of air. To purge the autoclave headspace, three cycles of charging the reactor with H_2 to 10 bar and venting were carried out with no agitation. The autoclave was then immersed in an ice-water bath. A head pressure of 14 bar was charged and the agitator started at 200 rpm. Chilling the vessel to reduce the vapour pressure of chlorobenzene was a precautionary measure. Once cooled to 5°C, the reactor pressure was once again vented and recharged to 14 bar. To degas the polymer solution, H_2 was purged continuously through the reactor headspace while agitating at 1200 rpm for 20 minutes. The reactor pressure was then vented and the ceramic band heater installed.

Achieving the desired reaction conditions required pressurizing the system to approximately 80% of the target value and initiating the temperature controller. The increase in the temperature of the sealed autoclave provided the remaining 20% of the pressure set point. Once the chosen conditions had been attained, the system was allowed a minimum of 45 minutes to equilibrate. During this period all of the reactor components would warm up, causing a slight rise in the overall system pressure. A failure to observe this equilibration time resulted in an uptake plot that was adversely influenced by this pressure increase. Experiments performed above 30 bar or those suspected of a duration greater than 40 minutes were allowed an additional 30 minutes to stabilize.

The H_2 uptake monitoring program employed two user-specified, data logging intervals. The first was of short duration and was designed to monitor the reaction during its initial stages where the reaction rates are greatest. The second interval could be initiated by the operator to avoid the unnecessary collection of data during periods of slow hydrogenation. Once activated, the program waited one logging interval before starting to record the time, reaction temperature and amount of H_2 consumed. At this point, the reference isolation valves V1

and V2 were closed and the catalyst bucket dropped, dispersing the powder in the polymer solution using an agitation rate of 1200 rpm. For extremely fast reactions the cooling unit was manually started as the catalyst was dispersed. This technique could limit the influence of the initial exotherm to less than a 1°C temperature rise.

Each experiment was allowed to proceed until gas consumption ceased. The reactor was then brought to 50°C using the cooling unit before venting off the pressure. The autoclave was disassembled and a sample of the HNBR solution cast onto a NaCl plate for infra-red analysis. The remainder of the product was isolated by precipitation with ethanol and drying under vacuum. The autoclave was then reassembled containing about 150 cm^3 of acetone and agitated to remove residual polymer solution. After this rinse, the reactor was blown dry with air before commencing the next trial.

The final degree of olefin conversion measured by gas uptake was confirmed by infra-red analysis (Marshall et al., 1990). Spectra of solvent cast films were collected on a Nicolet 520 FT-IR spectrophotometer. Select samples were analyzed by both ^1H and ^{13}C $\{^1H\}$ NMR on a Bruker 200 MHz spectrometer. Dilute solution viscosities (1g of HNBR / 100 ml 2-butanone) of fully saturated HNBR were measured at 35°C using a Ubbelohde capillary viscometer. This data is reported in the discussion of catalyst selectivity found in Chapter 6.

3.1.4 Experimental Design

Of principal interest in a kinetic study is the functional relationship between the rate of the reaction and the conditions under which it is carried out. The rate of NBR hydrogenation is known to be influenced by factors such as the concentration of catalyst, olefin, nitrile, and H_2 as well as the reaction temperature. As is clearly demonstrated in Section 3.2.2, the dependence of the hydrogenation rate on [C=C] is strictly first order for both $RhCl(PPh_3)_3$ and $RhH(PPh_3)_4$. The response of the process to changes in the remaining factors has been explored according to a statistical framework.

Factor combinations for experiments employing $RhCl(PPh_3)_3$ have been assigned on the basis of a central composite design structure (Box et al., 1978). This consists of a two level factorial design coupled with univariate experiments. While a rigorous central composite strategy provides guidelines for assigning the univariate factor levels, these have been augmented by experiments which lie within these combinations. Together, the factorial and univariate series provide an efficient means of studying the influence of factors acting alone or in combination. Selection of concentrations and temperatures considered weighing precision, polymer solution viscosities and limitations on the reaction rates that the apparatus could control and monitor effectively. The univariate factor combinations have been duplicated for $RhH(PPh_3)_3$ to gain a rudimentary understanding of the kinetic behaviour of this system. Tables AII-A and AII-B of Appendix II list the factor combinations explored.

3.2 Results and Discussion

3.2.1 Interfacial Mass Transfer

As an hydrogenation is initiated the concentration of H_2 in the condensed phase is depleted. The deviation of $[H_2]$ from its equilibrium level is then countered by the physical dissolution of H_2 from the vapour phase. Therefore, while all reactions requiring interfacial mass transfer must operate with a reactant concentration below its equilibrium level, it is desirable to minimize the deficiency. A failure in this respect will produce kinetic measurements that are confounded by mass transfer limitations. To prevent such a condition, an assessment of the rate of physical dissolution of H_2 into an NBR solution has been carried out.

The rate at which H_2 is absorbed by an agitated liquid is represented by equation 3.1.

$$\frac{dc_{H2}}{dt} = \frac{k_l A}{V}(c^*_{H2} - c_{H2}) \qquad 3.1$$

where c_{H2} = Bulk H_2 concentration; mole/L
c_{H2}^* = Equilibrium H_2 bulk concentration; mole/L
k_l = Gas-liquid mass transfer coefficient; m/s
A = Gas-liquid interfacial area; m^2
V = Liquid phase volume; m^3

Given an initial bulk concentration of hydrogen, $c_{H2,o}$, equation 3.1 may be integrated to yield equation 3.2.

$$c_{H2}(t) = c^*_{H2} - (c^*_{H2} - c_{H2,o}) \exp(\frac{-k_l A}{V} t) \qquad 3.2$$

This result has been applied to the gas uptake system to assess its mass transfer capability.

The interfacial mass transfer trials were analogous to hydrogenation experiments. An 150 cm^3 chlorobenzene solution containing 3.60g of Krynac 38.50 was charged to the reactor and purged of atmospheric gases. At room temperature the system was allowed to reach equilibrium under 1 bar of H_2 before stopping the agitator. Under stagnant conditions, the system was slowly pressurized to 23.7 bar. The gas uptake program was then activated with a data logging interval of 2 seconds. At t=0, the agitator was started at the desired rate in order to initiate the physical dissolution process.

The results observed for various agitation rates are illustrated in Figure 3.2 along with their regressed k_lA/V values. At the 1200 rpm agitation rate used throughout the kinetic studies, k_lA/V was approximately 0.31 s^{-1}. It is instructive to examine the bulk H_2 concentration that such a physical dissolution process can support when driven by the reaction rates measured in this work. For a hydrogenation reaction obeying a 1st order rate law,

$$\frac{d[C{=}C]}{dt} = \frac{d[H_2]}{dt} = -k' [C{=}C] \ .$$

Suppose a reaction carried out with $[C{=}C]_o$=275 mM, T=170°C, P_{H2}=23.7 bar were to yield a pseudo-first order rate constant, k', of 0.01 s^{-1} (see experiment #30, Table AII-A). The maximum reaction rate produced in a batch process would be

$$\left.\frac{d[H_2]}{dt}\right|_{max} = -k' [C{=}C]_o$$
$$= -0.01\ s^{-1} * 275\ mM$$
$$= -2.75\ mM/s$$

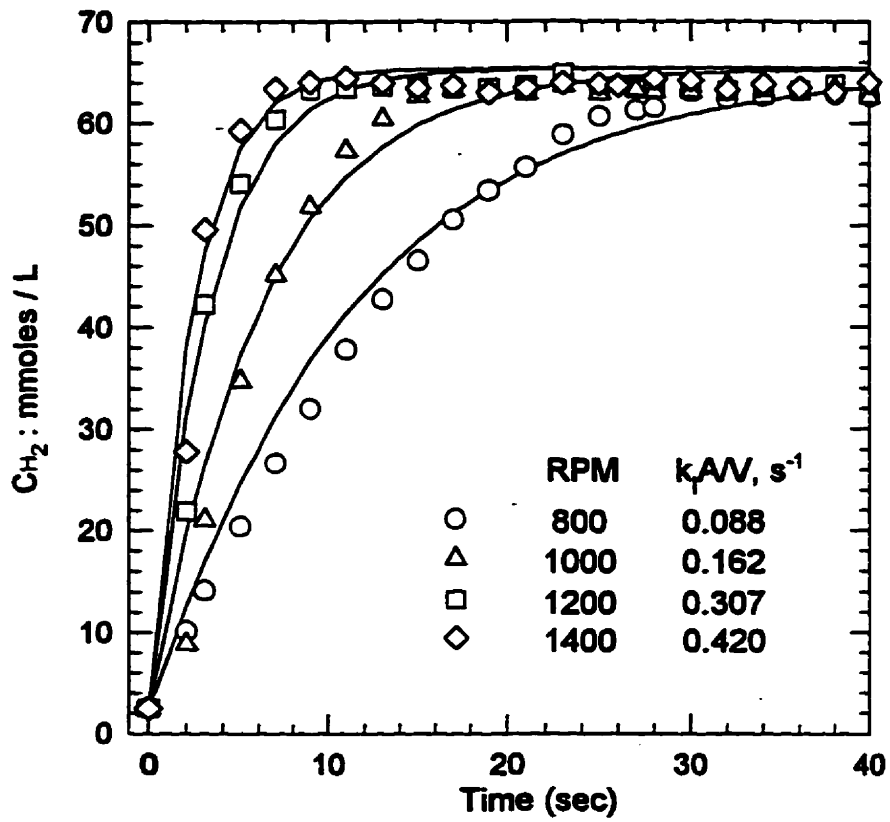

Figure 3.2: Physical H_2 adsorption into an NBR solution

Using equation 3.1,

$$\frac{d[H_2]}{dt} = \frac{k_l A}{V}(c^*_{H2} - c_{H2})$$

$$= 2.75\ mM/s$$

The equilibrium concentration of H_2 under these conditions is 105 mM. The bulk H_2 concentration supported by dissolution would be,

$$c_{H2} = 105\ mM - \frac{2.75\ mM/s}{0.31 s^{-1}}$$

$$= 96.1\ mM$$

For such a rapid hydrogenation, the bulk is depleted of H_2 by no more than 8.5% of its equilibrium level. It is therefore clear that mass transfer processes have a marginal influence on the hydrogenation rates acquired in this study.

3.2.2 Selectivity of NBR Hydrogenation

Over the range of process conditions studied, both $RhCl(PPh_3)_3$ and $RhH(PPh_3)_4$ functioned as efficient catalyst systems for the quantitative hydrogenation of NBR in chlorobenzene. Representative hydrogen uptake profiles corresponding to the saturation of olefin are presented in Figure 3.3. That the reaction profiles are well represented by a simple first-order regression model would indicate that neither system is appreciably selective to the *cis/trans* olefin isomerization of the copolymer under these reaction conditions. There is an insufficient amount of *vinyl* functionality in Krynac 38.50 to assess whether terminal unsaturation is strongly favoured as has been reported for mild reaction conditions (Mohammadi and Rempel, 1987; Hjortkjaer, 1974).

The influence of high reaction temperatures and pressures on the behaviour of $RhCl(PPh_3)_3$ is also demonstrated by its response to ketone solvents. At 100°C and 60 bar, Oppelt et al. (1976) report that 2-butanone and cyclohexanone promote the selective reduction of *vinyl* versus internal butadiene isomers. Under the conditions employed in this study (145°C, 23 bar), no greater than 5% conversion was achieved with either solvent. In each case, an uncharacterized black precipitate was noted to be dispersed in the reaction solution. Mohammadi and Rempel (1987) report no such effect at 65°C, suggesting that catalyst deactivation in these solvents is promoted by excessive reaction temperatures and/or pressures.

Infra-red and NMR analysis of the hydrogenated product revealed that no detectable reduction of nitrile unsaturation results from the use of either catalyst. The ^1H and $^{13}C\{^1H\}$ NMR spectra of select HNBR samples were consistent with those of Mohammadi and Rempel (1987) and Bhattacharjee et al. (1991). This would suggest that the oil resistance of the material is not compromised by the hydrogenation process. However, trace levels of

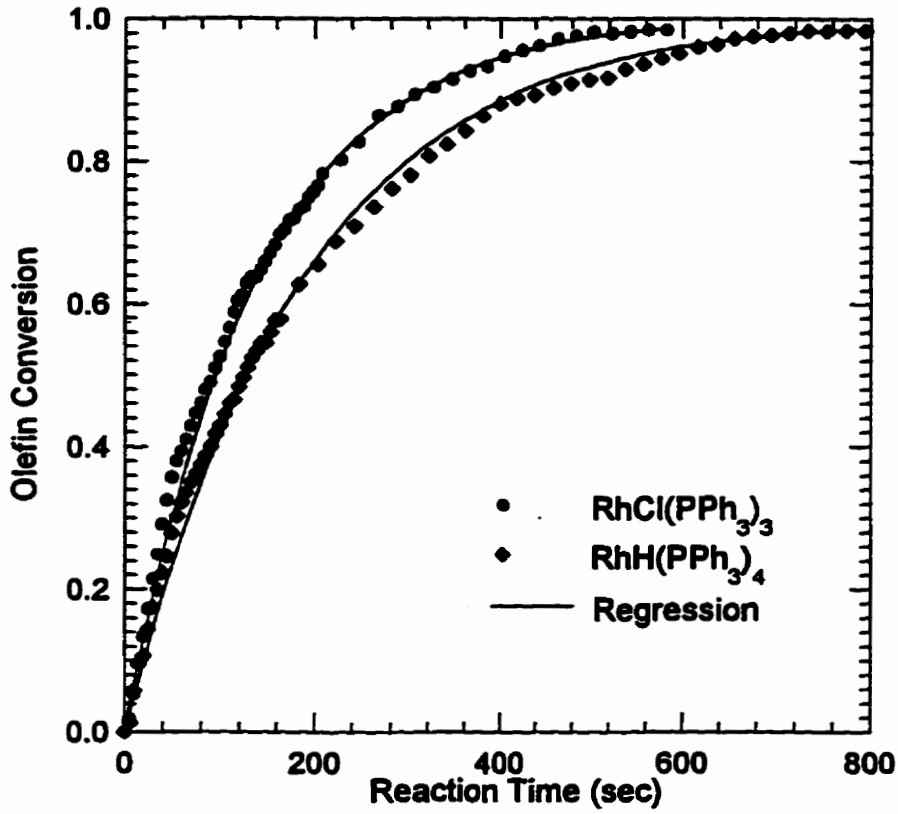

Figure 3.3: Representative NBR conversion profiles; $[Rh]_T$=80 μM, [RCN]=172 mM, $[PPh_3]$=4.0 mM, PH_2=23.7 bar, T=433.2 K

nitrile hydrogenation, well below the detection threshold of spectroscopic analysis, can lead to levels of polymer crosslinking that adversely effect the processability of the product (McManus and Rempel, 1995). Therefore, an alternative means of assessing crosslinking is required to measure the overall impact of the hydrogenation process. This subject is dealt with in detail in Chapter 6.

3.2.3 Kinetics of NBR Hydrogenation

The conversion profiles presented in Figure 3.3, along with all those observed in this study, adhere to the first-order rate model represented by Equation 3.3.

$$-\frac{d[C=C]}{dt} = k' [C=C] \qquad 3.3$$

Regression estimates of k', the apparent first-order rate constant, may be used in place of the raw data to represent the hydrogenation rate. The functional relationship between the rate of hydrogenation and concentrations of H_2, Rh, C≡N and PPh_3 as well as temperature has been explored by measuring the response of k' to specific combinations of factor levels (Section 3.1.4). The rate constants derived from these experiments are tabulated in Appendix II, Tables AII-A and AII-B for $RhCl(PPh_3)_3$ and $RhH(PPh_3)_4$, respectively.

An experiment of Bhattacharjee et al. (1991) has been reproduced in this work for comparative purposes. Under identical reaction conditions ([Rh]=200μM, [PPh_3]=7.6 mM, [RCN]=150 mM, P_{H2}=54.5 bar and T=100°C) the rate constant derived using the techniques detailed in Section 3.1.3 was nearly 10 times that reported by Bhattacharjee et al. (1991). While only 1.3 hours were required to produce a fully saturated product, the cited work reports an 11 hour reaction time. Operating at 100°C and 60 atm, Oppelt et al. (1976) achieved 100% conversion within 4.5 hours. Barring any misquotation of the amount of catalyst used by Bhattacharjee et al. (1991), it is possible that the addition of $RhCl(PPh_3)_3$ to the polymer solution prior to the purging of oxygen could have had a deleterious effect on the catalytic activity (Baird et al., 1966; Strohmeier, 1977).

The results obtained from the univariate series of experiments are illustrated in Figures 3.4 to 3.8. In each case the response of $RhH(PPh_3)_4$ paralleled that of $RhCl(PPh_3)_3$, though at a lesser rate. Figure 3.4 demonstrates the linear response of k' with changes in the concentration of catalyst precursor, $[Rh]_T$. Note that each experiment of this series was carried out under a constant Rh:PPh_3 ratio to safeguard the stability of the catalyst. Despite varying [PPh_3], a first order dependence holds throughout the data set. With respect to [H_2], both systems exhibit a first to zero order dependence as the system pressure is increased (Figure 3.5). The conversion of P_{H2} to [H_2] was accomplished by direct measurement of the solubility of hydrogen in chlorobenzene/NBR solutions (Chapter 2).

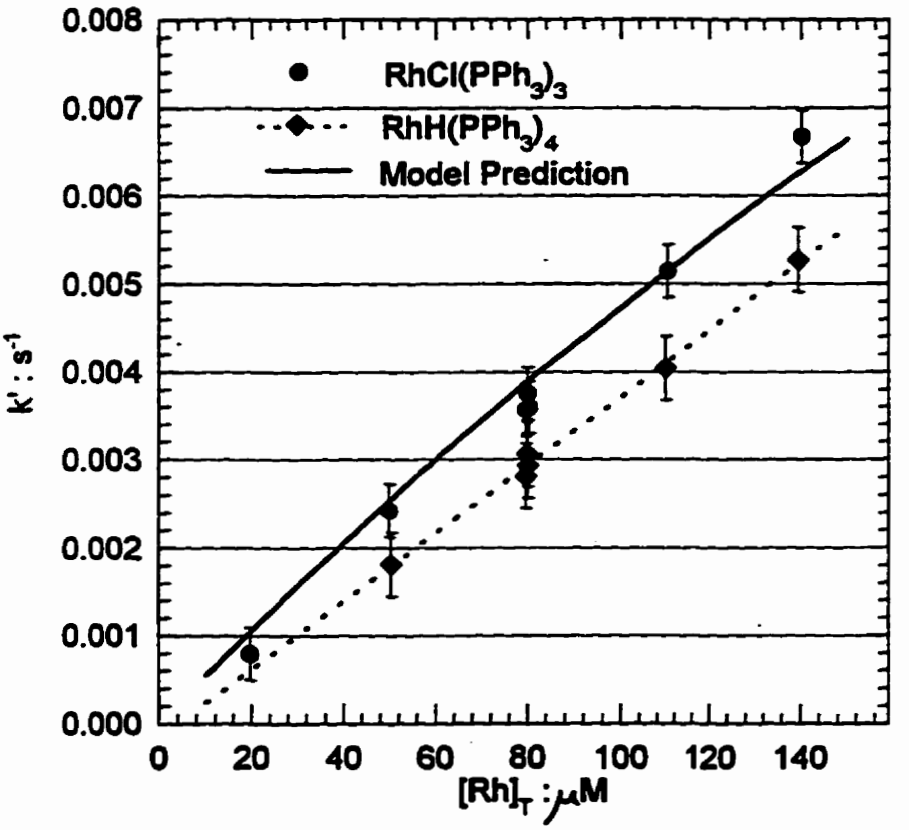

Figure 3.4: Influence of catalyst loading on the hydrogenation rate; [RCN]=172 mM, [PPh_3]=4.0 mM, P_{H2}=23.7 bar, T=418.2 K

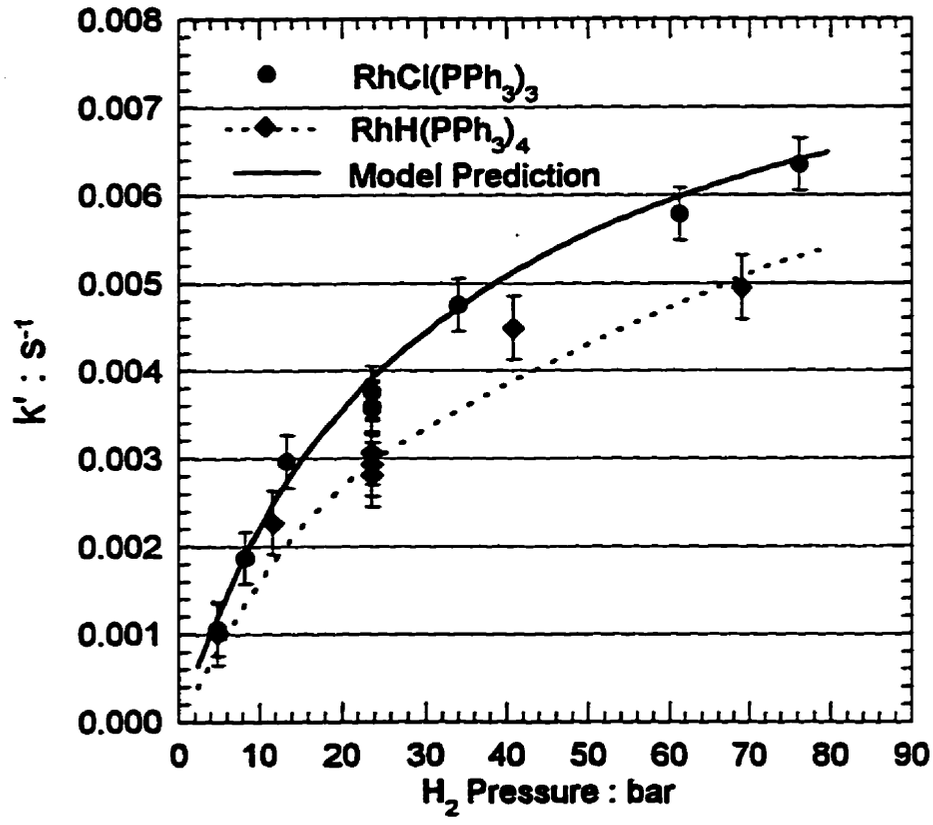

Figure 3.5: Influence of hydrogen pressure on the hydrogenation rate; $[Rh]_T$=80 μM, [RCN]=172 mM, $[PPh_3]$=4.0 mM; T=418.2 K

The influence of PPh_3 dissociation equilibria on the hydrogenation rate has been determined by varying the amount of added phosphine from a PPh_3:$[Rh]_T$ ratio of 10:1 to a ratio of 70:1. The data presented in Figure 3.6 suggest that at the reaction conditions employed, free PPh_3 has a marginal effect on hydrogenation activity. It is therefore likely that PPh_3 dissociation equilibria favour the dissociated products to a greater extent than seen at temperatures near ambient. Our experience has shown that although both catalysts are capable of quantitative hydrogenation, their behaviour becomes increasingly erratic below a $[PPh_3]$:$[Rh]_T$ ratio less than 20:1.

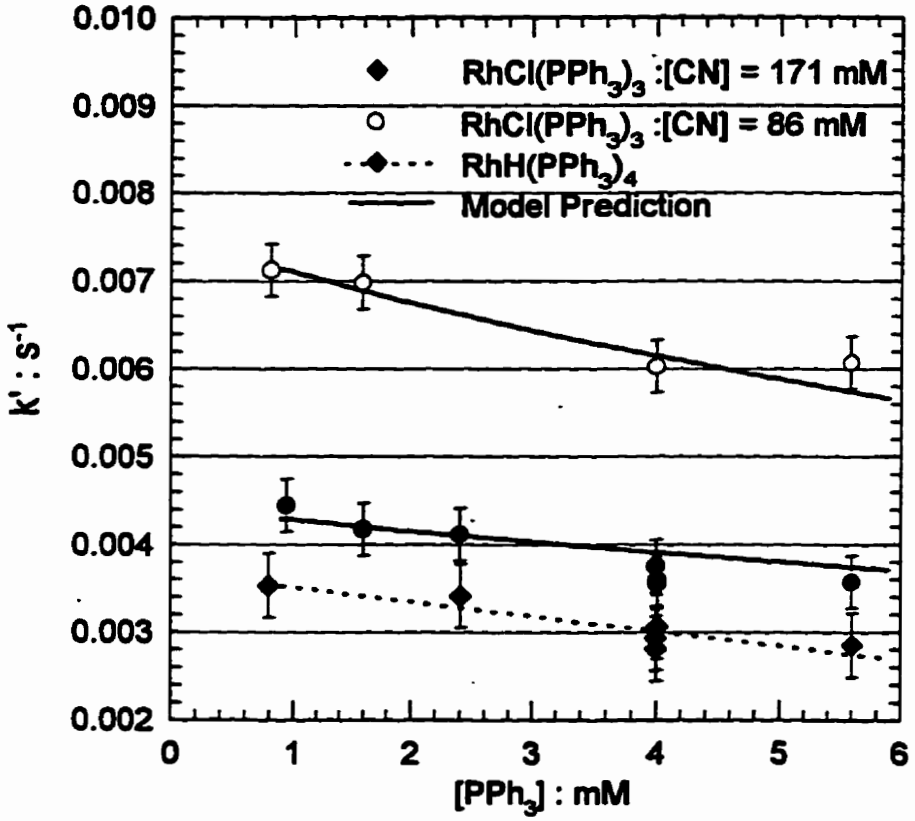

Figure 3.6: Influence of added PPh_3 on the hydrogenation rate; $[Rh]_T$=80 μM, P_{H2}=23.7 bar, T=418.2 K

The inhibiting effect of nitrile on the olefin hydrogenation rate has been identified by Mohammadi and Rempel (1987). Figure 3.7 illustrates the effect of varying the polymer loading. That the coordination of nitrile to a catalytic intermediate is responsible for the

reduction in activity is supported by an absence of the effect for styrene-butadiene rubber (Table AII-A). A similar effect is reported by Schrock and Osborn (1976) who identified a strong coordination of acetonitrile as responsible for lessening the hydrogenation activity of a cationic rhodium complex. At the temperatures and pressures used in this work, identifying the influential modes of nitrile coordination is difficult.

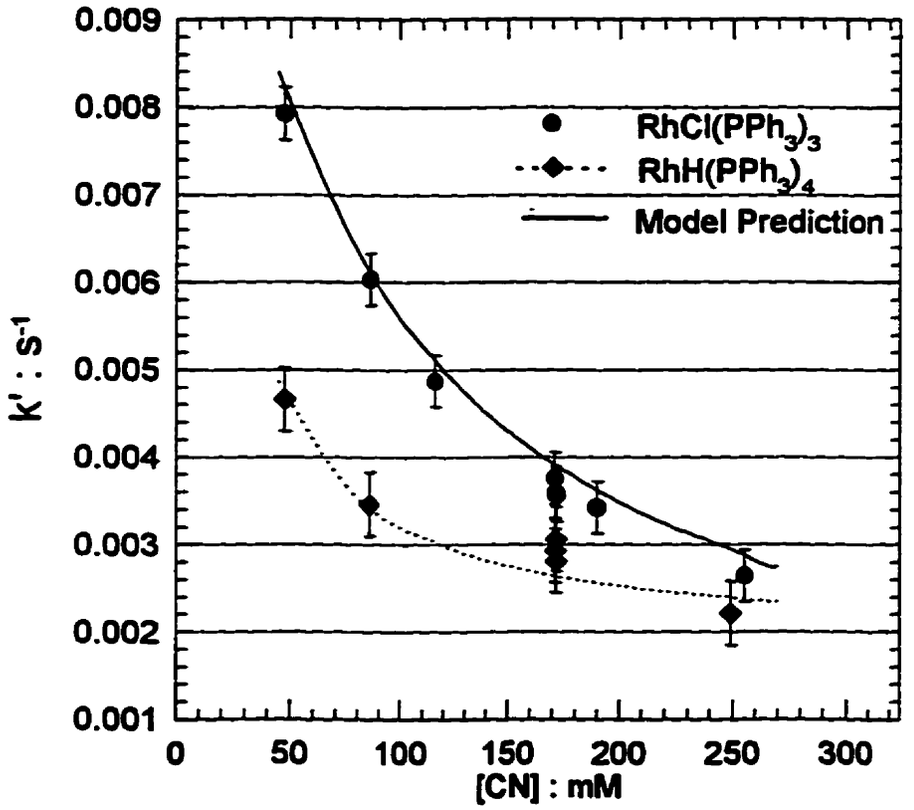

Figure 3.7: Influence of nitrile unsaturation on the hydrogenation rate; $[Rh]_T$=80 μM, $[PPh_3]$=4.0 mM, P_{H2}=23.7 bar, T=418.2 K

The Arrhenius plot provided in Figure 3.8 illustrates the influence of temperature on the rate of hydrogenation. Over the range of 130-170°C for $RhCl(PPh_3)_3$ and 115-160°C for $RhH(PPh_3)_4$, a linear response is observed, from which an apparent activation energy of 73.5 kJ/mole for the former and 57.4 kJ/mole for $RhH(PPh_3)_4$ is derived. These estimates provide further evidence that the experiments were free of mass transfer limitation. For $RhCl(PPh_3)_3$, Bhattacharjee et al. (1991) report a value of 22 kJ/mole without providing

sufficient data to rationalize the discrepancy. Nevertheless, the values derived from this study are more consistent with homogeneous catalytic processes.

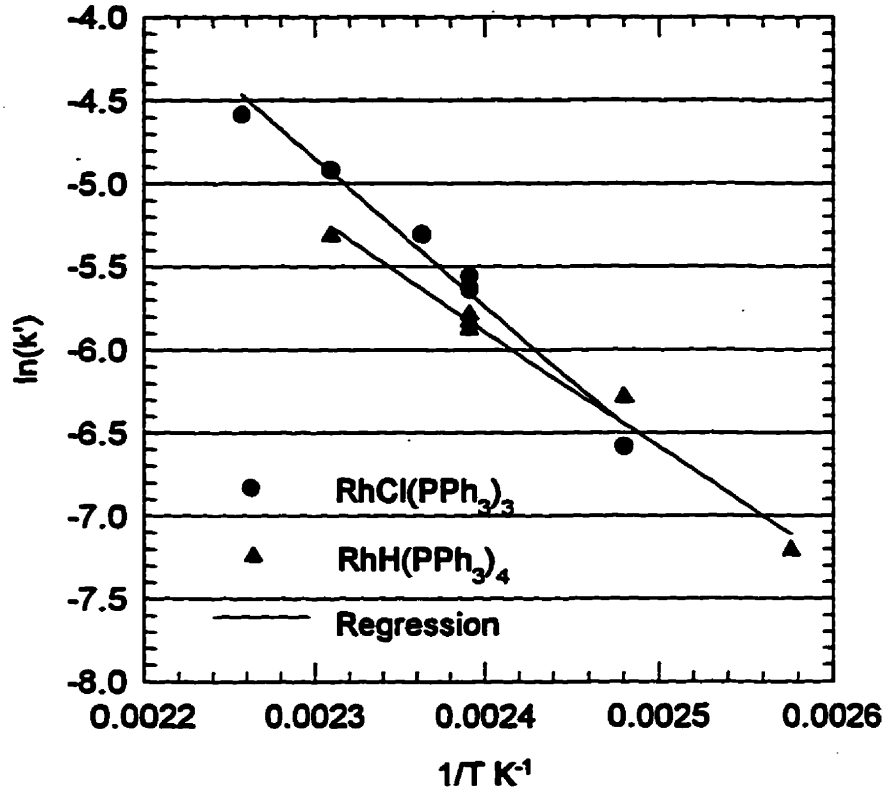

Figure 3.8: Arrhenius plot for the hydrogenation of NBR;
$[Rh]_T$=80 μM, [RCN]=172 mM, $[PPh_3]$=4.0 mM, P_{H2}=23.7 bar

A thorough kinetic study improves our knowledge not only of how each factor effects k' alone (as probed by the univariate experiments) but whether or not factors act in combination. The 2^3 factorial component of the experimental design (experiments 31-40, Table AII-A) provides a means of assessing the significance of such joint factor interactions. The results of an analysis of variance listed in Table 3.1 prove that in addition to strong main group influences ($[H_2]$, [RCN] and $[PPh_3]$), a highly significant $[H_2]$*[RCN] interaction operates within the kinetic mechanism. $[H_2]$*$[PPh_3]$ and [RCN]*$[PPh_3]$ interactions are somewhat weaker, as may be expected based on the marginal influence of PPh_3 at these reaction conditions. The existence of a three factor interaction is not supported.

Table 3.1: 2^3 Factorial Design; Analysis of Variance

Source	Sum-of Squares	DF	Mean Square	F-Ratio	P
$[H_2]$	8.30E-06	1	8.30E-06	1476.	0.0007
[RCN]	3.45E-06	1	3.44E-06	611.0	0.002
$[PPh_3]$	3.37E-07	1	3.37E-07	59.8	0.016
$[H_2]$*[RCN]	2.43E-07	1	2.43E-07	43.2	0.022
$[H_2]$*$[PPh_3]$	4.09E-08	1	4.09E-08	7.27	0.114
[RCN]*$[PPh_3]$	2.01E-08	1	2.01E-08	3.57	0.199
$[H_2]$*[RCN]*$[PPh_3]$	1.60E-08	1	1.60E-08	2.85	0.233
Error	1.12E-08	8	5.62E-09		

3.2.4 Catalytic Pathways of the $RhCl(PPh_3)_3$ and $RhH(PPh_3)_4$ Systems

The catalytic chemistry of Rh(I) phosphine complexes has been extensively researched, resulting in a greater understanding of trace intermediates that bring about the observed kinetic behaviour (Jardine, 1981; James, 1973). While an extrapolation of this knowledge to severe reaction conditions may not be straightforward, it is proposed that strong parallels exist between the chemistry underlying this work and that documented at mild reaction conditions. Figure 3.9 illustrates a catalytic mechanism that is consistent both with the kinetic data and our understanding of the coordination chemistry of $RhCl(PPh_3)_3$ in solution.

That $RhCl(PPh_3)_3$ oxidatively adds molecular hydrogen to form the six coordinate dihydride according to Equation 3.4 is well established (Halpern, 1973).

$$RhCl(PPh_3)_3 + H_2 \overset{K}{\rightleftharpoons} RhClH_2(PPh_3)_3 \qquad 3.4$$

Mohammadi and Rempel (1987) provide evidence that at 65°C and under 1 bar of H_2 the reaction is quantitative towards formation of the dihydride. The comparative ease of hydrogen activation relative to the addition of the bulky olefin is believed to favour the "hydride pathway" shown in the catalytic mechanism.

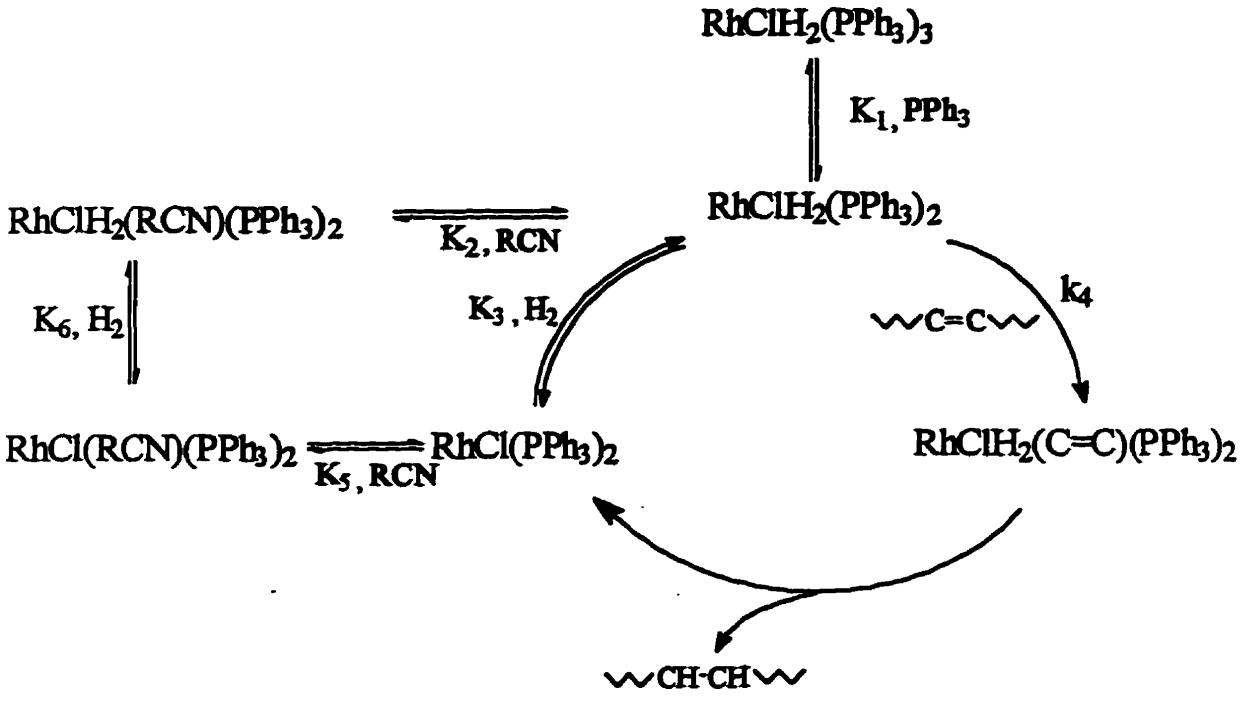

Figure 3.9: Proposed mechanism for the $RhCl(PPh_3)_3$/NBR system

The dissociation of phosphine from $RhClH_2(PPh_3)_3$ according to Equation 3.5, while not appreciable at room temperature, is likely to be encouraged by the temperatures used in this study.

$$RhClH_2(PPh_3)_3 \overset{K_1}{\rightleftharpoons} RhClH_2(PPh_3)_2 + PPh_3 \qquad 3.5$$

As the coordination of olefin to $RhClH_2(PPh_3)_2$ is not facile, a direct assignment of the rate determining step as the insertion of olefin into the Rh-H bond is not warranted. It is possible that the initial coordination of the substrate is rate limiting in this case. Therefore, we have chosen to represent the rate determining step with Equation 3.6.

$$RhClH_2(PPh_3)_2 + C{=}C \overset{k_4}{\rightarrow} RhClH_2(C{=}C)(PPh_3)_2 \qquad 3.6$$

Given that coordinatively unsaturated complexes are often presumed to associate with solvent, that a potential ligand such as nitrile may inhibit the hydrogenation cycle is not surprising. $[Rh(CO)(MeCN)(PPh_3)_2]^+ClO_4^-$ has been prepared (Booth et al., 1976) and $[Rh(PPh_3)_3(MeCN)][BF_4]$ has been analyzed crystallographically by Pimblett et al. (1985). As stated earlier, Schrock and Osborn (1976) report that the use of acetonitrile as a solvent has a deleterious effect on the hydrogenation activity of $[Rh(diene)(PPh_3)_2]^+A^-$. To date, a detailed study of the propensity of nitrile to associate with complexes derived from $RhCl(PPh_3)_3$ is lacking, although Ohtani et al. (1979) have presented some spectrophotometric data on the system.

As nitrile likely coordinates by σ-donation of its lone pair, it experiences little of the steric hinderance experienced by the olefin resident in NBR. It may therefore compete effectively with olefin for coordination to unsaturated complexes. Equations 3.7 and 3.8 illustrate two possible modes of nitrile coordination that could be capable of bringing about the observed inhibitory behaviour.

$$RhClH_2(PPh_3)_2 + RC{\equiv}N \overset{K_2}{\rightleftharpoons} RhClH_2(RC{\equiv}N)(PPh_3)_2 \qquad 3.7$$

$$RhCl(PPh_3)_2 + RC{\equiv}N \overset{K_5}{\rightleftharpoons} RhCl(RC{\equiv}N)(PPh_3)_2 \qquad 3.8$$

Having few means to probe the nitrile coordination chemistry at severe reaction conditions, the importance of these reactions may only be assessed using the kinetic data. Statistical measures of the agreement between the observed data and derived catalytic mechanisms, while not proving the validity of a model, may aid in the discrimination between alternatives. When applied to a rate expression based solely on Equation 3.7, an analysis of variance and residuals proved this simple model to be ill-equipped to account for the degree of nitrile inhibition. While an expression founded on Equation 3.8 alone proved to be satisfactory, the propensity of $RhCl(RCN)(PPh_3)_2$ to oxidatively add H_2 (Ohtani et al., 1979) would suggest an overall mechanism as illustrated in Figure 3.9.

Provided that Equation 3.6 adequately represents the rate determining step, Equation 3.3 may be written in the form of Equation 3.9.

$$-\frac{d[C=C]}{dt} = k_4\,[RhClH_2(PPh_3)_2]\,[C=C] \qquad 3.9$$

The conversion of $[RhClH_2(PPh_3)_2]$ to the total amount of rhodium $[Rh]_T$ used in each experiment is accomplished using a material balance (Equation 3.10).

$$\begin{aligned}[Rh]_T = {} & [RhClH_2(PPh_3)_3] + [RhClH_2(PPh_3)_2] \\ & + [RhCl(PPh_3)_2] + [RhCl(RC\equiv N)(PPh_3)_2] \\ & + [RhClH_2(RC\equiv N)(PPh_3)_2]\end{aligned} \qquad 3.10$$

Applying the equilibrium relations defined in Figure 3.9, the concentration of $RhClH_2(PPh_3)_2$ may be substituted into Equation 3.9 to provide the functional relationship between k' and the process factors studied (Equation 3.11).

$$k' = \frac{k_4K_1K_3[Rh]_T[H_2]}{K_1+K_1K_3[H_2]+K_3[H_2][PPh_3]+K_1K_5[RC\equiv N]+K_1K_2K_3[H_2][RC\equiv N]} \qquad 3.11$$

The results of an analysis of variance listed in Table 3.2 suggest that the derived rate expression complies with the observed hydrogenation kinetics over the range of process conditions studied. Although this result is insufficient to definitively certify the model, it indicates that its fit is superior to all other options explored.

Table 3.2: Model analysis of variance results

Source	Sum-of-Squares	DF	Mean-Square
Regression	7.092E-04	5	1.418E-04
Residual	1.512E-06	30	5.042E-08
Total	7.107E-04	35	
Corrected	9.588E-05	34	

Regression estimates for the parameters derived from equation 3.11 are provided in Table 3.3 along with their associated error estimates. Note that K_6 is not independent and may be derived from the other model parameters. An interpretation of these estimates must be done

with extreme caution, given the high degree of parameter correlation which accompanies models of this form. The residual plot shown in Figure 3.10 demonstrates none of the systematic patterns produced by other possible kinetic pathways. The model predictions are plotted in Figures 3.4 to 3.7 along with the raw experimental data.

Table 3.3: Model parameter estimates

Parameter	Estimate	A.S.E.	Lower <95%> Upper	
k_4,(mMs)$^{-1}$	1.19	0.17	0.85	1.53
K_1, mM	1.44	0.38	0.67	2.21
K_2, mM^{-1}	3.98E-02	5.94E-03	2.76E-02	5.19E-02
K_3, mM^{-1}	3.41E-03	2.06E-04	2.99E-03	3.83E-03
K_5, mM^{-1}	2.71E-02	3.20E-03	8.12E-03	4.61E-02
K_6, mM^{-1}	6.28E-03	3.78E-04	5.51E-03	7.05E-03

Compared to $RhCl(PPh_3)_3$, the $RhH(PPh_3)_4$ system has received relatively little attention. The results of this investigation would suggest that the underlying chemistry of the two systems is similar. Indeed, a catalytic mechanism derived using $RhH_3(PPh_3)_2$ as the active species is equipped to account for the kinetic data. However, ascertaining whether coordination of hydrogen precedes or follows the addition of olefin is less straightforward than for $RhCl(PPh_3)_3$, while the use of model discrimination techniques is limited by the similarity of rate expressions derived from either assumption. Therefore, given the complexity of the system, an assignment of a reaction mechanism is not warranted based on this kinetic data alone. Research directed at identifying important reaction intermediates is required before such a process may be unequivocally assigned.

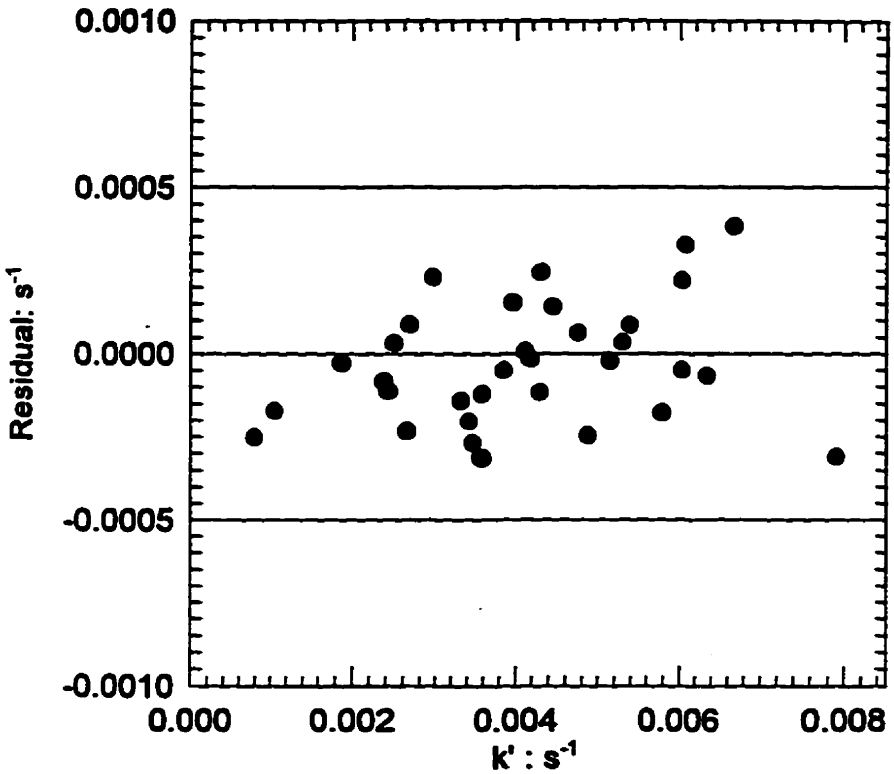

Figure 3.10: Residual plot of (k'_{actual} - k'_{model}) versus k'

Chapter 4

Spectroscopic Characterization of $OsHCl(CO)(L)(PR_3)_2$
1a: R=Cy, L=vacant; **1b**: R=*i*Pr, L=vacant
2a: R=Cy, L=O_2; **2b**: R=*i*Pr, L=O_2

Kinetic investigations define the overall response of a reactive system to variations in operating conditions. For elementary reactions, the interpretation of rate data in terms of a reaction mechanism may be straightforward. This is not the case for catalytic hydrogenations. For these reactions, the derivation of a reaction pathway requires a greater understanding of the chemistry which underlies the observed kinetics. A knowledge of the structure and reactivity of the complexes present during hydrogenation increases the likelihood that a mechanism will not only fit the experimental data, but better reflect the true nature of the process. To support the kinetic study of the osmium technology (Chapter 5), the reactivity of **1** and **2** have been characterized to the extent possible by nuclear magnetic resonance (NMR) spectroscopy.

Fortunately, previous research has resolved many of the structure and reactivity issues of relevance to NBR hydrogenation (See Chapter 1.1). The dynamics of H_2 coordination to **1b** have been thoroughly characterized by Bakhmutov et al. (1996) while the propensity of **1a,b** to coordinate with O_2 and small olefins has been identified by Moers et al. (1974) and Esteruelas and Werner (1986). Unexplored elements which concern NBR hydrogenation include the fate of **2a,b** when exposed to hydrogenation conditions and the capacity of the nitrile and olefin resident in NBR to coordinate with **1a,b**. More fundamental considerations centre on the lability of bound phosphine and CO at the extreme conditions employed for the kinetic experiments.

In this chapter, the NMR studies that have enhanced our knowledge of the forementioned reactions are detailed. In most cases, data on both **1a** and **1b** have been acquired, although quantitative studies have centred on the PCy_3 system due to its greater commercial potential. To ensure that the structure and distribution of the reaction products observed in

the NMR work reflected those encountered during the kinetic studies, temperatures exceeding 130°C and pressures up to 52 bar were employed. These *in situ* measurements were made possible by the loan of a high-pressure, sapphire NMR tube by Professor T.B. Marder of the Department of Chemistry, University of Waterloo.

4.1 Experimental

4.1.1 Materials.

PCy_3, $PiPr_3$, PCp_3 and $PtBu_3$ were used as received from Strem Chemicals Inc. while $PMetBu_2$ was synthesized by Dr. N.T. McManus of our laboratory. A ^{31}P NMR spectrum of this product was consistent with $PMetBu_2$. Both **1a** and **1b** were synthesized by refluxing $OsCl_3*3H_2O$ (Strem Chemicals Inc.) with the required phosphine in methoxyethanol and ethanol respectively, in accordance with the method of Esteruelas and Werner (1986). **2a,b** were prepared by exposing a suspension of **1a,b** in hexane to an atmosphere of O_2 as detailed by Esteruelas et al. (1989).

Hydrogen gas of 99.99% purity was obtained from Linde-Union Carbide Inc. Samples of NBR were those used throughout the kinetic studies (Krynac 38.50 from Bayer Rubber Inc). Low molecular weight polybutadiene (Mn=1000, *cis/trans/vinyl* = 30/30/40) was purchased from Scientific Polymer Products. Monochlorobenzene from Fisher Chemicals Ltd. was used without purification as was the d^6-toluene purchased from Cambridge Isotopes Ltd.

4.1.2 High-Pressure Sample Preparation and Analysis

A detailed description of the sapphire NMR apparatus used in this work has been published by Roe (1985). It consisted of a 5 mm O.D. sapphire tube attached by a thermoset resin to a titanium valve assembly. As this was the first application for the apparatus at the University of Waterloo, the assembly underwent rigorous hydrostatic testing. While full of water, it successfully withstood several heating/cooling cycles between 25°C and 140°C under an N_2 pressure of 700 psi. Roe (1985) recommended a maximum operating pressure

of 2000 psi for an apparatus of this type. This testing procedure was repeated periodically to confirm the mechanical integrity of the apparatus.

Other procedures were routinely followed to ensure the safety of both the operator and the NMR instrument. When under pressure, the apparatus was transported within a polymethylmethacrylate protective shield. Rather than using the air-lift mechanism, the sample was lowered into the spectrometer magnet using a string attached to the valve assembly. Its correct location in the probe was ensured by using a custom-made Kel-F spinner. Under no conditions was an attempt made to spin the sapphire apparatus.

Solutions for NMR analysis were prepared and handled either in a dry-box or using standard schlenk techniques. High pressure samples were prepared within a dry-box environment by charging the sapphire tube with the test solution and fixing the titanium valve. The sealed assembly was removed from the dry-box and inserted into its protective shield for pressurization. To replace the N_2 atmosphere, 24 bar of H_2 were charged to the tube and vented for a total of ten cycles. The two phases were mixed by repeatedly inverting the shield that housed the pressurized tube. The desired system pressure was established, the titanium valve sealed, and the system checked for leaks.

^{31}P and ^{1}H NMR spectra were recorded on a Bruker AC-200 MHz spectrometer while ^{13}C NMR measurements were acquired on an AC-300 MHz instrument. ^{1}H NMR chemical shifts were referenced to TMS using the residual methyl protons of toluene-d^8 at δ 2.09 or, in the case of benzene-d^6, to the resonance at 7.15 ppm. ^{13}C NMR spectra were referenced to TMS using the aromatic carbon resonance at δ 137.5. ^{31}P signals were referenced using 86% H_3PO_4 as a standard. Temperatures above ambient were calibrated against an 80% solution of ethylene glycol in DMSO-d^6 while those below 25°C were measured using a 4% solution of methanol in CD_3OD.

4.2 Results and Discussion

^1H, ^{31}P NMR spectroscopic data and prevalent IR stretching frequencies of all the complexes studied are listed in Table AIII of Appendix III. Owing to the greater solubility of $P\textit{i}Pr_3$ complexes, the signal-to-noise ratios of their NMR spectra are generally superior to those acquired for their PCy_3 analogues. Therefore, while both systems have been characterized, the spectra used to illustrate the discussions are those of the $P\textit{i}Pr_3$ system.

Fate of the dioxygen adducts 2a,b under hydrogenation conditions

Traces of O_2 will displace olefin or molecular hydrogen from **1a,b** to form the corresponding dioxygen adducts **2a,b** (Esteruelas et al., 1988; Moers et al., 1974). The remarkable stability of **2a,b** and their virtually inevitable presence suggests they be used directly in kinetic studies. Andriollo et al. (1989) have proven the efficacy of **2b** for the hydrogenation of phenylacetylene. However, they observed an induction period at 23°C after which the hydrogenation rate was essentially identical to that of **1b**. They attributed the effect to a slow displacement of O_2 by the substrate. To clarify the role of **2a,b** as catalyst precursors, their fate when exposed to extreme hydrogenation conditions has been monitored by ^{31}P NMR. The results are illustrated in Figure 4.1.

Under N_2 at 23°C, a $^{31}P\{^1H\}$ spectrum of **2b** yields a singlet at 23.1 ppm in toluene. At 65°C and under 24 bar of H_2, evidence for **2b** is lost while the characteristic singlet of $OsH(H_2)Cl(CO)(P\textit{i}Pr_3)_2$ (**3b**) at 36 ppm evolves. The process has also been observed for the **2a-3a** system by ^1H NMR. Note also that refluxing **2a** in methoxyethanol with an excess of PCy_3 regenerates **1a** in good yields. This suggests the transformation of **2a,b** to **3a,b** proceeds by a dissociation of O_2 followed by dihydrogen coordination, rather than by a direct displacement reaction.

Over time, a solution of **2a,b** maintained at 65°C generated phosphine oxide at the expense of the **1a,b** product. Therefore, the presence of dissolved oxygen is expected to have a deleterious effect on catalytic activity. However, the release of oxygen from **2a,b** is

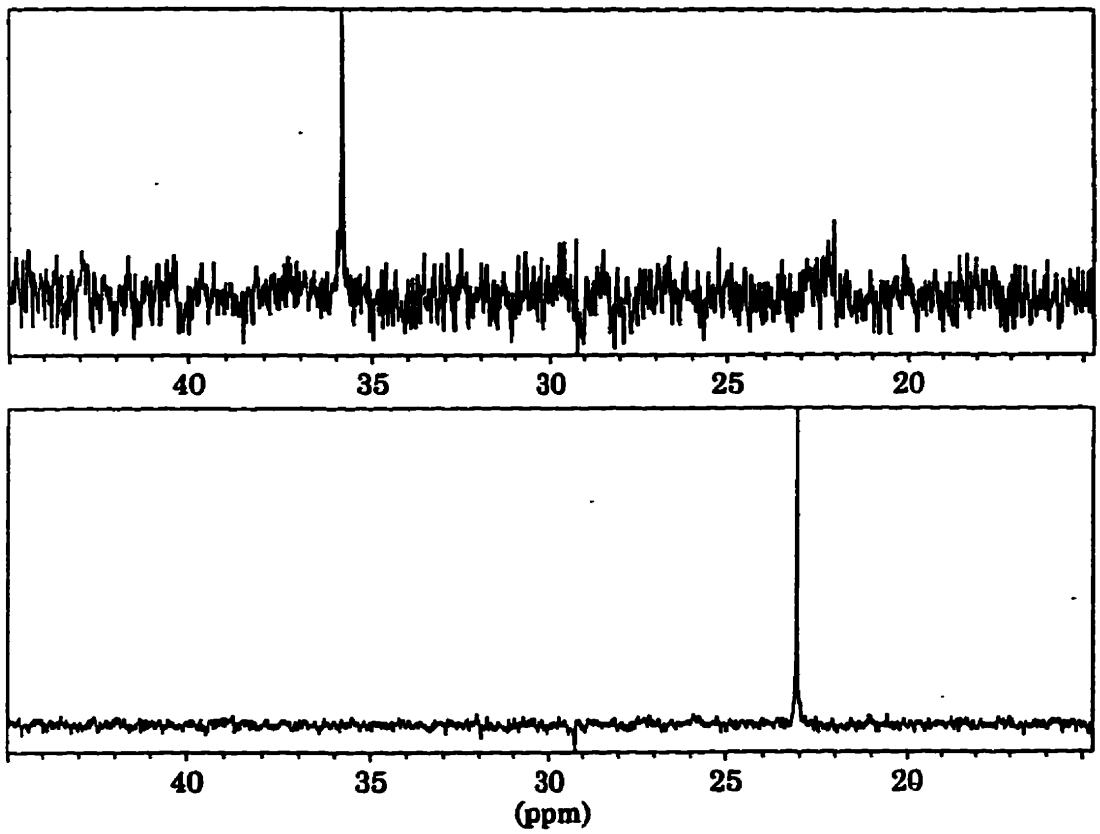

Figure 4.1: ^{31}P NMR spectra illustrating the transformation of **2b** to **3b**; P_{H2}=24 bar, T=65°C

unlikely to be influential if μM concentrations of catalyst are used. Under these conditions, the partial pressure of released O_2 from **2a** is sufficiently small that its liquid phase concentration is insignificant. It may therefore be concluded that the catalytic behaviour observed from **2a,b** should be identical to that of their precursors **1a,b**.

Nitrile coordination mode and equilibrium

The ability of nitrile to diminish catalytic activity has been reported for a number of efficient hydrogenation systems. Mohammadi and Rempel (1987) have observed the inhibition of $RhCl(PPh_3)_3$ by the nitrile within NBR as has Martin et al. (1991) for the $RuHCl(CO)(PCy_3)_2$ system. In a study of $OsH_2(dcpe)_2$, Farnetti et al. (1992) attributed the relatively low rate of PhHC=CH-CN hydrogenation to a competitive coordination of nitrile

to the metal centre. As there are no published reports of such a reaction for **1a,b**, there is a need to establish the mode and significance of nitrile coordination for the NBR system.

A room temperature ^{31}P $\{^1H\}$ spectrum of **1a** contains a singlet at 36.7 ppm while **1b** exhibits a broad resonance at 47.9 ppm. The addition of 1 equivalent of benzonitrile produces a colour change from brown to pale yellow as sharp new singlets appear at 14.5 ppm and 24.3 ppm for **1a,b** respectively. These correspond with spectra of the isolated products $OsHCl(CO)(R'CN)(PR_3)_2$ (**6a** R=Cy; **6b** R=*i*Pr; R'=Ph). ^1H NMR spectra of **6a,b** show the hydride resonance shifted significantly downfield from the starting complexes, suggesting it is *trans* disposed to PhCN (Figure 4.2). Precedents for nitrile complexes of this type are abundant. Gilbert and Wilkinson (1969) have prepared $RuCl_2(RCN)_2(PPh_3)_2$ by heating under reflux $RuCl_2(PPh_3)_3$ with benzonitrile. A recent report by Schlaf et al. (1996) describes the reactivity of *trans*-$[Os(\eta^2\text{-}H_2)(CH_3CN)(dppe)_2](BF_4)_2$. In both cases σ-donation from the nitrogen lone pair is the accepted mode of nitrile coordination.

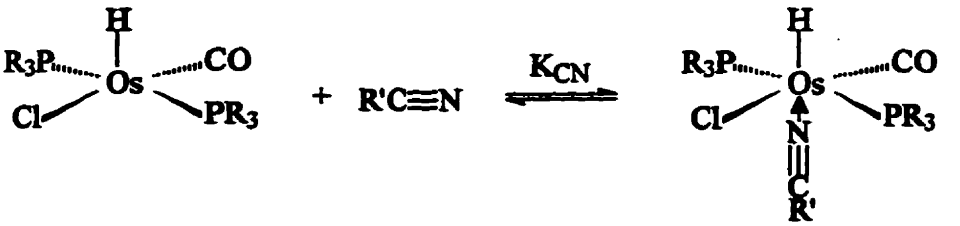

Figure 4.2: Nitrile coordination equilibrium to form **6a,b**

Having characterized the nitrile complexes **6a,b**, it remains to be evaluated whether this association can be influential at the conditions used for hydrogenation. Figure 4.3 illustrates a variable temperature, ^{31}P NMR study of the interaction of **1b** with 1.25 equivalents of benzonitrile at high pressures of H_2. At -4°C and 52 bar, two singlets corresponding to **3b** and **6b** are resolved. Based on the intensity of the signals, the coordination of nitrile is favoured at this temperature. Reducing the system pressure by half produces the expected shift of the equilibrium towards **6b**.

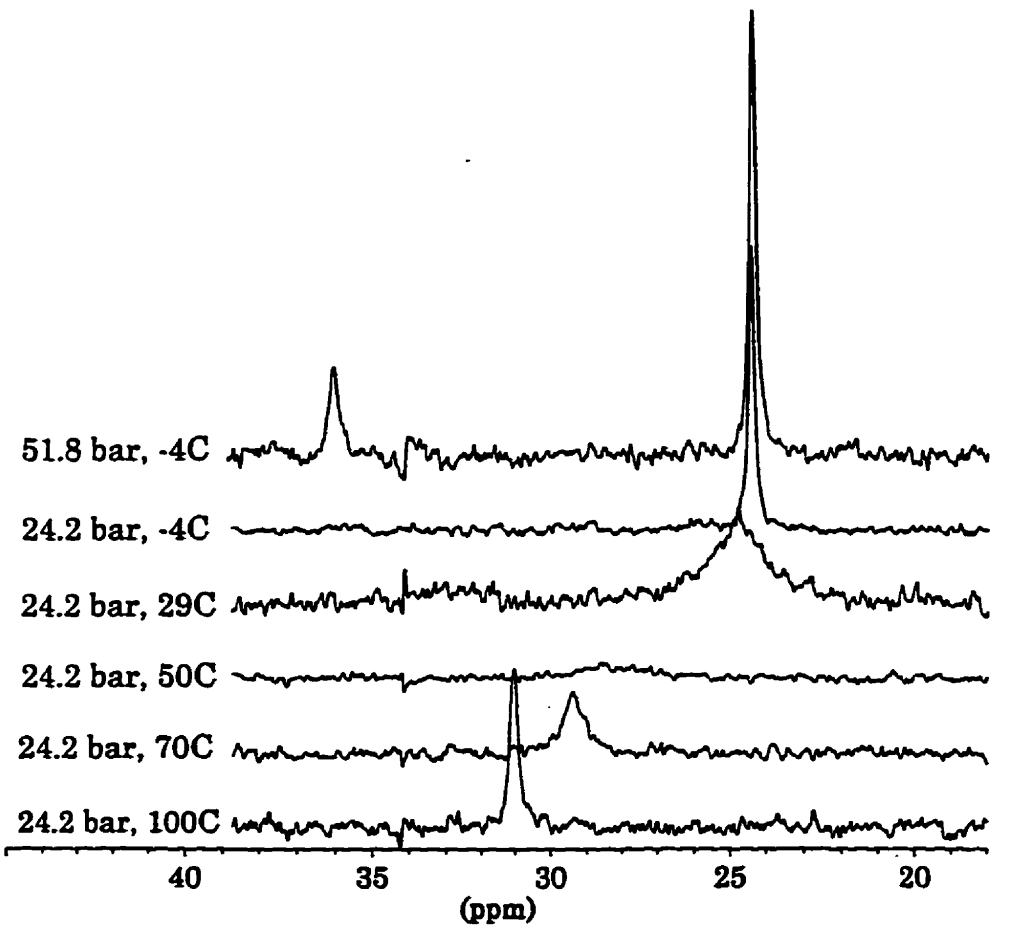

Figure 4.3: Variable temperature ^{31}P $\{^1H\}$ study of the **3b-6b** equilibrium; 1.25 eq. PhCN

Warming the system to 29°C produces two exchange broadened signals, one at approximately 32.5 ppm and a more abundant resonance at 24.5 ppm. These coalesce at 50°C as the system reaches the fast exchange limit of the NMR timescale. At 70°C and beyond, the chemical shift of the exchange averaged Os(η^2-H_2)/Os(RCN) signal is evidence of an equitable distribution between the two complexes despite the higher concentration of H_2 relative to RCN. This clearly demonstrates the potential of nitrile to compete with H_2 for the metal centre at conditions approaching those used for NBR hydrogenation. The shift in the distribution of **3b** and **6b** suggests operating at elevated temperatures to minimize nitrile inhibition.

With the mode and significance of benzonitrile coordination to **1a,b** established, it is a relatively simple matter to quantify the **1a-6a** exchange process for hydrogenated NBR (Figure 4.2). In the fast exchange domain (above 70°C), the position of the exchanged average signal relative to the chemical shifts of **1a** and **6a** reflect their relative abundance in solution. It follows that

$$\frac{[6a]}{[1a]} = \frac{\delta_{avg}-\delta_{1a}}{\delta_{6a}-\delta_{avg}} = X .$$

Mass balances on the total amount of osmium and nitrile yield:

$$[Os]_t = [1a]+[6a]$$

$$[RCN]_o = [6a]+[RCN].$$

Therefore, given the initial concentrations of **1a** and nitrile charged to the system, the equilibrium constant K_{cn} may be derived as follows:

$$K_{cn} = \frac{X}{[RCN]_o - \frac{X}{1+X}[Os]_t}$$

The ^{31}P chemical shifts of **1a** and **6a** measured as a function of temperature are listed in Table 4.1. Although **6a** undergoes rapid ligand exchange, estimates of δ_{6a} were made possible by using a large excess of nitrile to saturate the system. By pushing the equilibrium far to the right (Figure 4.2), the observed signal effectively represented that of **6a**. Linear regressions of δ_{1a} and δ_{6a} versus temperature were used to derive estimates for the temperatures employed in the exchange analysis.

Also presented in Table 4.1 are the measured chemical shifts (δ_{avg}) for the exchange averaged **1a** system containing 0.99 equivalents of the nitrile residing within hydrogenated Krynac 38.50. The equilibrium constants calculated at each temperature are plotted in Figure 4.4.

Table 4.1: **1a - 6a Equilibrium study by ^{31}P {^{1}H} NMR Hydrogenated Krynac 38.50 in chlorobenzene**

Temp.	δ_{1a}	δ_{6a}*	Temp	δ_{avg}+	X	K_{CN}, M^{-1}
23°C	37.17	13.86	77.5°C	18.50	4.595	3050
50°C	37.37	---	93.5°C	21.04	2.560	914
70°C	37.55	14.28	115°C	25.84	1.085	204
110°C	37.78	14.68	133°C	29.76	0.503	65.6
132°C	37.95	15.03				

* [1a] = 0.0161 M; [RCN] = 0.645 M.
+ [1a] = 0.0120 M; [RCN] = 0.0119 M.

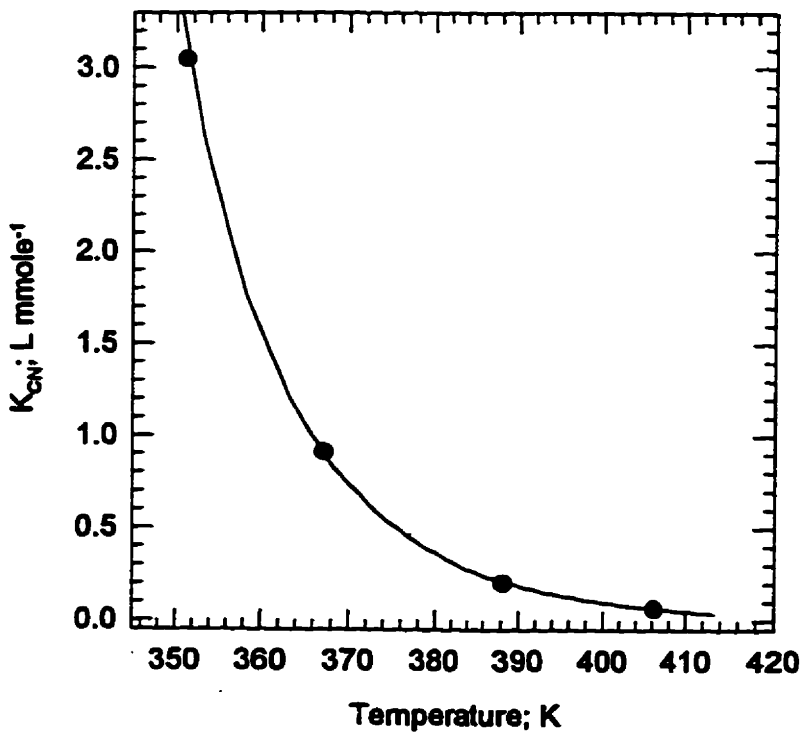

Figure 4.4: K_{CN} versus temperature for the 1a-Krynac system

Coordination of polymeric olefin to 1a,b

The potential of small olefins to coordinate with **1a,b** has been previously demonstrated (Moers et al., 1974; Esteruelas and Werner, 1986). From the information available, it appears that the Os(η^2-C=C) association is weak for olefins which lack an electron withdrawing substituent. Given that the olefin resident within NBR is at least 3 bonds removed from the potentially activating nitrile, a similar osmium-olefin bond strength may be expected. The steric bulk of the polymer is another concern, especially for the predominant *trans* butadiene isomer of Krynac 38.50 (78% *trans*, 18% *cis*, 4% *vinyl*). While an olefin complex of **1a,b** may not be the predominant species in solution, that it must be activated by the metal centre to be hydrogenated justifies a further study.

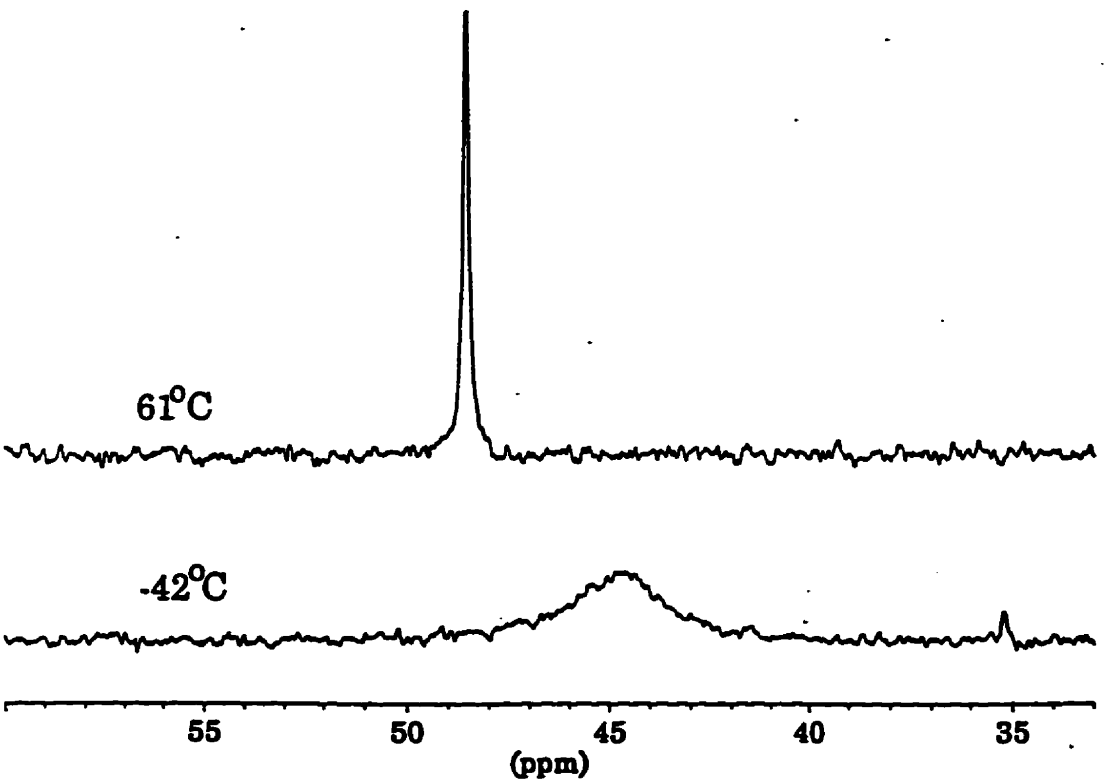

Figure 4.5: Variable temperature ^{31}P {^1H} spectra of **1b** under N_2

Preliminary attempts to examine the coordination of olefin residing within NBR were complicated by the more favourable association of **1a,b** with nitrile. As a result, this study focused on a low molecular weight polybutadiene homopolymer having a *cis/trans/vinyl*

distribution of 30/30/40. Before describing its interaction with **1b**, it is necessary to comment on the ^{31}P $\{^1H\}$ NMR spectrum of **1b** in isolation. Figure 4.5 illustrates the changes in the solution behaviour of **1b** with temperature. While a sharp singlet is observed above 23°C, cooling the system produces broadening and chemical shift migration that is likely caused by changes in the conformation of the complex in solution.

The influence of a 10:1 and a 30:1 ratio of olefin:osmium on the phosphorus spectrum of **1b** is shown in Figure 4.6. At 61°C, neither spectrum was perturbed by the polymer from that of pure **1b**. However, a noticeable difference in the degree of broadening is detected at room temperature between the 10:1 and 30:1 spectra, indicating that while the degree of olefin coordination is marginal, it is nonetheless present. At -27°C both systems exhibit a new resonance at 10.8 ppm in addition to the broadened **1b** signal. Cooling the system a further 15°C virtually eliminates residual **1b** while producing either an ill-resolved doublet or a second phosphorus resonance. As it is difficult to rationalize a mechanism by which the phosphines become inequivalent, it is most likely that the coordination of a different olefin isomer to **1b** is responsible for the second signal. Based on steric considerations, coordination of the *vinyl* and *cis* isomers of polybutadiene should be favoured over the relatively bulky *trans* structure.

H_2 coordination to 1a to form the dihydrogen complex 3a

The dynamics of H_2 coordination to **1b** have been examined by Bakhmutov et al. (1996). In a thorough research effort they have shown coordinated H_2 to be in rapid exchange with free molecular hydrogen while participating in an Os-H/Os(η^2-H_2) exchange process (see scheme below). The distribution of osmium between **1b** and **3b** at equilibrium has also been quantified as a function of temperature by direct measurements of K_{H2}.

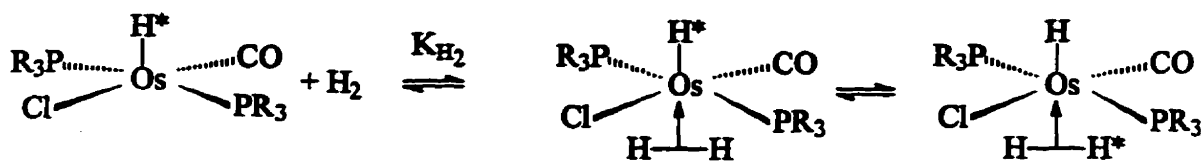

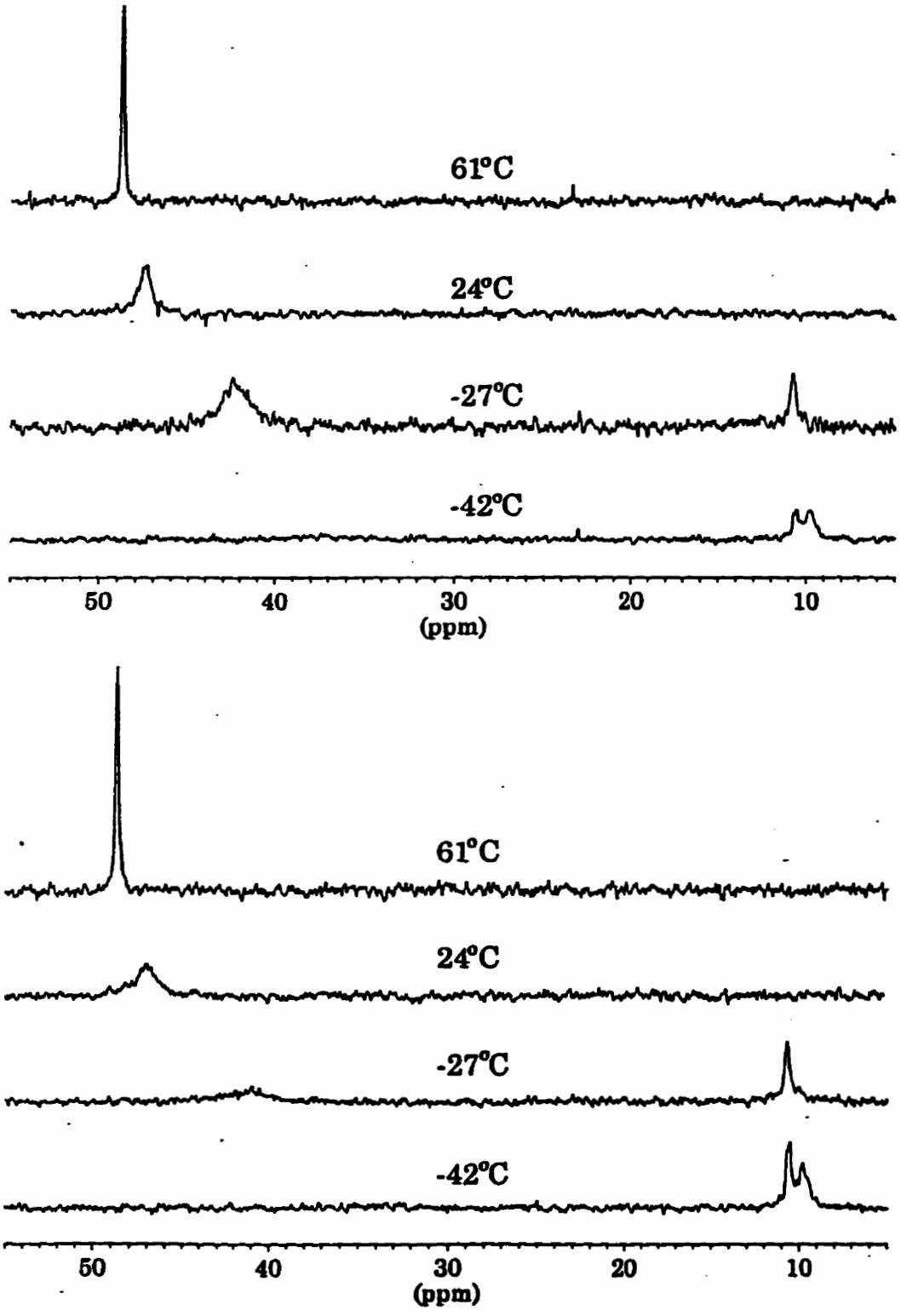

Figure 4.6: **Polybutadiene olefin coordination to 1b;**
Upper, 10:1 [C=C]:[Os] ratio; Lower, 30:1 [C=C]:[Os] ratio

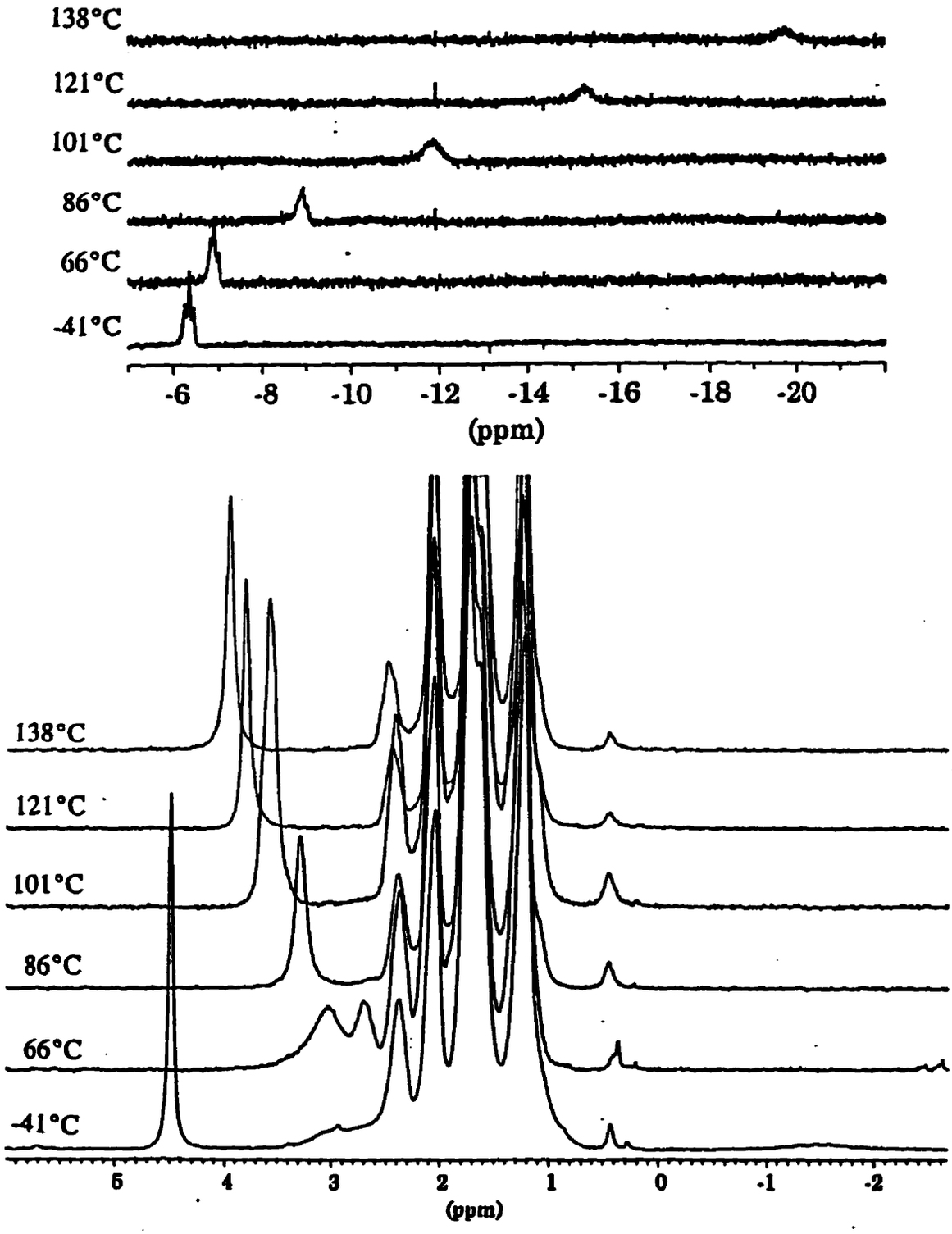

Figure 4.7: ^{1}H NMR spectra of the **1a** - **3a** system under rapid exchange
Upper: Os-H resonance, Lower: PCy_3, Os-(η^2-H_2) region

As the PCy_3 system is of primary interest in this work, the method devised by Bakhmutov et al. (1996) to estimate K_{H2} has been adopted to quantify the **1a-3a** equilibrium. The relative abundance of **1a** and **3a** was determined from the exchanged averaged ^1H chemical shift of the hydride resonance while the distribution of free and coordinated H_2 was measured from the exchanged averaged dihydrogen resonance (Figure 4.7). A known concentration of total osmium charged to the sample is all that is required to estimate $K_{H2} = [3a] / [1a][H_2]$. The results of the variable temperature ^1H analysis are provided below.

Table 4.2: K_{H2} versus temperature

Temp,K	δ_{avg},H_2	δ_{avg},Os-H	K_{H2},M^{-1}
411.2	4.12	-23.80	15.1
393.9	4.02	-19.55	25.6
374.2	3.86	-15.35	51.5
360.1	3.63	-11.80	122
339.7	3.33	-8.85	375
306.6	3.04	-6.85	2345
$[Os]_T = 6.68*10^{-3}M$			
δ_{H2}(free)= 4.50 ppm		δ_{3a}= -6.31 ppm	
δ_{H2}(bound)= -1.52 ppm		δ_{1a}= -32.65 ppm	

Mechanisms of phosphine exchange

Martin (1991) observed that 1 equivalent of added PCy_3 severely inhibited the catalytic activity of $RuHCl(CO)(PCy_3)_2$. A similar influence of free phosphine was reported Farnetti et al. (1992) for the $OsH_2(dcpe)_2$ system. In the case of unsaturated complexes like **1a,b**, phosphine inhibition may result from the coordination of PR_3 to the metal centre. Although there is no evidence to support the addition of a bulky phosphine, Esteruelas and Werner (1986) have added PMe_3 and $POMe_3$ to **1b** and the PPh_3 analogue of **1** is a tris-phosphine complex. On the other hand, free phosphine may inhibit hydrogenation by discouraging a necessary dissociation reaction. Were the active complex to possess but one phosphine, additional PR_3 could reduce its solution concentration.

A ^{31}P spectrum of **1a,b** in toluene at 100°C shows no evidence for phosphine dissociation. Conversely, no signs of PR_3 addition to **1a,b** were observed in a room temperature spectrum of **1a,b** with excess ligand present. Therefore, the likelihood of directly confirming either mode of phosphine inhibition is small. However, the rates of exchange between bound and free phosphine may provide a clue of the type of transition state capable of the osmium system (Figure 4.8). Evidence in favour of an associative exchange mechanism would suggest that a trisphosphine intermediate complex can be created. Data supporting a dissociative pathway would indicate a monophosphine transition state facilitates the exchange reaction. It should be noted however, that the transition state for phosphine exchange may or may not be representative the nature of the complex responsible for olefin hydrogenation.

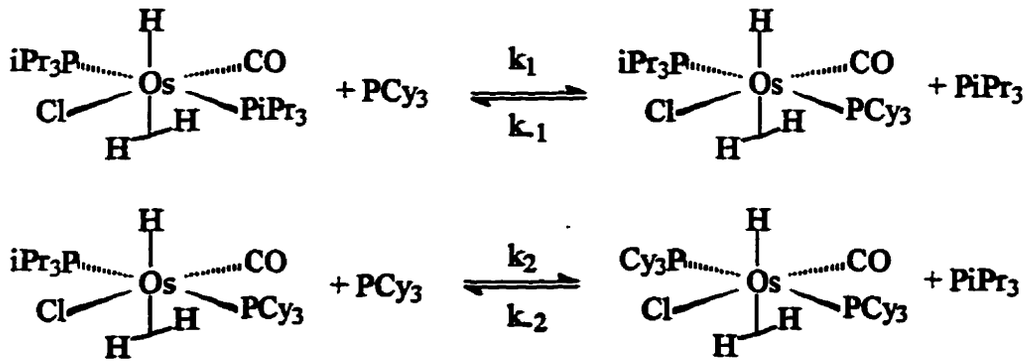

Figure 4.8: Phosphine exchange equilibria

Attempts to employ spin-saturation labelling to measure k_1 and k_{-1} failed, as the rate of phosphine exchange was insufficient to support the technique. Therefore, a traditional kinetic study was undertaken where the concentration of the exchange products was monitored with time. In a typical experiment, a known mass of **1b** (approximately 0.03g) was combined with the required amount of phosphine in 1g of toluene-d^8. This solution was charged to the sapphire tube and pressurized to 24 bar with H_2. At 23°C no phosphine exchange was detected during the time required to prepare the sample. Therefore, time zero was marked by its insertion into the preheated probe. The evolution of exchange

products observed in one of four **3b**-PCy_3 exchange experiments is presented in Figure 4.9 while a plot of the decay of [**3b**] observed for all of the trials follows in Figure 4.10. A complete listing of the acquired data is provided in Appendix AIII.

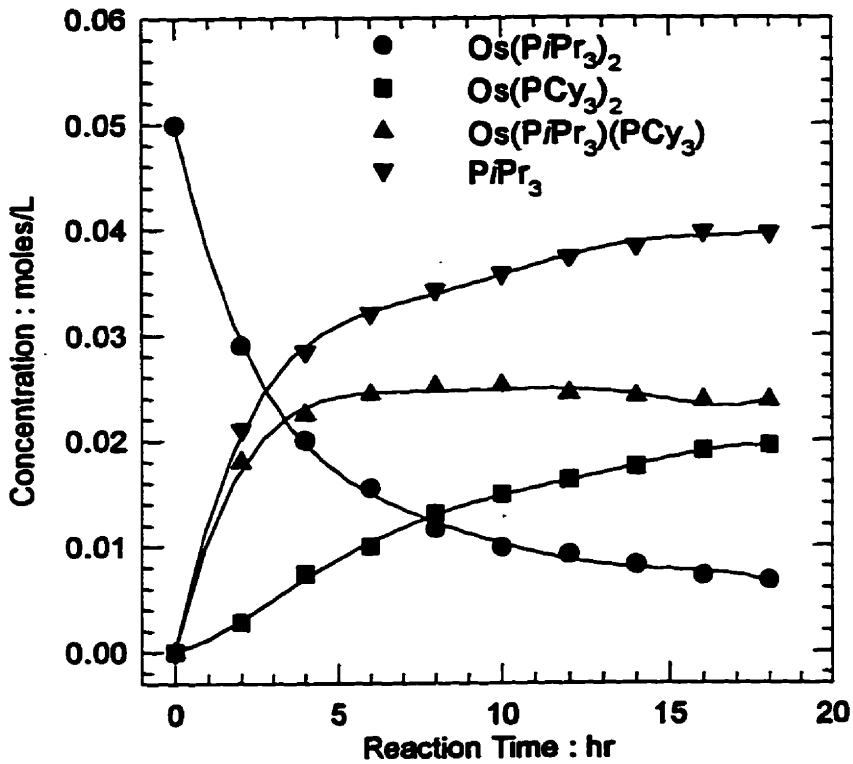

Figure 4.9: Exchange product concentrations versus time, Os=$OsH(H_2)Cl(CO)$; P_{H2}=23.7 bar, T=71°C, $[PCy_3]_o$=0.32M

Based upon the exchange experiments performed at $[PCy_3]$=0.1 M (Figure 4.10), the results were reproducible. Note that while the degree of substitution is related to the thermodynamic stability of the exchange products, it is the rate with which the system approaches its equilibrium that is of interest to this work. In this respect, the different systems are remarkably similar. To quantify the transformation of **3b** into $OsH(H_2)Cl(CO)(PiPr_3)(PR_3)$, k_1 and k_{-1} defined in Figure 4.8 have been fitted to the second

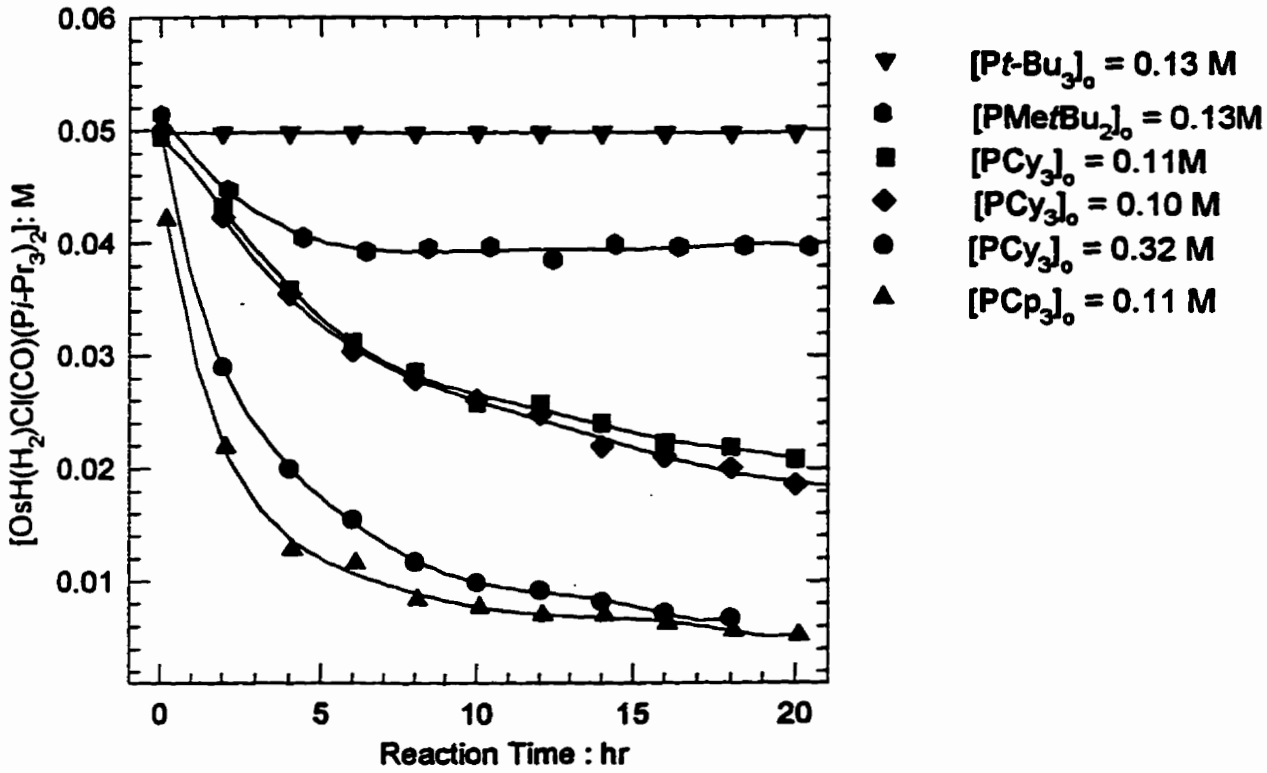

Figure 4.10: **[3b]** versus time for different phosphine systems; P_{H2}=24 bar, T=71°C

order rate expression

$$-\frac{d[3b]}{dt} = k_1[3b][PR_3] - k_{-1}[OsH(H_2)Cl(CO)(PiPr_3)(PR_3)][PiPr_3] \ .$$

Estimates of k_1 represent the inherent rate of the forward substitution reaction for a given phosphine type and concentration. Regression values of k_1 and k_{-1} are listed in Table 4.3.

From this limited set of data, the reaction rate appears to be independent of the nature and abundance of the entering phosphine as no significant differences in k_1 for the PCy_3 and P*Met*Bu_2 experiments are observed. That P*t*Bu_3 does not participate in an exchange process is not surprising, given its extraordinary cone angle of 180°.

Table 4.3: Phosphine exchange rate constants

PR_3	$[PR_3]$ M	k_1 $(M*hr)^{-1}$	Lower<95%>Upper		k_{-1}	Lower<95%>Upper	
PCy_3	0.10	0.814	0.729	0.899	0.461	0.148	0.773
PCy_3	0.11	0.873	0.802	0.945	1.246	0.358	1.469
PCy_3	0.32	0.842	0.762	0.922	0.531	-0.055	1.117
$PMeBu_2$	0.13	0.773	0.677	0.870	17.04	12.98	21.10
$PtBu_3$	0.13	0.000	-----	-----	-----	-----	-----
PCp_3	0.11	2.72	2.48	2.96	0.714	0.113	1.314

The PCp_3 experiment is somewhat disconcerting. Unlike the other trials, the PCp_3 exchange spectra did not satisfy a material balance on phosphorus or osmium in the early stages of the reaction. Whether this was due to a shift in the instrument during the experiment or to a difference in the relaxation times between the various complexes cannot be determined at present. While the derived rate constants are clearly unlike those of the other series, the qualitative agreement of the Cp_3 experiment suggests that the **3b** phosphine exchange process may indeed be tentatively declared independent of the incoming phosphine character.

Indifference to the nature and amount of the entering group is evidence for a dissociative-type mechanism for an exchange process. While little else is known of the reaction intermediate (particularly whether H_2 is involved), this result lends qualified support to the potential of the osmium system to form a mono-phosphine transition state.

Stability of bound CO under hydrogenation conditions

While the displacement of CO from either **1a,b** or **3a,b** is not expected, ^{13}C NMR provides a simple means of verifying its presence under hydrogenation conditions. A toluene solution of **1b** was pressurized to 24 bar with H_2 and heated to 100°C while recording the proton decoupled ^{13}C NMR spectrum shown in Figure 4.11. In addition to the isopropyl

carbon resonances at 19.4 and 24.5 ppm, a broad singlet at δ177.2 is observed which may be assigned to an osmium-bound CO ligand. The lack of expected ^{31}P-^{13}C coupling most likely reflects the relatively poor resolution of the spectrum rather than any exchange mechanism. Note that the ^{31}P spin-saturation labelling trials demonstrated that phosphine exchange rates are insufficient to produce an exchange averaged CO signal. It may therefore be assumed that CO remains coordinated during NBR hydrogenation.

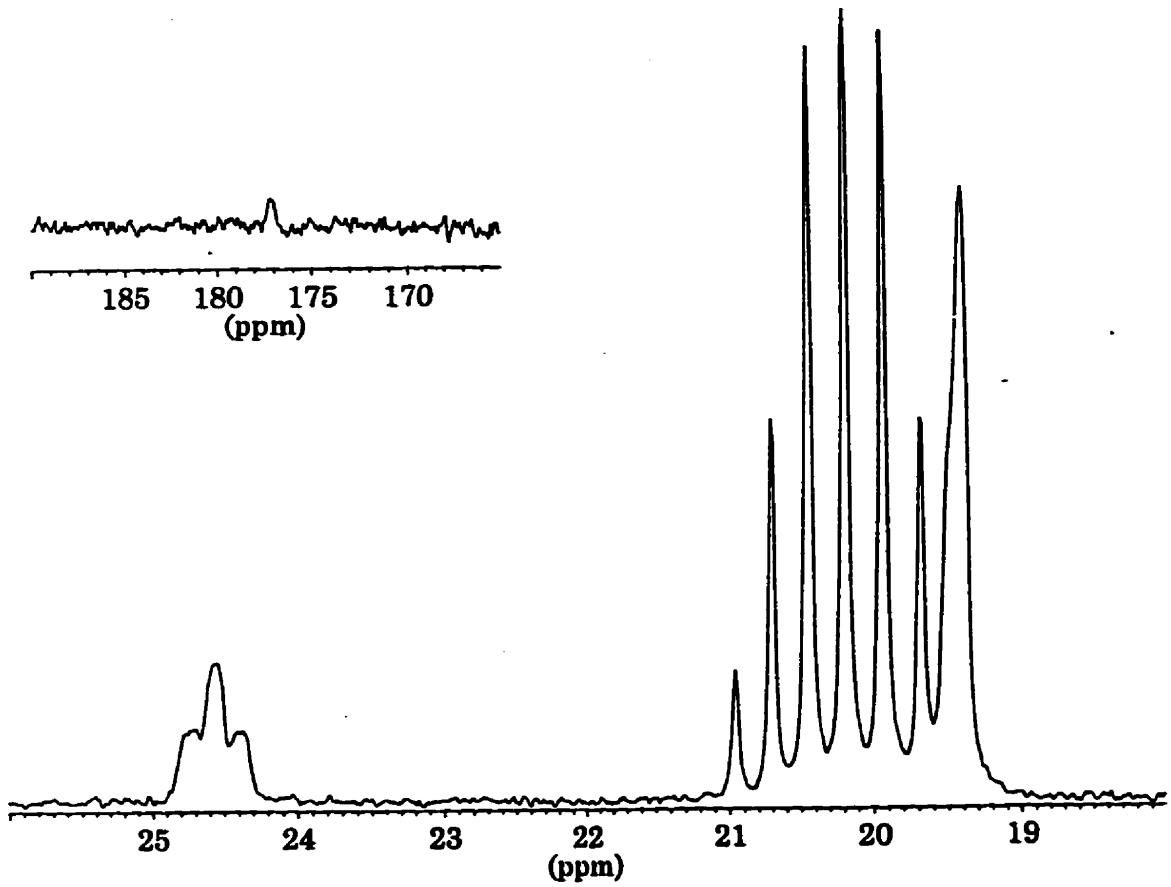

Figure 4.11: ^{13}C {^{1}H} spectrum of **1b**; P_{H2}=24 bar, T=98°C

Chapter 5

Kinetics of Olefin Hydrogenation by $OsHCl(CO)(O_2)(PCy_3)_2$; 2a

A major objective of this thesis is to assess the merits of the osmium technology while furthering our understanding of its underlying chemistry. This chapter summarizes the core of the project, a comprehensive kinetic study of the selective hydrogenation of NBR by **2a**. The range of operating conditions chosen for this work paralleled those employed in the rhodium study (Chapter 3) to facilitate a direct comparison of the two systems. However, a detailed assessment of the economic potential of the osmium technology is beyond the scope of the project. Only distinct advantages and shortcomings associated with the new catalyst system are highlighted.

In addition to providing a means of appraising the activity of **2a**, the kinetic studies further our basic knowledge of this class of complexes. Kinetic data is important in its own right, given the scarcity of literature devoted to osmium catalysis and the absence of research performed under extreme conditions. Interpretations of rate data can be equally constructive, should they provide a solid foundation upon which greater understanding may be built. The status of an evolving reaction mechanism has therefore been inserted into the discussion of the kinetic measurements.

5.1 Experimental

5.1.1 Materials, Apparatus and Procedures

The preparations of **2a,b** as well as the source of the reagents have been provided in Chapter 4.1. The acrylonitrile-butadiene copolymer studied (Krynac 38.50 from Bayer Rubber Inc.) contained 62% butadiene by weight which was distributed as 78% *trans*, 16% *cis*, 6% *vinyl*. The styrene-butadiene rubber employed was Finaprene 410 from Petrofina. Dec-1-ene, purchased from Aldrich Chemical Co., was purified by vacuum distillation, stored under N_2 and used promptly. The solvents employed (monochlorobenzene, acetone

and 2-butanone) were used as received from Fischer Chemical Co. The purity of H_2 purchased from Linde-Union Carbide was reported to be 99.99%.

The apparatus, operating procedures and product characterizations were identical to those detailed in Chapter 3.1, with one exception. Where the addition of PCy_3 was required, the phosphine was not combined with the polymer solution as PPh_3 had been. Rather, a separate glass bucket was fashioned to hold the PCy_3 within the catalyst addition device. Both the catalyst and the phosphine were charged to the solution once the system was purged of atmospheric gases. Note that the handling time of the phosphine in air was minimized to limit potential oxidation.

5.1.2 Design of the Kinetic Experiments.

Specific combinations of factor levels have been selected according to a structured design. Of principal interest were the influences of the concentrations of **2a**, nitrile and H_2 on the rate of hydrogenation. Of secondary interest was the effect of varying the reaction temperature or adding PCy_3 to the system. Principal factor combinations conformrd to a central composite structure (Box et al., 1978), consisting of a univariate or "one-at-a-time" series to study the influence of each factor while holding all others constant, and a two-level factorial series of experiments to identify joint interactions (Figure 5.1). The influence of various substrates, added phosphine and temperature have been investigated by univariate experiments alone.

The basic central composite structure shown in Figure 5.1 has been expanded to include a survey of [**2a**]*[H_2] interactions. Selection of the factor levels ([**2a**], [RCN], [H_2]) considered catalyst weighing precision, the viscosity of the polymer solution and the hydrogenation rate which the apparatus could effectively control and monitor. As chlorobenzene boils at 132°C, a base reaction temperature of 130°C was chosen for safety concerns. Table AIV of Appendix IV lists all of the combinations of factor levels explored.

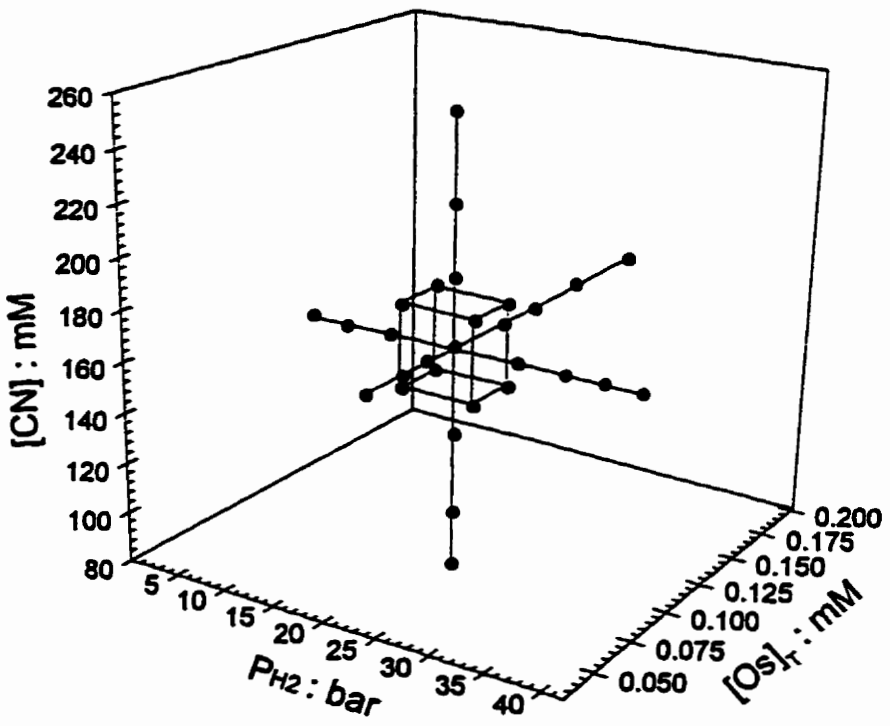

Figure 5.1: Principal factor combinations studied; T=130°C

The experiments were generally performed in randomized blocks. While not rigidly defined, each block focused upon a particular component of the overall design ie. 2^3 factorial series, [RCN] series, etc. The central combination ([**2a**]=80 μM, [RCN]=172 mM, P_{H2}=23.7 bar, T=130°C) was periodically repeated to detect shifts in hydrogenation activity evolving with time.

5.2 Results and Discussion

Exposed to traces of O_2, **1a,b** readily form their corresponding dioxygen adducts **2a,b**. Complex **2a** in particular is extremely robust, showing no signs of degradation over the course of months when left in air. This unique stability, coupled with its virtually inevitable presence, has led to its adoption as the catalyst precursor for this work. The

transformation of **2a,b** into the dihydrogen adducts **3a,b** has been demonstrated by NMR (Chapter 4). Under the reaction conditions employed, the catalytic behaviour of **2a,b** is expected to be identical to that of **1a,b**.

In the early stages of this research it was discovered that the PCy_3 complex **2a** demonstrates superior activity for NBR hydrogenation over that of **2b**. Due to its greater commercial potential, the **2a** system has therefore been the focus of the kinetic study. A final preliminary issue centres on the choice of chlorobenzene as solvent for the process. Unlike its ruthenium analogue which is unaffected by acetone or 2-butanone (Martin, 1991), **2a** cannot function in ketone solvents. This is likely due to the coordination and insertion of the ketone as described by Esteruelas and Werner (1986). In any event, the problems arising from the use of ketones constrained the choice of solvent to chlorobenzene.

5.2.1 Hydrogenation Profile for the **2a**/Krynac 38.50 System

Under all reaction conditions, **2a** proved to be an efficient catalyst for the quantitative hydrogenation of the olefin moiety within NBR. Both ^1H and ^{13}C NMR spectra of the product were consistent with those published by Mohammadi and Rempel (1986) and Bhatachjaree et al. (1991) for HNBR obtained from the $RhCl(PPh_3)_3$ catalyst system, indicating that **2a** does not promote a significant reduction of nitrile. Further discussion of undesirable side reactions are the subject of Chapter 6.

In contrast to the Rh(I) catalysts, the activity of **2a** is not independent of the *cis/trans/vinyl* isomerization of olefin within of the copolymer. Figure 5.2 illustrates a representative olefin conversion profile of the hydrogenation of NBR by **2a**. In early stages of the reaction, a transient period of heightened activity is consistently observed. As the system temperature was logged along with the conversion profile, it is known that reaction exotherm was effectively controlled by the apparatus and was not responsible for the effect. Indeed, a careful examination reveals the overall olefin conversion profile to be the

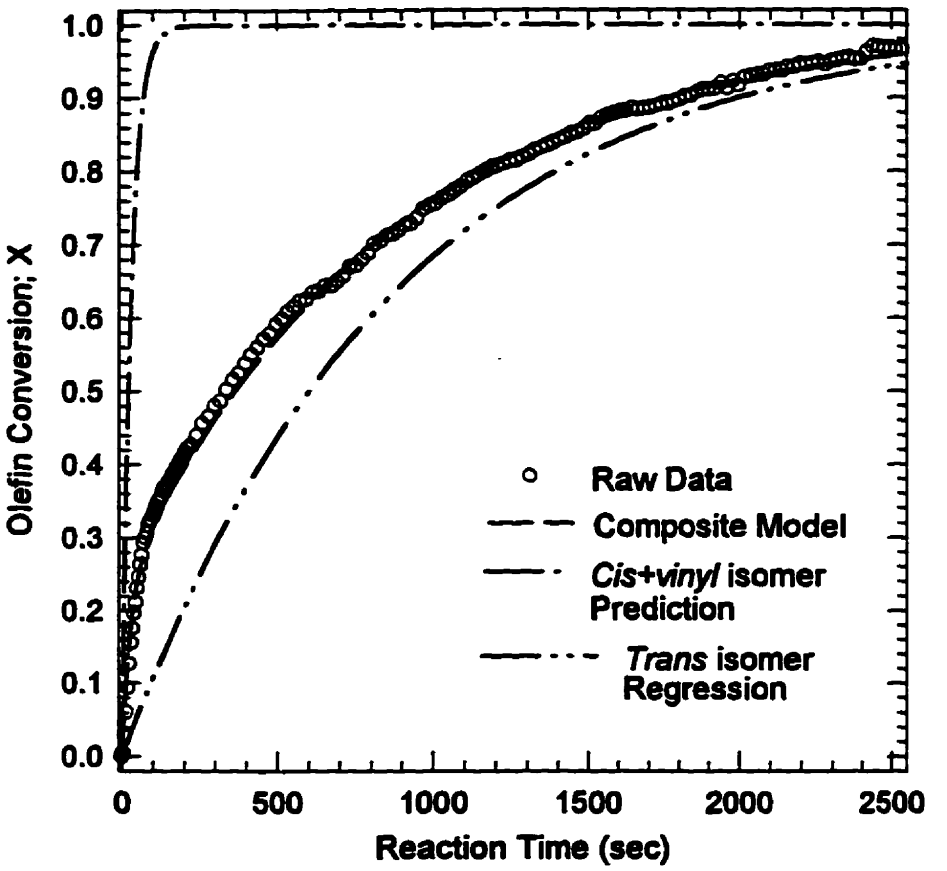

Figure 5.2: Conversion vs. time profile; [2a]=110μM, [RCN]=172mM, P_{H2}=14bar, T=130°C.

superposition of two distinct processes. This is more clearly illustrated in the log plot comprising Figure 5.3.

For a single first order reaction, a plot of ln(1-X) versus time is a linear function defined by its slope, k', the first order rate constant and an intercept of (0,0). Figure 5.3 resolves two distinct domains of hydrogenation activity. A relatively short-lived period of rapid hydrogenation is followed by a more moderate, and strictly first-order reaction rate. A regression of the latter data from 35% to 95% conversion according to

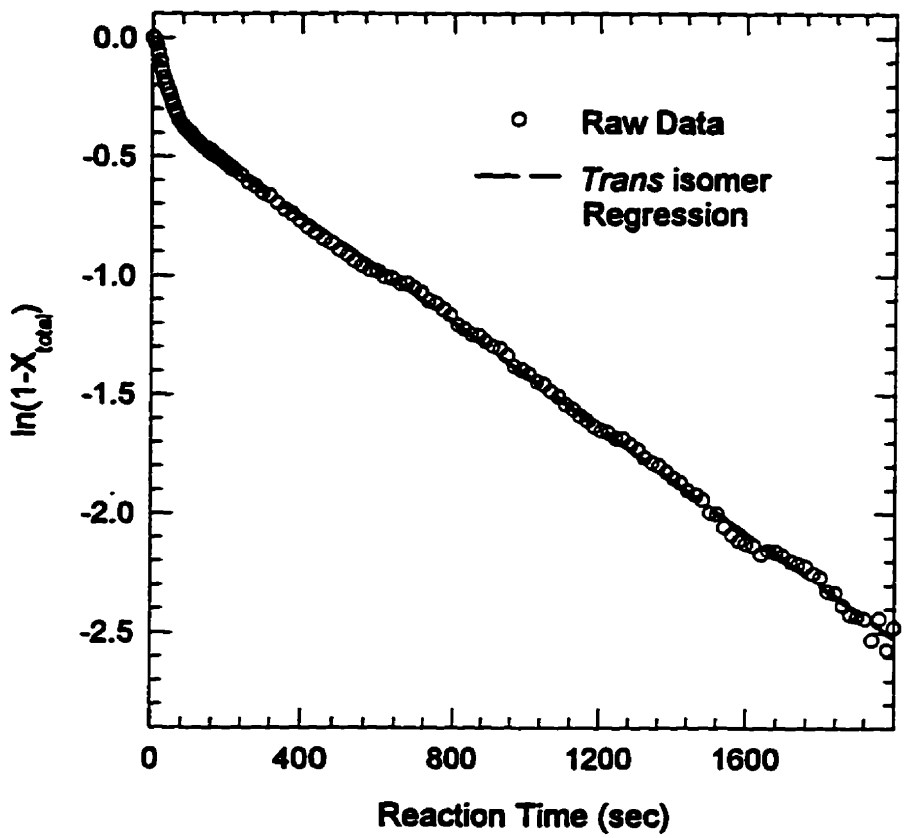

Figure 5.3: Ln plot of the X versus time data shown in Figure 5.2

$$[C{=}C] = [C{=}C]_o * e^{-k't}$$

yielded k' = $1.15*10^{-3}$ s^{-1} and $[C{=}C]_o$ = 209 mM. The total loading of 3.59 g of NBR corresponds to [C=C] = 275 mM. Given that Krynac 38.50 is reported to contain approximately 78% *trans* olefin, 0.78 * 275 mM = 214 mM of *trans* olefin was charged to the reactor. Six kinetic experiments, each run at different conditions, yielded $[C{=}C]_o$ = 206.8+/-2.0 mM despite producing a wide range of hydrogenation rates.

Using an 75% *trans* olefin content, the (*cis* + *vinyl*) conversion versus time profile was derived by correcting the raw uptake data with the regressed *trans* conversion profile.

Note that at 4% abundance, there is an insufficient amount of *vinyl* functionality to account for the initial surge of activity. For the (*cis* + *vinyl*) profile, an estimate of $k'_2 = 3.1*10^{-2}$ s^{-1} was derived. The predicted overall (*cis* + *vinyl* + *trans*) conversion profile derived using k' and k'_2 fits the observed data satisfactorily as illustrated in Figure 5.2. Any difference in the activity of **2a** towards the *vinyl* and *cis* isomers cannot be resolved from the conversion profile.

As commercial interests require a complete saturation of the copolymer backbone, the rate at which **2a** hydrogenates the 78% abundant *trans* isomer of Krynac 38.50 is most important. At 130°C and pressures up to 41 bar, *trans* C=C conversion abides by a first order rate expression as depicted in Figure 5.3. Therefore, the dependence of the hydrogenation rate on [**2a**], [RCN], $[H_2]$ and temperature has been quantified by measuring the response of k' (derived from approximately 35% to 95% olefin conversion) to the factor combinations detailed in Section 5.1.2.

5.2.2 2^3 Factorial Design Results

A two-level factorial design was applied in the $RhCl(PPh_3)_3$ study to determine the significance of interactions between factors which influence the hydrogenation rate (Chapter 3). This strategy has been revisited to identify similar interactions between [**2a**], [RCN] and P_{H2} acting within the osmium reaction mechanism. The factor combinations and derived rate constants are listed in Appendix IV, Table AIV. The results of an analysis of variance (ANOVA) treatment of the acquired data are summarized by Table 5.1.

Not surprisingly, the variance test statistics demonstrate the significance of main factors ([**2a**], [RCN] and $[H_2]$). More importantly, all two-factor joint interactions appear to be significant at the 95% confidence level. This indicates the influence of a factor on the rate of hydrogenation is dependent upon the levels of the others. For instance, the impact on k' created by increasing the amount of **2a** is dependent on the reaction pressure employed. Note that a [**2a**]*[RCN]*$[H_2]$ interaction is not statistically significant.

Table 5.1: ANOVA results of the 2^3 factorial experiments

Source	Analysis of Variance Sum of Squares	DF	Mean - Square	F-Ratio	P
[Os]	4.35E-06	1	4.35E-06	198	6.28E-07
P_{H2}	3.20E-05	1	3.20E-05	1460	2.43E-10
[RCN]	4.52E-06	1	4.52E-06	206	5.43E-07
[Os]*P_{H2}	1.12E-07	1	1.12E-07	5.12	5.45E-02
[Os]*[RCN]	1.72E-07	1	1.72E-07	7.86	2.31E-02
P_{H2}*[RCN]	4.16E-07	1	4.16E-07	19.0	2.43E-03
[Os]*P_{H2}*[RCN]	2.10E-08	1	2.10E-08	0.959	0.356
Error	1.75E-07	8	2.19E-08		

Having identified the importance of factors acting alone and in combination, the factorial component of the central composite design has provided a sound basis for further study. The univariate series of experiments expanded the number of factor levels, the results of which are provided in the following discussion.

5.2.3 Univariate Kinetic Experiments

*Influence of the concentration of **2a** on the hydrogenation rate*

The hydrogenation of styrene catalyzed by **1b** at 60°C, 1 bar H_2, is reported to be first order with respect to the concentration of the catalyst precursor (Andriollo et al., 1989). Martin et al. (1991) observed a similar response for the ruthenium analogue of **1a**, $RuHCl(CO)(PCy_3)_2$, acting upon Krynac 38.50 at 160°C, 41 bar. It is therefore not unexpected that plots of k' versus **[2a]** at various pressures yield a linear relationship (Figure 5.4). This first order response of the hydrogenation rate to changes in **[2a]** indicates that the concentration of the active complex is linearly proportional to the precursor loading employed ie. k' α **[2a]**. This is strong evidence for a mononuclear active species.

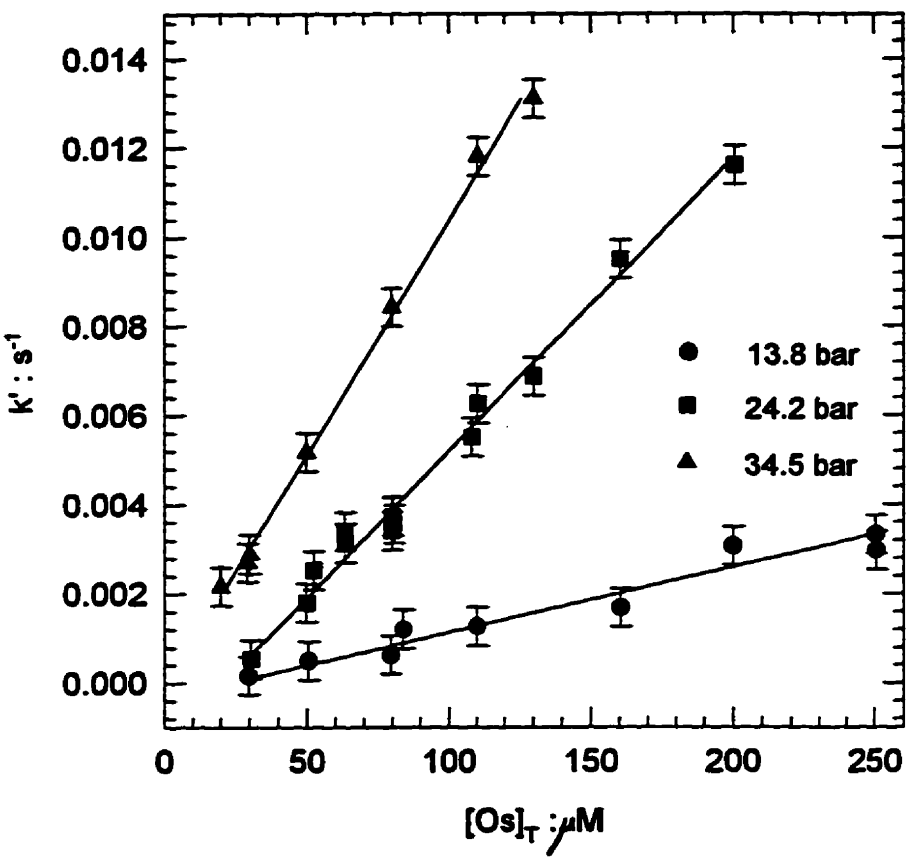

Figure 5.4: Influence of [2a] on the hydrogenation rate; [RCN]=172mM, T=130°C

Inhibition of the hydrogenation rate by nitrile

The potential of nitrile to coordinate with **1a,b** has been characterized by NMR (Chapter 4). Its influence on the rate of hydrogenation is demonstrated in the k' versus [RCN] plot comprising Figure 5.5. Conversion profiles for first order systems are, by definition, independent of the amount of olefin charged to the reactor. Therefore, increasing the initial concentration of an olefin such as 1-decene would have no effect on a conversion versus time profile. Figure 5.5 indicates that elevated NBR loadings, with their corresponding increases in the concentration of nitrile, inhibit the catalytic activity of **2a**. This influence may be rationalized by a competitive coordination of the nitrile residing within NBR to **1a** as illustrated by Figure 4.2 and demonstrated in the NMR spectra of

Figure 4.3. However, an increase in the concentration of potentially poisonous components of the polymer (mercaptan, carboxylate, etc.) may contribute to the observed decrease in k' that is associated with a higher rubber loading.

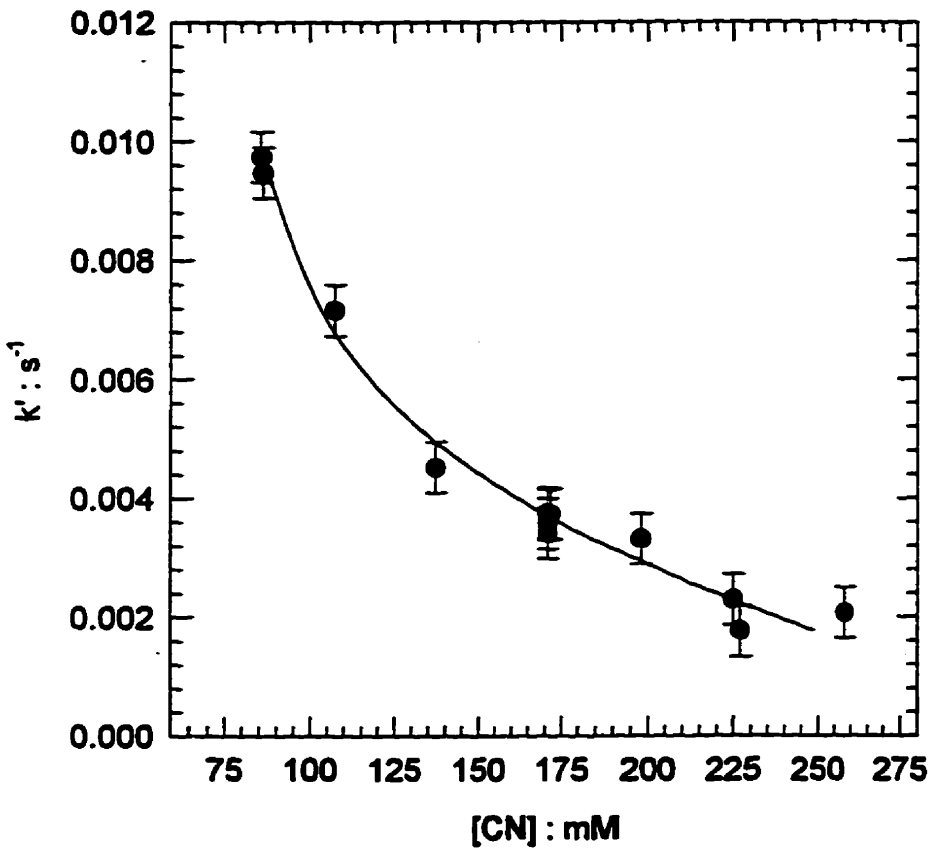

Figure 5.5: Influence of [RCN] on the activity of **2a**; [**2a**]=80μM, P_{H2}=23.7bar, T=130°C

Influence of [H_2] on the hydrogenation rate

The H_2 univariate experiments of Chapter 3 demonstrated the first to zero order dependence of k' on P_{H2} that is characteristic of the rhodium(I) catalysts. Martin et al. (1992) have, using the same apparatus employed in this work, observed a linear relationship between k' and P_{H2} for the $RuHCl(CO)(PCy_3)_2$ system. In contrast, the behaviour illustrated by Figure 5.6 is not only unexpected, but unprecedented. At 130°C

and pressures up to 41 bar, a distinct second order dependence of k' on the hydrogen pressure is observed. 27 experimental trials at three different catalyst loadings demonstrate the consistent second order response of k' to $[H_2]$ as well as the first order relationship between k' and [2a]. Note that 5 replicates of the central reaction conditions ([2a]=80 μM, [RCN]=172 mM, P_{H2}=23.7 bar, T=130°C) yielded 3.57 +/- 0.19 s^{-1}. This remarkable precision suggests that the second order result is a real effect. It may therefore be concluded that up to 41 bar, k' α [2a]*$[H_2]^2$.

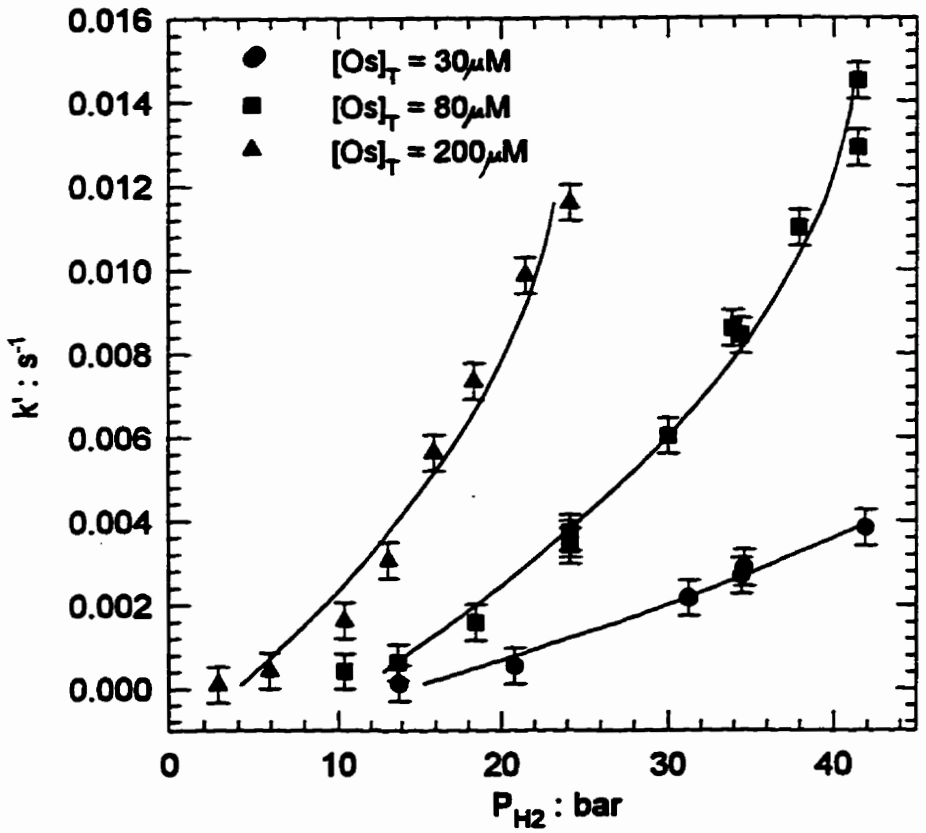

Figure 5.6: Influence of P_{H2} on the reaction rate; [RCN]=172mM, T=130°C

The apparent second order response of 2a to the system H_2 pressure implies that a truly unique mechanism underlies the observed process. In some form, two molecules of H_2 must generate the active species or interact with it in the reaction's rate determining step.

Recall that the **[2a]** univariate experiments support a mononuclear active complex. Therefore, it would appear that two molecules of H_2 are involved with a single metal centre to facilitate the hydrogenation.

While the second order effect of H_2 is intriguing from a fundamental standpoint, it is also of considerable industrial interest. An extrapolation of the rate data in Figure 5.6 to the pressures commonly associated with commercial HNBR processes (up to 100 bar) suggests that an osmium-based process could operate efficiently using trace amounts of **2a**. To investigate this potential further, the 30 μM univariate pressure series has been extended to 80 bar. Representative olefin conversion profiles acquired at these elevated pressures are presented in Figure 5.7.

Each of the conversion versus time plots demonstrate the transient activity attributed to the preferential hydrogenation of the *cis* isomer within NBR. Beyond 25% conversion, the 20.6 bar profile displays an exemplary first order response to olefin concentration to yield $k' = 0.55*10^{-3}\ s^{-1}$. At 29.6 bar, the system retains the first order behaviour with $k' = 3.84*10^{-3}\ s^{-1}$. To this point, **2a** demonstrates the expected behaviour, first order in olefin, second order with respect to $[H_2]$. However, increasing the pressure to 51.7 bar raises the reaction rate by a margin which is somewhat less than that projected by a second order mechanism. This trend continues until little difference in activity is observed between the 62 and 80 bar experiments. Clearly, the reaction order with respect to hydrogen evolves from second towards zero order as the system pressure is increased.

Of significance is the shift in the appearance of the olefin conversion profiles. With each increase in pressure, the conversion versus time plots tend towards a zero order dependence with respect to olefin. No longer is the rate of olefin reduction proportional to its concentration. Rather, an intermediate reaction order is observed according to;

$$-\frac{d[C{=}C]}{dt} = \frac{a\,[C{=}C]}{b + c\,[C{=}C]}$$

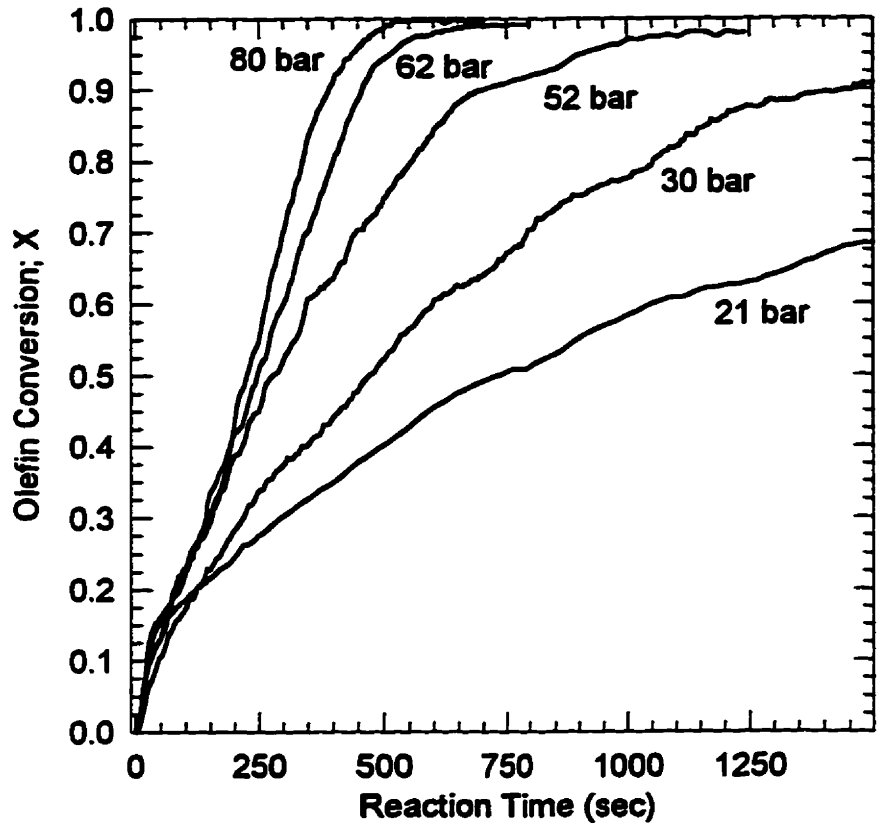

Figure 5.7: Conversion profiles observed at high pressures; [2a]=30μM, [RCN]=172mM, T=130°C

where a,b and c are constants. At low reaction pressures, c[C=C] is apparently much smaller than b to provide an overall order with respect to olefin of one. As the pressure is raised, c[C=C] approaches b to reduce the overall order towards zero. Note also that as the high pressure reactions proceed, the reaction returns to a first order behaviour at high conversions. Clearly the constant, c, must be dependent upon the concentration of H_2 in the condensed phase. Its functional relationship to [H_2] is discussed in greater detail in the latter stages of Section 5.2.3.

An alternate explanation for the reduced orders of olefin and hydrogen appeals to mass transfer arguments. As the reaction rate approaches the rate which the apparatus can

replenish consumed hydrogen, the kinetic data no longer represents the intrinsic behaviour of 2a. Under a severe mass transfer limitation, the influence of H_2 and olefin would yield to those factors controlling the rate of hydrogen dissolution such as agitation and impeller design. To assess the possibility that the forementioned observations could be attributed to mass transfer effects, it is necessary to revisit the data presented in Chapter 3.2.1.

For a 150 cm^3 solution containing 3.6g of Krynac 38.50, the aggregate mass transfer coefficient, k_lA/V, at 1200 rpm was 0.307 s^{-1}. From the conversion versus time profile at 80 bar (Figure 5.7), the maximum rate of hydrogen consumption was 4 mmoles $H_2L^{-1}s^{-1}$. Therefore,

$$4.0\ mmole\ H_2\ L^{-1}s^{-1} = 0.307 s^{-1}\ (c^*_{H2} - c_{H2})\ .$$

At 80 bar and 130°C, the equilibrium concentration of hydrogen, c_{H2}* equals 325mM. Substituting this value into the above expression yields:

$$4.0\ mmole\ H_2L^{-1}s^{-1} = 0.307\ s^{-1}\ (325\ mM - c_{H2})$$

$$c_{H2} = 309\ mM\ .$$

To support the maximum reaction rate reported in Figure 5.7, the bulk concentration of hydrogen would be depleted from its equilibrium value by just 15.5 mM, a difference of just 4.7%. It may therefore be concluded that mass transfer limitations have little effect, if any, on the diminished reaction orders observed in the high pressure series of experiments.

Influence of substrate: Part A - Styrene-butadiene rubber

Like NBR, Styrene-butadiene rubber (SBR) is a random copolymer produced by free-radical, emulsion polymerisation. Examining its hydrogenation provides a means of studying the osmium technology in the absence of nitrile. Figure 5.8 illustrates a conversion versus time profile for the hydrogenation of Finaprene 410. Analogous to NBR hydrogenation, the rate of *trans* butadiene saturation is less than that of the *cis* isomer. Beyond the transient period (Finaprene contains approximately 60% *trans* double bonds) the reaction follows a first order profile as revealed by the ln plot provided in the same figure.

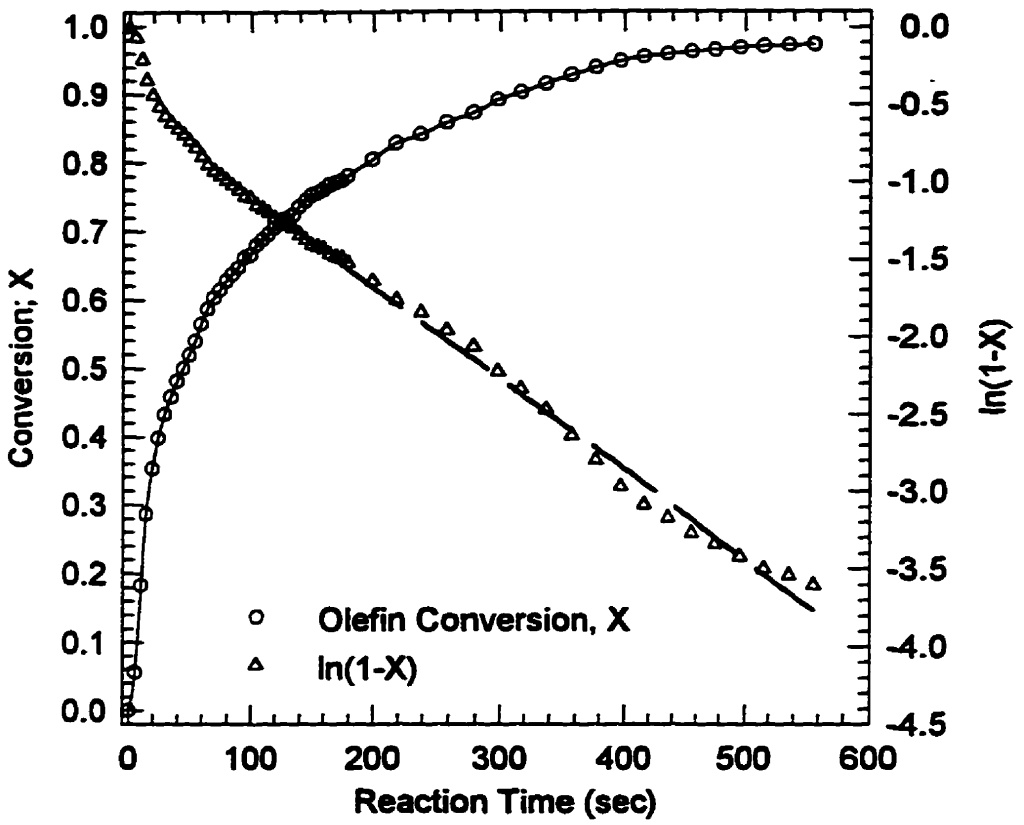

Figure 5.8: Styrene-butadiene rubber hydrogenation;
[2a]=80μM, [C=C]$_o$=400mM, P_{H2}=24.7bar, T=130°C

The apparent first order rate constant, k', representing the reaction illustrated by Figure 5.8 is $5.42*10^{-3}$ s^{-1}. Unlike the NBR system, this reaction rate is unaffected by the amount of polymer charged to the reactor (Table 5.2). This is the expected response of a first order process in which cofunctionality within the copolymer does not inhibit the reaction. It is interesting that the SBR hydrogenation rate is not simply an extrapolation of the NBR data to zero [RCN] (See Figure 5.5). This is a good example of the deceptive complexity of transforming polymeric substrate. Reactivities must be assessed directly and comparisons between polymeric systems made with caution.

Table 5.2: Influence of the SBR loading on k'

$[C=C]_o$, mM	$k'*10^3$, s^{-1}
138	4.94
275	5.39
400	5.42

[2a]=80μM, P_{H2}=24.2 bar, T=130°C

A significant development has come from measuring the response of the **2a**/SBR system to a variation of the reaction pressure. Over a wide range of P_{H2}, the reaction rate is zero order with respect to $[H_2]$, as was previously observed for NBR at high pressures. The olefin conversion profiles were consistently first order. Without a coordinating functional group such as nitrile in the system, the reaction orders with respect to [C=C] and $[H_2]$ are first and zero respectively.

Table 5.3: Styrene-butadiene rubber hydrogenation

H_2 Pressure (bar)	$k'_{trans}*10^3$, s^{-1}
5.24	3.85
10.4	3.60
24.2	3.85
31.2	3.69
38.2	4.08

[2a] = 60μM, $[C=C]_o$ = 275mM
[RCN] = 0 mM, T=130°C

In the case of NBR, the development of a zero order hydrogen dependence was accompanied by a reduction of the order with respect to olefin. This SBR result suggests a

rate expression of the form;

$$-\frac{d[C=C]}{dt} = \frac{A\,[Os]_T\,[H_2]^2\,[C=C]}{B + C\,[C=C]\,[H_2] + D\,[H_2]^2}.$$

According to this expression, the term D $[H_2]^2$ must be less than (B + C[C=C]$[H_2]$) to produce the experiments summarized by Table 5.3.

Influence of substrate: Part B - 1-Decene

While a second order dependence on $[H_2]$ has no precedent, Esteruelas et al. (1992) report a zero order response for the hydrogenation of benzylideneacetone by the PMe*t*Bu$_2$ analogue of **1a**. The reaction conditions used in the work were considerably milder than those employed throughout this study ($[Os]_T$ = 2.5mM, T = 60°C and P_{H2} = 0.70 - 1.26 bar). Therefore, the behaviour of a simple olefin at intermediate reaction conditions has been examined to bridge the two research efforts.

The reaction profiles acquired for the hydrogenation of 1-decene by **2a** are presented in Figure 5.9. Over the considerable pressure range investigated, the data revealed a very marginal improvement in the rate of hydrogenation by increasing $[H_2]$. Consistent with the reduction of the *trans* isomer of SBR, the system remains first order with respect to olefin at all reaction pressures.

Effect of added PCy_3 on the activity of 2a

Farnetti et al. (1992), in their investigation of benzylideneacetone hydrogenation by $OsH_2(dcpe)_2$, observed that the addition of PPh_3 to the system produced a marked decrease in the catalytic activity. They assigned the effect to a hinderance of a phosphine dissociation process that is believed to produce the active complex. In a study of $RuHCl(CO)(PCy_3)_2$, Martin (1991) discovered a similar inhibition by the addition of PCy_3. One equivalent of phosphine relative to the catalyst reduced the hydrogenation activity to less than one half. The influence of PCy_3 on **2a** appears to be equally severe (Figure 5.10). While exerting a strong effect on the hydrogenation rate, added phosphine appears

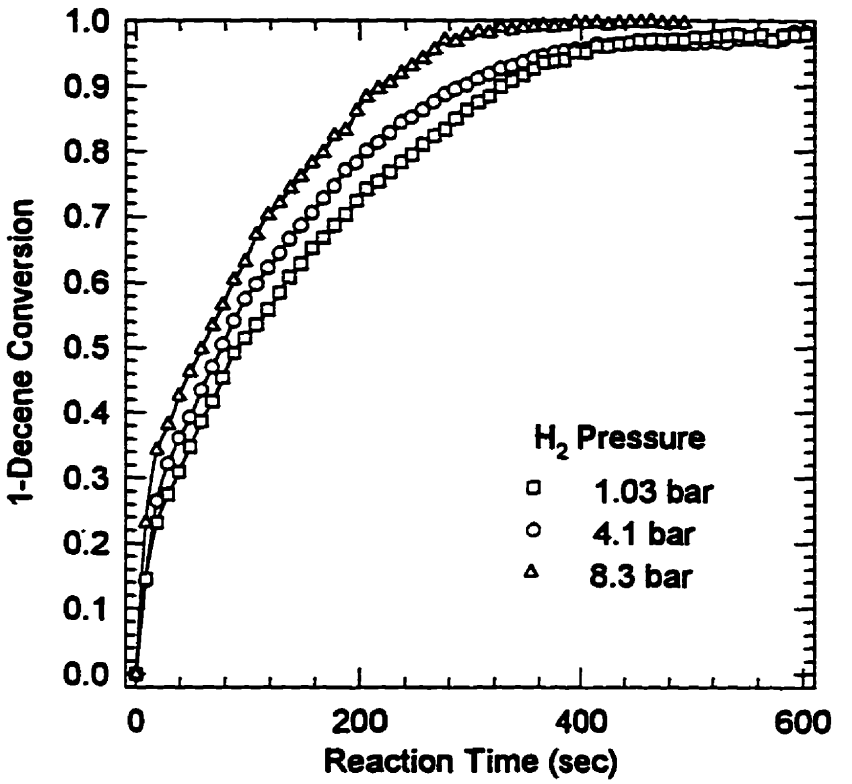

Figure 5.9: Hydrogenation of 1-decene by **2a**; [**2a**]=20μM, [C=C]$_o$=210mM, T=110°C

to reduce the order with respect to olefin in a manner similar to that observed at elevated pressures. This joint [C=C][PCy_3] interaction is ill-defined at present.

Whether PCy_3 inhibits hydrogenation by coordinating to **1a** or by hindering a necessary dissociation of phosphine is of consequence to the reaction mechanism. It is instructive to recall the level of inhibition produced by nitrile, which is a good ligand for **1a**. At a solution concentration of 172 mM, a batch reaction time of 200 seconds is required to produce an 99.5% olefin conversion (Figure 5.10). In contrast, just 0.08 mM of PCy_3 lengthens the reaction time to 2000 seconds. Given that there is no evidence of the coordination of a third phosphine to **1a**, it is unlikely that an inhibition by PCy_3 is due to an associative-type mechanism.

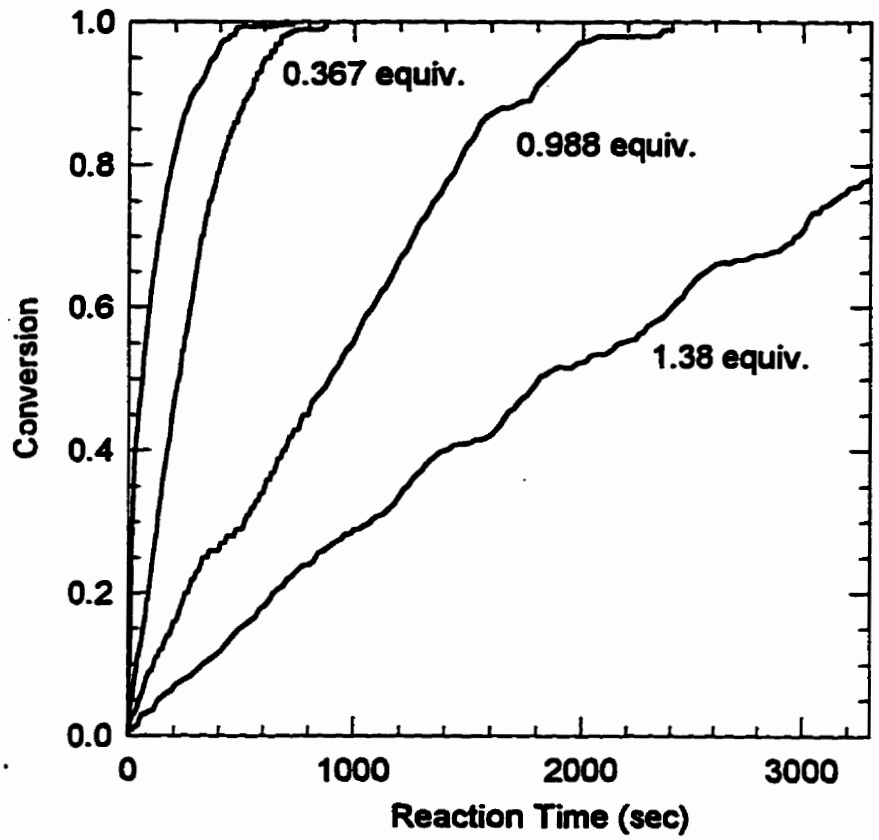

Figure 5.10: Influence of added PCy_3 on the **2a** system;
[**2a**]=80μM, [RCN]=172mM, P_{H2}=23.7bar, T=145°C.

On the other hand, under no conditions has the dissociation of PCy_3 from either **1a** or **3a** been observed. Therefore, a monophosphine complex would necessarily be extremely reactive and/or present in trace quantities. While not comprehensive, there is limited evidence to support a dissociative intermediate in the process of phosphine exchange (Chapter 4). At 24 bar H_2 and 70°C, the exchange data supported a mechanism in which the loss of a PR_3 ligand initiates the process, although no monophosphine complex was observed directly. Were a similar dissociative process required to initiate olefin hydrogenation, trace amounts of added PCy_3 could influence an already unfavourable equilibrium, thereby lowering the observed reaction rate.

Influence of temperature on the hydrogenation activity of 2a

The response of k' to a variation of temperature between 120°C and 140°C has been measured. The sensitivity of k' to $[H_2]$, combined with the strong influence of temperature on the Henry's constant of the system (Chapter 2), suggested that the temperature range be limited to +/- 10°C of the base value. An Arrhenius treatment of the acquired data is illustrated in Figure 5.11. The ln(k') versus 1/T expression yields a correlation coefficient (R^2) of 0.985 and a random distribution of residuals. An apparent activation energy of 96 kJ/mole is derived from the function's slope.

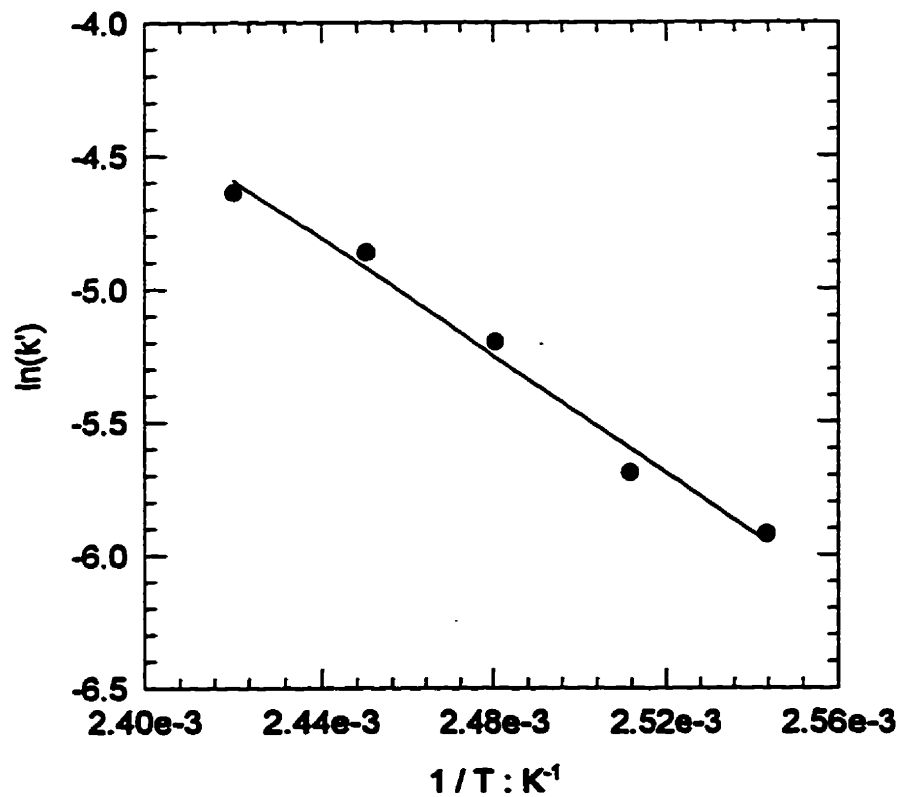

Figure 5.11: Arrhenius plot over the 120°C to 140°C range;
[2a]=80μM, [RCN]=156 mM, P_{H2}=24 bar

The linearity of the Arrhenius plot suggests that a single reaction mechanism supports hydrogenation. Independent hydrogenation processes operating concurrently would produce

a non-linear response as each component would possess a unique activation energy. Mechanisms that use a parallel reaction scheme to rationalize the unusual behaviour of **2a** are therefore inconsistent with the observed temperature response.

5.2.4 Supplementary Kinetic Data

Perturbing a reactive system in a controlled manner may provide useful information regarding the roles of reaction components in the mechanism. In the present work, the response of the osmium system to a variation in the isotope of hydrogen and the nature of its phosphine ligand has been probed. While not a comprehensive review of the influence of additives, the additional data acquired for simple acids and bases have direct relevance to the project objectives. The results of this work are provided in Table 5.4.

Table 5.4: Supplementary Kinetic Data

Catalyst	Variation	$k'*10^3$, s^{-1}
2a	24.2 bar H_2	3.57 +/- 0.19
2a	24.2 bar D_2	2.17 +/- 0.64
2b	24.2 bar H_2	1.41
2b	29.0 bar H_2	3.11
2b	33.9 bar H_2	4.82
2a	2 eq. [NEt_3]	2.91
2a	25 eq. Octylamine	1.54
2a	5.5 eq. Proton Sponge® 1,8-bis(dimethylamino)napthalene	3.55
2a	15 eq. Acetic Acid	1.38
2a	0.4 ml H_2O	3.19

$[Os]_T$=80 μM, [RCN]=172 mM, T=130°C, P_{H2}=24.2 bar unless specified

Deuterium isotope effect

The absolute activation energy of any reaction a complex undergoes is unchanged by an isotope substitution. What is effected is the vibrational energy of the substituted bond, as

its ground state energy is reduced with an increase in the isotope atomic mass. Should the bond be directly involved in the transition state, the replacement of an atom by a heavier isotope (such as deuterium substitution for hydrogen) raises the **relative** activation energy, thereby reducing the reaction rate. In the case of hydrogenation, k'_{H2}/k'_{D2} is a simple indicator for the cleavage of a bond to hydrogen in the rate determining step.

Two trials employing D_2 (99.99% purity; Linde-Union Carbide) were carried out to identify a potential influence on **2a**. The data presented in Table 5.4 demonstrate a kinetic isotope effect, k'_{H2}/k'_{D2}, of 1.64. This clearly establishes the significance of an Os-H bond in the rate determining step of the mechanism.

Hydrogenation activity of the $PiPr_3$ analogue, 2b

In each of the **2b** experiments a preferential hydrogenation of the *cis* isomer of NBR was observed. The first order rate constants obtained for the *trans* olefin reductions indicate that, consistent with the PCy_3 analogue, **2b** is second order with respect to $[H_2]$ over the range of conditions examined. It is interesting to note that the $PiPr_3$ system is incapable of the activity demonstrated by the bulkier tricylcohexylphosphine catalyst system.

Influence of additives on the activity of 2a

Organic acids and bases have been prescribed for use with the group 8 catalysts to improve their selectivity (McManus and Rempel, 1995). Common examples are acetic acid and octylamine, both of which have been screened for an effect on the activity of **2a**. The data indicates that additives capable of associating with the metal centre have a detrimental influence on the hydrogenation rate. Their influence on the product quality is the subject of Chapter 6.

It should be noted that a very strong, non-coordinating base (1,8-bis(dimethylamino) naphthalene) proved to be of no consequence to the reaction rate. The chloride could be eliminated by a mechanism involving the heterolytic cleavage of hydrogen;

$$M\text{-}Cl + H_2 + base \rightarrow M\text{-}H + H^+\text{-}base\ Cl^-.$$

That no change is observed from the addition of the base suggests that such a process is not relevant to this catalytic system.

5.3 Mechanistic Interpretation of the Kinetic Data

By their nature, reactions comprising the catalytic cycle are difficult, if not impossible, to identify for the **2a** system. While the NMR studies of Chapter 4 have characterized important equilibria that act on the periphery of the catalytic cycle, complexes within it are extremely reactive, precluding their isolation or study by standard spectroscopic means. Therefore, a catalytic pathway must be developed, not from direct observations of reaction intermediates, but from inferences on kinetic data and arguments regarding coordination numbers, and electron counting schemes. The ultimate test of a proposed catalytic cycle is its consistency with the kinetic observations. It is therefore subject to review as a greater understanding of the system is developed.

5.3.1 Independently Characterized Elements of the Reaction Mechanism

Besides identifying the prevalent complexes that may exist during hydrogenation, certain elements of the reaction mechanism have been amenable to study by NMR. The activation of **2a** by displacement of O_2 has been demonstrated as well as the propensity of **1a** to coordinate with H_2 and the nitrile residing within NBR. The contribution of this research to the catalytic mechanism is summarized by Figure 5.12.

The competitive coordination of nitrile to **1a** produces the diminished hydrogenation activity that is associated with increased NBR loadings. ^{31}P NMR spectra have provided evidence to support this assertion, while quantifying the **1a-6a** equilibrium for Krynac 38.50. The addition of H_2 to **1a** has also been characterized by NMR, yielding the equilibrium constant K_{H2}. Variable temperature studies of a solution of **1b** with 1.25 equivalents of benzonitrile under 24 bar H_2 suggest that nitrile coordination is favoured

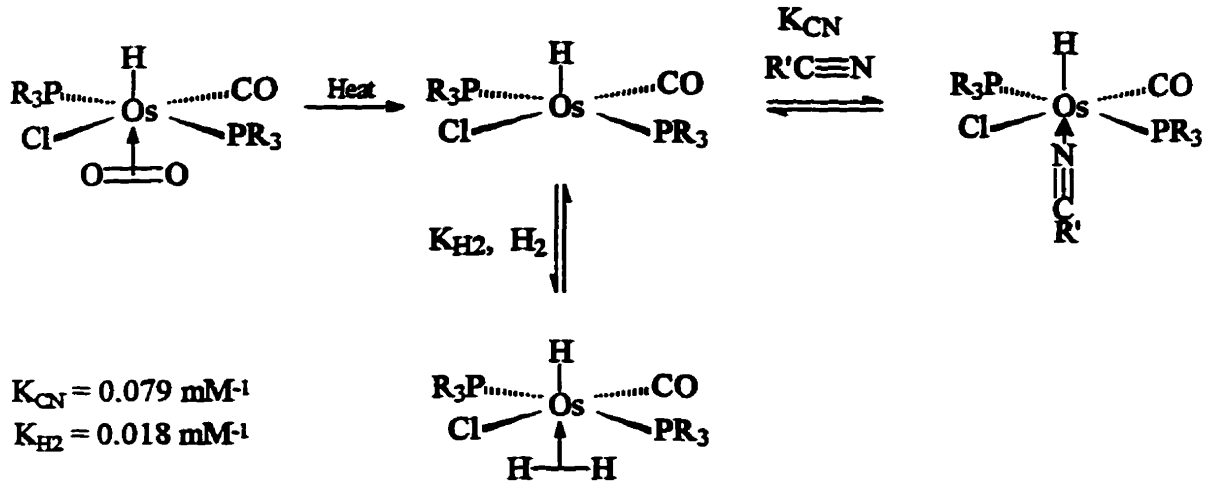

Figure 5.12: Characterized reactions related to NBR hydrogenation; T=130°C.

over H_2 at the temperatures relevant to NBR hydrogenation. However, a more equitable distribution between **3b** and **6b** was observed as the temperature was increased.

The NMR studies have shown that under the conditions employed in the hydrogenation experiments, **6a** and **3a** are the predominate complexes in solution. No other complexes have been detected. Furthermore, the broad singlets observed in the NMR spectra of **1a** when combined with benzonitrile under H_2 indicate that the system is in rapid exchange relative to the NMR timescale. This would suggest that the complexes shown in Figure 5.12 are able to achieve their equilibrium concentrations during hydrogenation.

The role of free PCy_3

As little as one equivalent of PCy_3 added to **2a** had a dramatic effect on its ability to hydrogenate Krynac 38.50. This may be rationalized by two mechanisms; the competitive coordination of PCy_3 to **1a** (Scheme I, Figure 5.13) or the inhibition of a required PCy_3 dissociation from **3a** (Scheme II, Figure 5.13).

$$OsHCl(CO)(PCy_3)_2 + PCy_3 \rightleftharpoons OsHCl(CO)(PCy_3)_3 \qquad \text{Scheme I}$$

$$OsH(H_2)Cl(CO)(PCy_3)_2 \rightleftharpoons OsH(H_2)Cl(CO)(PCy_3) + PCy_3 \qquad \text{Scheme II}$$

Figure 5.13: Plausible mechanisms for phosphine inhibition

The addition of phosphine to a solution of **1a** or **3a** produced no ^{31}P NMR evidence to support the coordination of a third phosphine. Given the severity of the catalytic inhibition by PCy_3 relative to that produced by nitrile (an extremely good ligand for **1a**), it is unlikely that the association of an additional phosphine would produce the effect. There is, however, limited evidence to support Scheme II.

Variable temperature ^{31}P NMR spectra of **1a** under N_2 or H_2 demonstrated no evidence of a monophosphine complex nor any signs of exchange broadening which could be attributed to Scheme II. It is certain, however, that coordinated PCy_3 is labile as it undergoes exchange with free phosphine in solution. Tentative NMR evidence indicates this exchange process could be dissociative in nature, suggesting that a monophosphine transition state may be generated in trace quantities. Were PCy_3 dissociation to facilitate hydrogenation, small amounts of free phosphine would inhibit the formation of the active species, thereby reducing the observed activity. This is considered to be the most plausible explanation for the PCy_3 inhibition effect.

Note that the less sterically encumbered $PiPr_3$ system, **2b**, proved to be less active than the cyclohexyl analogue, **2a**. Were the formation of an active centre to be initiated by PR_3 dissociation, a smaller phosphine of similar electron donating capacity may be expected to yield an inferior hydrogenation rate. Accordingly, a bulky system such as an $PMetBu_2$ complex could provide superior activities than those measured for **2a**.

Founded on the above considerations, a phosphine dissociation step has been incorporated into the hydrogenation mechanism. The exchange studies suggest that this process is slow relative to the hydrogenation rates reported in Section 5.2. Therefore, Scheme II may facilitate the formation of the active complex but cannot be directly involved in the hydrogenation cycle. That is, the catalytic cycle is unlikely to involve PCy_3 loss, olefin transformation, followed by phosphine recoordination.

5.3.2 Inferences on the Mechanism from Kinetic Observations

To this point the discussion has focused upon equilibria acting on the periphery of the hydrogenation cycle. Having few means to characterize the system further, the remainder of the catalytic mechanism must be inferred from the response of the hydrogenation rate to variations in operating conditions.

The conceptually difficult element of the reaction mechanism is the requirement for two molecules of H_2 to either produce an active complex or participate in the rate determining step. Clearly, one molecule is added to **1a** to form the dihydrogen complex **3a**. However, under no conditions was a transformation of **3a** to a classical trihydride complex observed in the ^1H NMR studies of this system. Bakhumutov et al. (1996) have revealed an exchange process between the hydride and dihydrogen ligands of **3b**. However, their relaxation data suggests that a trihydride complex is not formed and could at most be a transition state for the exchange process.

The mechanism illustrated in Figure 5.14 assumes that the dihydrogen ligand of **3a** does not add oxidatively to the metal in such a manner to permit either the insertion of olefin or the reductive elimination of an alkyl ligand. While the η^2-H_2 ligand may indeed participate in the saturation of olefin, it is proposed that it cannot do so in the absence of a second molecule of hydrogen. This non-traditional theory is required to rationalize the unconventional behaviour observed for the **2a** system.

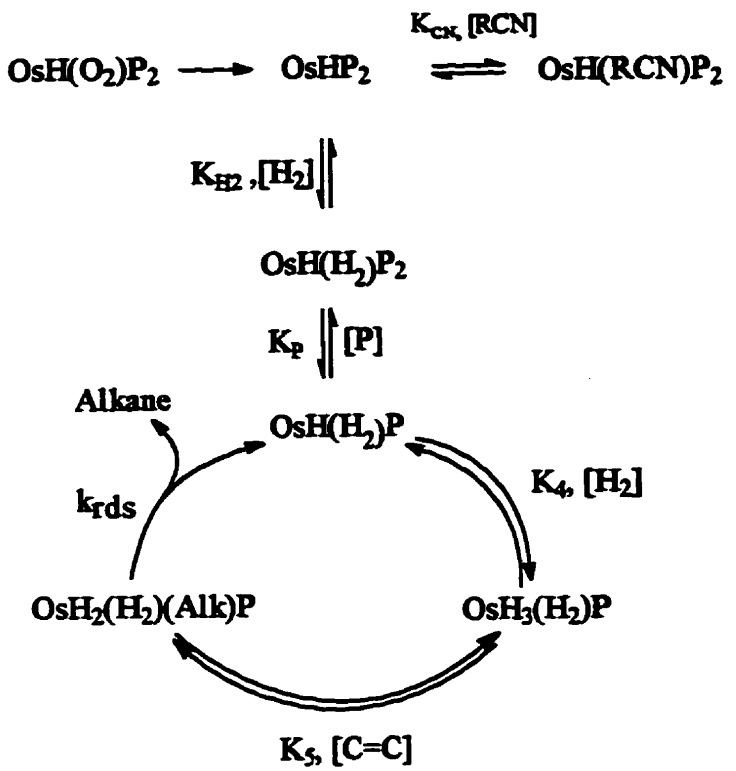

Figure 5.14: Proposed mechanism for NBR hydrogenation by **2a**

A deuterium isotope effect of 1.64 indicates that the rate determining step of the cycle involves the cleavage of a bond to hydrogen. This could be an insertion of olefin into an Os-H bond or a reductive elimination of an osmium-alkyl to yield the saturated product. The proposed mechanism suggests that the addition of olefin is a concerted addition-insertion into the hydride. In assigning a rate determining step, no discrimination between the insertion and elimination process has been made.

According to the proposed mechanism, the hydrogenation of olefin by **2a** abides by the following rate expression,

$$-\frac{d[C=C]}{dt} = k_{rds}\,[OsH_2(H_2)(Alk)P]\ . \qquad 5.1$$

Applying a steady state assumption to each of the equilibria leading to the formation of $[OsH_2(H_2)(Alk)P]$ provides a means of relating the concentrations of every species to the rate determining step. A mass balance on the total amount of osmium charged to the system, $[Os]_T$ yields the concentration of the active centre as a function of the total amount of **2a** charged to the system. A full derivation of the resulting rate expression is provided in Appendix IV;

$$-\frac{d[C=C]}{dt} = k_{rds}\,[OsH_2(H_2)(Alk)P]$$

$$= k_{rds}\frac{K_{H2}K_PK_4K_5\,[Os]_T\,[H_2]^2\,[C=C]}{[P](1+K_{CN}[CN]+K_{H2}[H_2]) + K_{H2}K_P[H_2] + K_{H2}K_PK_4[H_2]^2\,(1+K_5[C=C])} \qquad 5.2$$

The functional form of this rate expression is consistent with the behaviour of the **2a** system observed throughout the kinetic and NMR investigations.

The derived rate equation (5.2) suggests that unique responses observed in the kinetic studies represent limiting cases of the overall catalytic chemistry of **2a**. For example, the coordination of nitrile to **1a** is anticipated to produce more than a simple inhibitory effect. Being the dominant equilibrium in the mechanism, nitrile coordination may produce the observed second order dependence of the reaction rate with respect to hydrogen. Under conditions where $K_{CN}[P][RCN]$ is the predominant term of equation 5.2, the rate expression may be reduced to the form,

$$-\frac{d[C=C]}{dt} = \frac{\alpha\,[Os]_T\,[H_2]^2\,[C=C]}{\beta + K_{CN}[P][RCN]}$$

which is first order with respect to olefin and second with respect to $[H_2]$.

As the system pressure was increased, the behaviour of the **2a** system with respect to NBR hydrogenation became more complicated. The mechanism suggests that the system was no longer dominated by nitrile as the equilibria governing H_2 coordination became more

prevalent. A shift to a lower order is anticipated, culminating in a zero order dependence as extreme pressures are employed. Consistent with the high pressure NBR experiments, this shift in H_2 order is accompanied by a reduction in that of olefin.

The hydrogenation of olefins lacking nitrile functionality was unaffected by the concentration of H_2 as demonstrated for SBR and 1-decene reduction. Without nitrile in the system, equation 5.2 reduces to a form that represents a dramatic departure in the observed kinetics. As the concentrations of **6a** and **1a** are no longer significant to the mechanism at these conditions, equation 5.2 assumes the form;

$$-\frac{d[C=C]}{dt} = k_{rds}\frac{K_{H2}K_PK_4K_5\,[Os]_T\,[H_2]^2\,[C=C]}{[P] + K_{H2}K_P[H_2] + K_{H2}K_PK_4[H_2]^2\,(1+K_5[C=C])}.$$

It is clear that a zero order response with respect to $[H_2]$ is rationalized by this reduced form of the general case. Therefore, it may be contended that the catalytic cycle which underlies this rather simple behaviour is more complex than anticipated by Esteruelas et al. (1992).

In the process of developing the reaction mechanism a great many variations have been considered, none of which were consistent with the kinetic data. A reaction pathway in which olefin could be added to the monophosphine complex **prior** to the coordination of the second H_2 molecule (Figure 5.15) yields a rate expression of the form,

$$-\frac{d[C=C]}{dt} = k_{rds}\,[OsH_2(H_2)(Alk)P]$$

$$= k_{rds}\frac{\alpha\,[Os]_T\,[H_2]^2\,[C=C]}{[P]\,(1 + K_{CN}[RCN] + K_{H2}[H_2]) + K_{H2}K_P[H_2] + \beta[C=C][H_2]\,(1 + \gamma[H_2])}$$

This states that a zero order dependence on $[H_2]$ must be accompanied by a zero reaction order with respect to [C=C], a fact that is not born out in experimental data for SBR and decene hydrogenation.

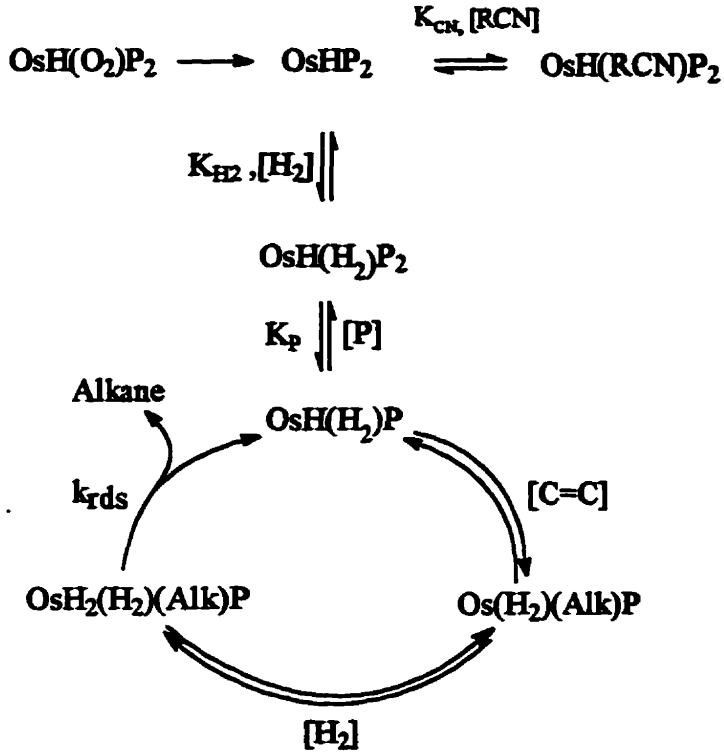

Figure 5.15: Alternative mechanism involving olefin coordination prior to H_2 addition

The strength of the proposed mechanism lies in its ability to rationalize the kinetic data without violating generally accepted arguments on feasible coordination numbers and electron counting schemes. While it is both unprecedented and unconventional, the proposal is no more so than the reliable kinetic data from which it is derived. Nevertheless, the mechanism is a provisional one. Further research into the role of phosphine in the system as well as the means by which **1a** activates molecular hydrogen is required to substantiate key assumptions. Until such time as these studies are carried out, the catalytic cycle presented in Figure 5.14 must be classified as tentative.

Chapter 6

Chemical Aspects of NBR Hydrogenation Selectivity

The Group 8 catalyst systems of the form, $MHCl(CO)(PCy_3)_2$ (**1a** M=Os; **7** M=Ru) have a number of advantages over the existing rhodium technology. In first place, the cost and price volatility of Os and Ru are substantially less than that of rhodium metal. Secondly, whereas the rhodium systems demand the addition of PPh_3, neither **1a** nor **7** require excess phosphine to maintain their stability at high temperatures and pressures. The osmium analogue has the further advantage of superior catalytic activity. Nevertheless, this new generation of HNBR catalysts has failed to displace the commercial Rh system due to the prevalence of an undesirable side reaction.

Unacceptable selectivity has plagued ruthenium catalyst development efforts from their onset. Although spectroscopic analysis revealed no evidence of substantial nitrile reduction, McManus and Rempel (1991) observed inordinately high intrinsic and Mooney viscosities of HNBR prepared using **7**. This signifies an increase in the molecular weight of the material from the chemical crosslinking of polymer molecules. The problem is particularly severe for PPh_3 complexes such as $RuCl_2(PPh_3)_3$ (Buding et al., 1991) and $RuHCl(CO)(PPh_3)_3$ (Rempel et al., 1989) which may crosslink HNBR to the point of gelation. Once compromised to this degree, the product has a virtually infinite molecular weight. This may complicate or preclude processing operations such as injection moulding, compounding and extrusion.

That a side reaction whose products are created in trace amounts may be responsible for gross changes in product quality is due to the high molecular weight of NBR. Given the material's molecular weight of approximately 150,000, a single crosslinking event could produce a molecule having an M_n of 300K. A second event occurring along the polymer chain (which now contains approximately 5500 monomer units) would produce a molecule with an M_n of 450K. Obviously very few crosslinking events are capable creating an unmanageable material, a fact which complicates efforts to characterize the process.

To date there have been no direct attempts to ascertain the structure of an HNBR crosslink or the mechanism by which one is created. McManus and Rempel (1995) suspected a metal catalyzed reduction of nitrile to be responsible for the process (Figure 6.1). This mechanism, first derived by von Braun et al. (1923) in a study of alkyl nitrile hydrogenation, has received tentative support from Martin (1991). In the course hydrogenating heptylcyanide using nickel salts at 20 bar H_2 and 120°C, von Braun and his coworkers reported a significant production of secondary amine. By this mechanism, polymer crosslinking could result from the addition of fully reduced nitrile to an imine intermediate located on a second polymer chain.

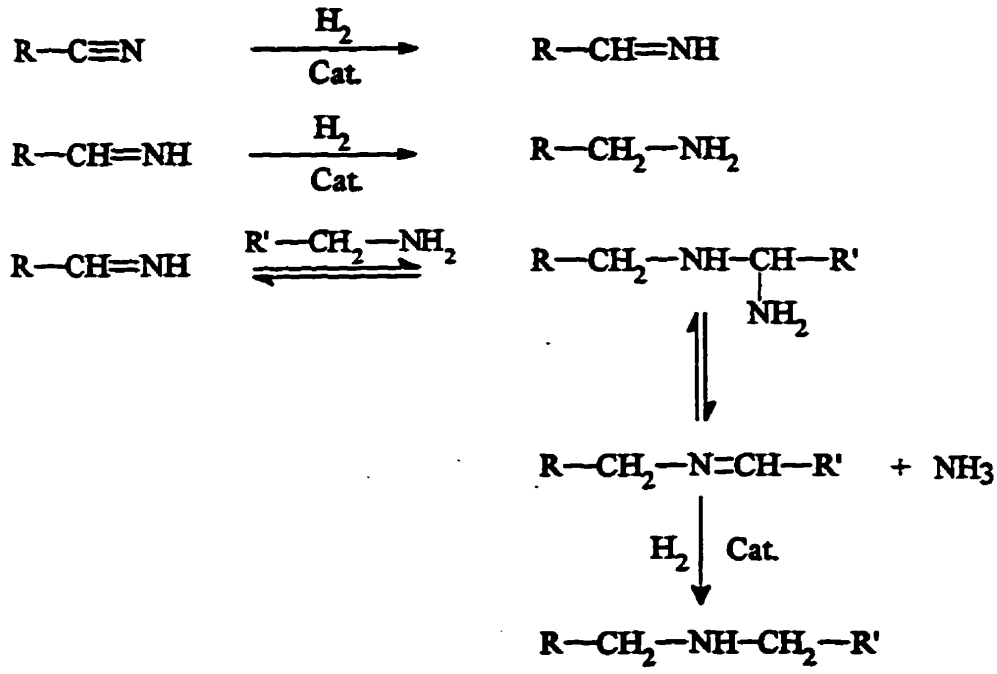

Figure 6.1: von Braun mechanism for NBR crosslinking

Strategies designed to minimize the crosslinking proficiency of 7 have had considerable success. McManus and Rempel (1991) have demonstrated the efficacy of primary amine additives to reduce the Mooney viscosity of HNBR produced by aryl and alkyl phosphine complexes of ruthenium. By competing with reduced nitrile for reactive imine sites, compounds such as octylamine are believed to yield benign amine additions. A second

approach employs organic or inorganic acid additives such as acetic acid (Rempel et al., 1993a) or ammonium sulfate (Rempel et al., 1993b). Both were found to control crosslinking by a mechanism presumed to involve the hydrolysis of imine or the protonation of amine to an inert ammonium salt (McManus and Rempel, 1995).

Although additives have improved the product quality derived from the ruthenium catalysts, they have not satisfied industrial concerns about selectivity. Given the cost of producing several tonnes of unmarketable product, a commercial process must eliminate crosslinking altogether. This would ensure a uniform product quality irrespective of process upsets or operator variability.

At present, neither the ruthenium nor osmium system has been developed to the point where the existing technology may be supplanted. The research detailed in this chapter quantifies the propensity of **2a** to crosslink NBR and provides mechanistic information on the selectivity of Group 8 catalysts in general. A direct assessment of the product quality derived from **2a** relative to that produced by rhodium(I) phosphine catalysts is presented. In addition, kinetic data on the evolution of polymer crosslinking and the efficacy of additives is interpreted within the context of plausible reaction mechanisms.

6.1 Experimental Methodology

Estimating the crosslink density of a sample is complicated by their infrequent appearance in a manageable sample. As discussed previously, the sensitivity of spectroscopic techniques is insufficient to detect the small number of crosslinks required to produce an undesirable viscosity. Therefore, the degree of polymer crosslinking must be inferred indirectly from molecular weight measurements. While not identifying the structure of crosslinks or their numerical frequency, the technique does characterize the process in a semi-quantitative manner.

In the present work, dilute solution viscosity has been used to monitor the shifts in molecular weight that are created by crosslinking. The method has the drawback of an

ambiguous relationship of viscosity (η) to molecular weight, especially for copolymers with composition or structural dispersity. Nevertheless, the space occupied by a macromolecule in solution is related to its molecular weight and evident in the solution's viscosity. Therefore, the viscosity of a dilute NBR solution relative to pure solvent (η_{rel}) provides a simple and effective means of measuring the consequences of crosslinking.

Having quantified the degree of crosslinking using η_{rel}, it is necessary to define an appropriate measure of the process selectivity. Throughout this work, a catalyst which produces no crosslinking is defined as completely selective for the transformation of NBR to a desirable HNBR product. The indicator used to quantify selectivity is the dilute solution viscosity of fully saturated (>98% hydrogenated) product. This designated viscosity, η_{rel}^{*}, represents the amount of crosslinking produced over the time taken to complete the hydrogenation process.

Unfortunately, η_{rel}^{*} is not a direct measure of the number of crosslinks in a sample and therefore has little meaning when viewed in isolation. However, η_{rel}^{*} measured as a function of the concentration of catalyst, H_2 and nitrile used in the hydrogenation can define the influence of these factors on the process selectivity. They also provide a means of comparing the performance of different catalyst systems. This was the rationale for measuring the η_{rel}^{*} of HNBR produced by **2a** as well as $RhCl(PPh_3)_3$ and $RhH(PPh_3)_3$ over a range of operating conditions. These data are presented in Section 6.3.1.

While selectivity measurements are essential to process design, they yield limited information on the evolution of crosslinking with time. Information of this sort requires measuring η_{rel} during the course of a hydrogenation and beyond 99.5% olefin conversion. Detailed in Section 6.3.2 is a series experiments which monitor the solution viscosity produced by the Rh, Ru and Os catalysts as a function of time. By examining η_{rel} as a time-evolving variable, a rudimentary understanding has been gained of the means by which crosslinks are formed and how this process may be curtailed.

6.2 Experimental

6.2.1 Materials

$RhCl(PPh_3)_3$, $RhH(PPh_3)_4$ and $OsHCl(CO)(O_2)(PCy_3)_2$ were prepared by the methods detailed in Chapters 3 and 5. The procedure employed by Martin (1991) was used to prepare $RuHCl(CO)(Sty)(PCy_3)_2$. Chlorobenzene and 2-butanone were used as received from Fisher Chemical Company. A single batch of acrylonitrile-butadiene copolymer (Krynac 38.50 from Bayer Rubber Inc.) was used without purification.

6.2.2 Sample Preparation Procedures

The procedures used to hydrogenate NBR were identical to those described in Chapter 3. However, two variations of sample collection were employed. The first series of samples comprise HNBR produced in the kinetics studies of Chapters 3 and 5. The progress of these hydrogenations was monitored by the gas uptake apparatus. Once H_2 consumption ceased (indicating >98% olefin hydrogenation), the reactor was brought to 50°C in about 10 minutes by activating the cooling system. The autoclave pressure was then vented and the sample isolated by precipitation with ethanol. This product was dried at 60°C under an aspirator vacuum (about 17 inHg) for 3 days. Analysis of this series of samples provided the selectivity data (η_{rel}^*) discussed in Section 6.3.1.

The second series of samples were collected at regular intervals during an hydrogenation reaction rather than at its completion. Access to the liquid phase was obtained by removing the H_2 uptake measurement equipment from the autoclave and installing a dip tube with a sampling valve. Approximately 16 cm^3 of polymer solution constituted each sample. All samples were precipitated with 100 cm^3 of ethanol immediately after collection to limit the exposure of dissolved olefin to the atmosphere at the reaction temperature. This HNBR was then pressed to remove solvent, washed with a further 10 cm^3 of ethanol and dried at room temperature under high vacuum for 3 days.

6.2.3 Product Characterization

Samples having <10% residual olefin were assigned a definite conversion by the infra-red method of Marshall et al. (1990). This included samples collected for the selectivity studies and those isolated in the latter stages of the crosslinking kinetic work. Low conversion samples were analyzed by ^1H NMR in $CDCl_3$ on a Bruker AC-300 spectrometer.

To assess the solution viscosity of a given polymer, 0.25000 +/- 0.00015g of the material was weighed and transferred to a 25 cm^3 volumetric flask. Approximately 15 cm^3 of 2-butanone was added and the flask shaken for 3 days. Experience showed that highly crosslinked samples required such an extended dissolution time. Therefore, the 3 day period was consistently observed for all samples. Once dissolved, the volume was brought to precisely 25 cm^3 and the solution was mixed thoroughly. This sample was then transferred to a Ubbelohde capillary viscometer through a coarse, sintered glass filter. This coarse filtration removed particulate and provided a means of detecting insoluble gel. Samples containing any insoluble HNBR could not be analyzed by viscometry. Raw data consisted of two measurements of the time required for the constant volume of solution to drain through the viscometer capillary. All viscosities were carried out at 35°C and reported as the elution time of the sample relative to that of pure 2-butanone at this temperature.

6.3 Results and Discussion

6.3.1 Selectivity of Osmium and Rhodium Catalyzed Hydrogenations

Measurements of η_{rel}^* have defined the selectivity of the osmium and rhodium catalysts over the range of conditions listed in Table 6.1. Direct comparisons of different η_{rel}^* estimates are valid, in that all of the HNBR analyzed had been fully saturated and therefore shared a common polymer backbone composition. As a result, an increase in η_{rel}^* reflects a rise in the degree of crosslinking alone. Figures 6.2 to 6.4 illustrate the selectivity as a function of the type and amount of catalyst as well as the hydrogen pressure and nitrile loading employed.

Table 6.1: Operating conditions for the selectivity studies

[Catalyst]:	20 μM - 155 μM
H_2 Pressure:	4.5 bar - 42 bar
[Nitrile]:	46 mM - 255 mM
Temperature:	
- Osmium Study:	130°C
- Rhodium Study:	145°C

Unfortunately, the precision of the measurements were compromised by an incomplete drying of the isolated polymer. The use of approximately 17 inHg of vacuum at 60°C may have been insufficient to remove residual chlorobenzene from all samples. This would result in a slight weighing error in the preparation of a solution for viscosity analysis. Nevertheless, the data does reveal definitive trends which may be interpreted as real effects.

In so far as the rhodium complexes produce the lowest viscosities of the known HNBR catalysts, they represent the standard for process selectivity. The η_{rel}^* measurements presented in Figures 6.2 to 6.4 indicate that irrespective of the reaction conditions employed, these catalysts produce a product of uniform quality. From an engineering standpoint this is favourable, as a rhodium process does not require accurate control strategies to yield a standard, marketable material. It should be noted that no statistically significant difference is observed between $RhCl(PPh_3)_3$ and $RhH(PPh_3)_4$.

The viscometric and spectroscopic analysis suggest that the Rh technology is completely selective for the hydrogenation of olefin in the presence of nitrile. This is in agreement with Yoshida et al. (1979) who have observed $RhCl(PPh_3)_3$ to be incapable of catalyzing alkyl nitrile hydrogenation. However, $RhH(PiPr_3)_3$ proved to be an efficient catalyst for this reaction. It is interesting to note that $RuHCl(CO)(PCy_3)_2$ crosslinks HNBR to a much lesser extent than its PPh_3 analogue (Rempel et al., 1991).

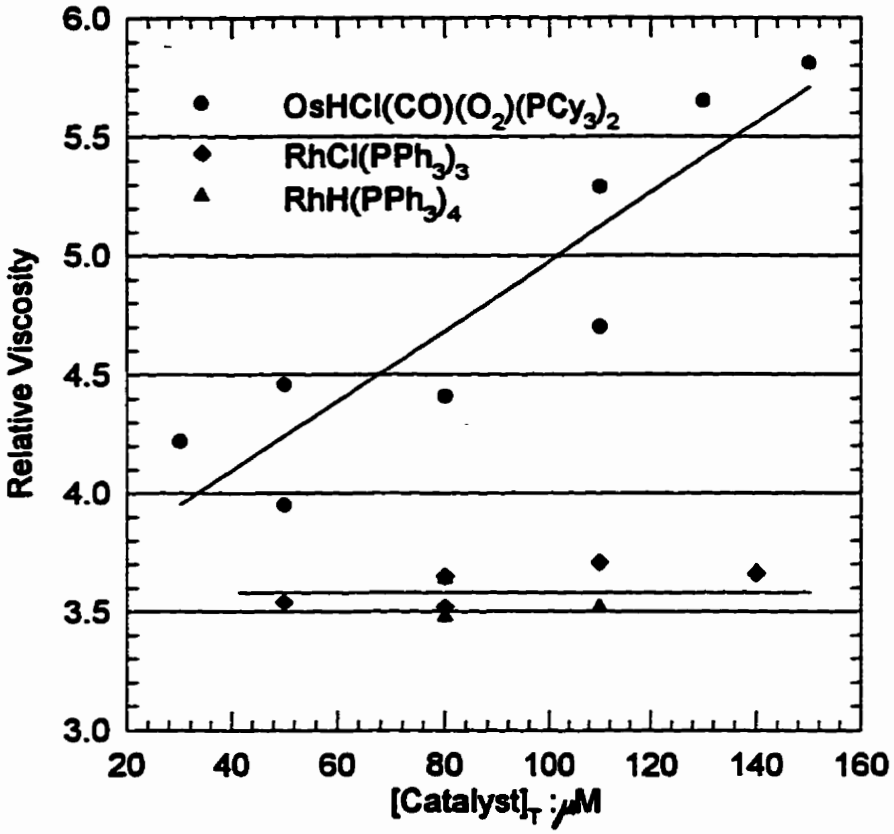

Figure 6.2: Selectivity as a function of total metal loading; [RCN]=172 mM, P_{H2}=24 bar

The η_{rel}^{*} data estimates in Figures 6.2 to 6.4 illustrate that under the conditions studied, **2a** was incapable of providing the selectivity demonstrated by the rhodium technology. Figure 6.2 indicates that the problem escalated as the catalyst loading was increased. This suggests that crosslinking must have a metal-catalyzed component. Therefore, the product quality cannot be improved by arbitrary measures designed simply to enhance the hydrogenation rate. If crosslinking were entirely non-catalytic, the selectivity could be improved by any means of improving the rate of hydrogenation, including employing more catalyst. Furthermore, barring any influence of the additional PPh_3, one might expect to observe crosslinking during the rhodium experiments.

Given the strong dependence of the hydrogenation rate on the system pressure (Chapter 5), that the relative rates of crosslinking and hydrogenation could be influenced disproportionately by a variation of $[H_2]$ is not unexpected. The limited data presented in Figure 6.3 demonstrates a substantial improvement in the selectivity of **2a** from the use of higher reaction pressures. Samples produced below 13 bar contained gelled polymer which was insoluble in 2-butanone at room temperature. While the trend toward lower η_{rel}^{*} is encouraging, it is unlikely that the selectivity of the osmium system can be improved to the level of the rhodium technology simply by increasing the reaction pressure.

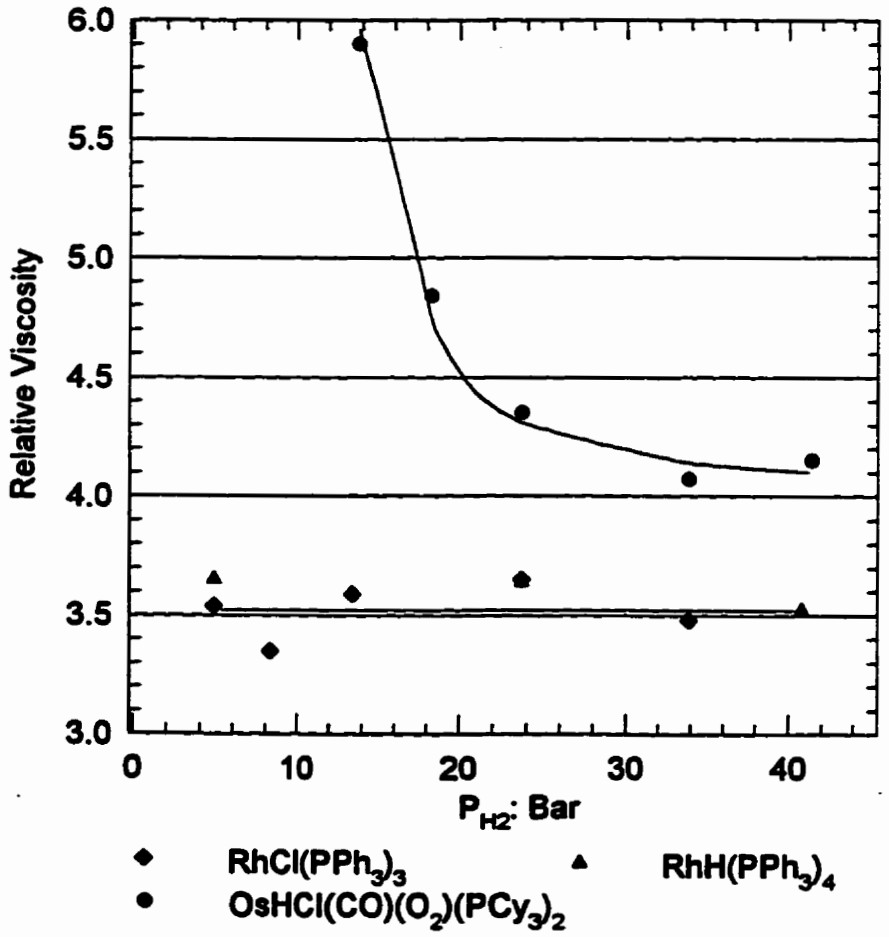

Figure 6.3 Influence of pressure on selectivity; [metal]=80μM, [RCN]=172 mM

Less favourable is the influence of polymer loading on η_{rel}^{*} (Figure 6.4). Over the limited range of concentration studied, the **2a** product viscosity increased as more nitrile was

charged to the process. This is consistent with the von Braun mechanism which assigns responsibility for crosslinking to the catalytic reduction of nitrile. An elevated [RCN] would therefore be expected to promote gelation. It is also possible that the coordination of nitrile has a more potent influence on the hydrogenation activity than on crosslinking. According to this argument, crosslinking need not involve nitrile in any form to produce a shift in selectivity. The relevance of potential nitrile hydrogenation mechanisms is discussed further in Section 6.4.

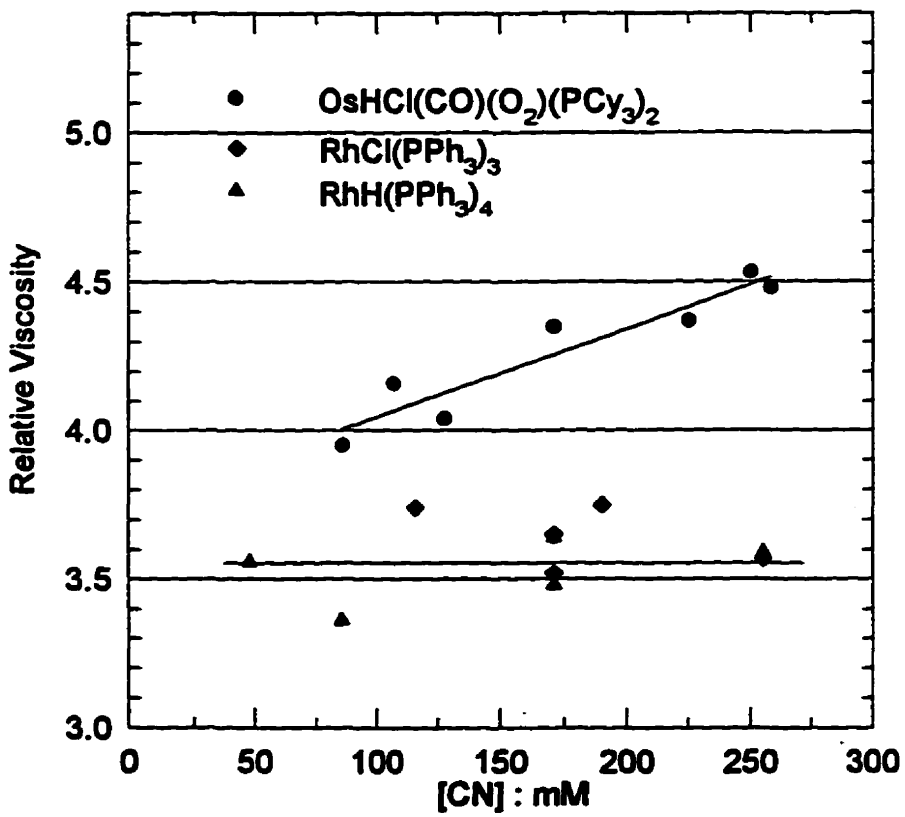

Figure 6.4: Selectivity as a function of NBR loading; [metal]=80μM, P_{H2}=24 bar

The relationship between η_{rel}^{*} and [RCN] appears to be a linear over the narrow range of conditions studied. However, given the limited amount of data and its variability, it is uncertain that the linearity holds over a wider domain. In fact, McManus et al. (1996) have revealed the potential of **2a** to produce an acceptable product at nitrile loadings that are four times the maximum shown in Figure 6.4, albeit at 83 bar and $[Os]_T$=20μM.

Although the selectivity of **2a** is not ideal, the data indicates that the process may be optimized through a judicious choice of operating conditions. From an economic standpoint it is desirable to minimize the amount of **2a** while utilizing a high reaction pressure and temperature to maintain an acceptable rate of hydrogenation. The selectivity data suggests this strategy would improve the product quality as well. Based on the limited nitrile data, operating at high NBR loadings could be problematic. However, more research is required to define the viscosity-nitrile relationship over a wider range of RCN concentration.

6.3.2 Preliminary Evaluation of Crosslinking Kinetics

A knowledge of how crosslinking evolves with time requires the periodic sampling of an HNBR solution both during and after the completion of the hydrogenation process. However, interpreting the viscosity of unsaturated HNBR is not straightforward. Hydrogenating the residual olefin in the polymer backbone alters both the solubility and the conformation of the molecule in solution. As a result, the viscosity of HNBR increases with olefin conversion in a manner that is independent of polymer crosslinking. This would preclude a direct assignment of η_{rel} to crosslinking were an appropriate correction not available.

Given the proven selectivity of $RhCl(PPh_3)_3$, a correlation between η_{rel} and the conversion of Krynac 38.50 can be defined in the absence of crosslinking. The η_{rel} versus conversion profile of $RhCl(PPh_3)_3$ has therefore been measured by periodically sampling an hydrogenation experiment. This relationship (illustrated in Figure 6.5) can be used to decouple the conversion dependence from η_{rel} measurements acquired in the osmium and ruthenium trials. The data were derived from two experiments employing $[RhCl(PPh_3)_3]$=95 μM, $[PPh_3]$=6.1 mM, [RCN]=917 mM, P_{H2}=83 bar at a temperature of 140°C.

According to the proposed nitrile reduction mechanism for crosslinking by the Group 8 catalysts (Figure 6.1), η_{rel} is expected to rise sharply during the hydrogenation as a result of

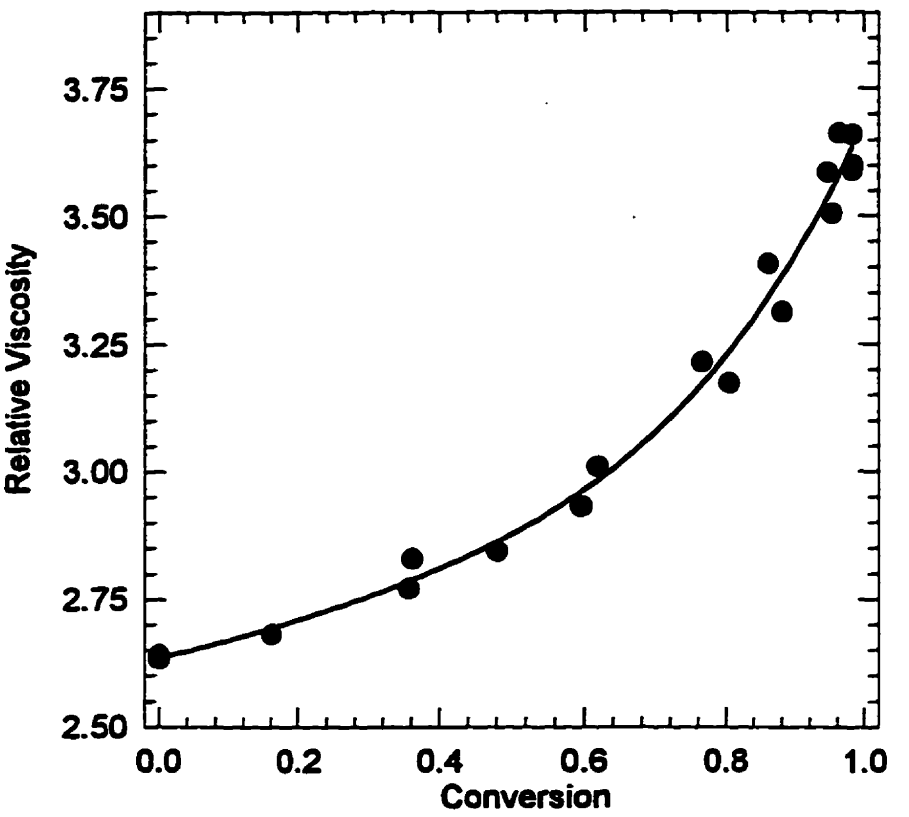

Figure 6.5 η_{rel} verses conversion produced by $RhCl(PPh_3)_3$

the conversion effect and continue to increase beyond 100% olefin hydrogenation. The η_{rel} versus time data for **2a**, comprised of four independent trials, is therefore unexpected (Figure 6.6). The broken line reflects the viscosity that a sample of HNBR with an equivalent conversion would have if produced by $RhCl(PPh_3)_3$. A third order polynomial regression of the rhodium η_{rel} versus conversion data (Figure 6.5) was used to derive the predicted profile from the **2a** conversion data.

In comparing the osmium η_{rel} data to the rhodium projections, it is clear that crosslinking occurs during all stages of the hydrogenation. However, beyond 99.5% conversion the viscosity approaches an asymptotic limit rather than continuing to increase. Therefore, η_{rel}

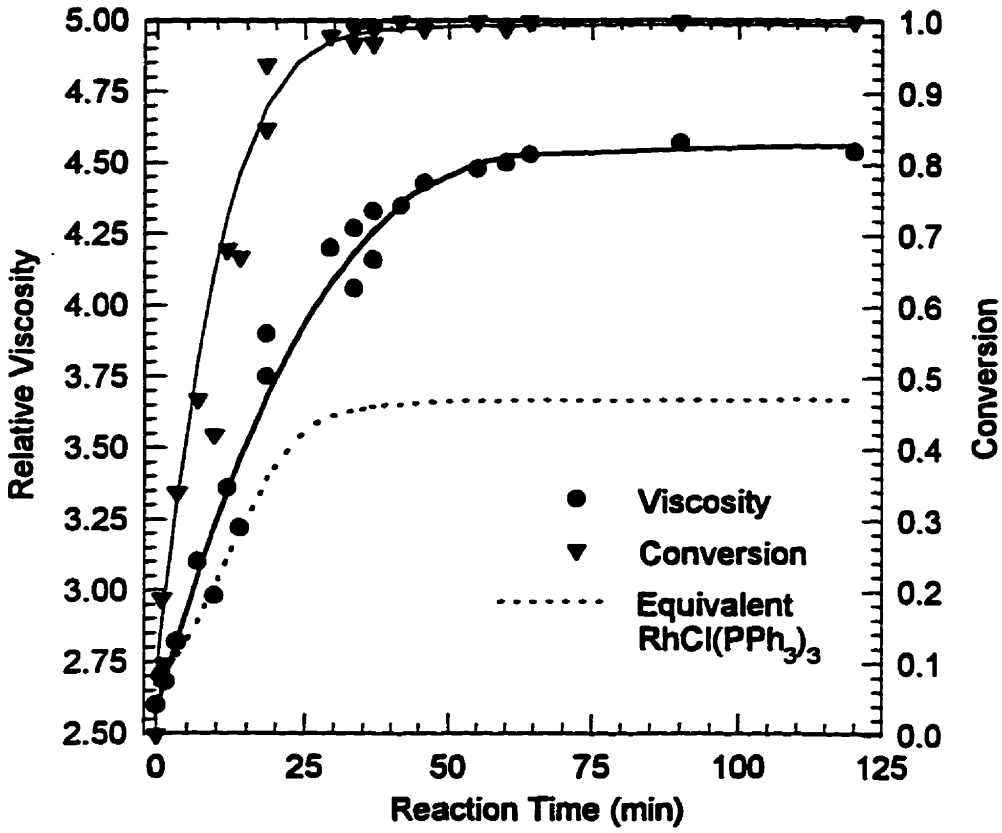

Figure 6.6: Conversion, η_{rel} versus time profiles; [2a]=80 μM, P_{H2}=23.7 bar, [RCN]=249 mM, T=130°C.

may be related to the degree of olefin conversion, which strongly suggests that crosslinking involves residual C=C reactivity.

To support this observation, fully saturated HNBR that had been isolated from an earlier osmium experiment was exposed to [Os]=80 μM, P_{H2}=23 bar, T=130°C for one hour. Based on the selectivity data presented in Section 6.3.1, this treatment should raise the viscosity to the point of gelation. In fact, no large-scale gel was formed.

Additional support for an olefin dependence was sought from the ruthenium catalyst, **7**. Having been the subject of an intense search for viscosity reducing additives, there exits a

broader knowledge of the crosslinking behaviour of this catalyst. Two independent experiments using this system are presented in Figure 6.7. Consistent with the osmium response, η_{rel} approaches a limit once hydrogenation is complete. In this case the viscosity parallels the conversion profile more closely than witnessed for **2a**. Note that a reaction temperature of 160°C was applied to compensate for the disparity between the hydrogenation activities of the ruthenium and osmium analogues.

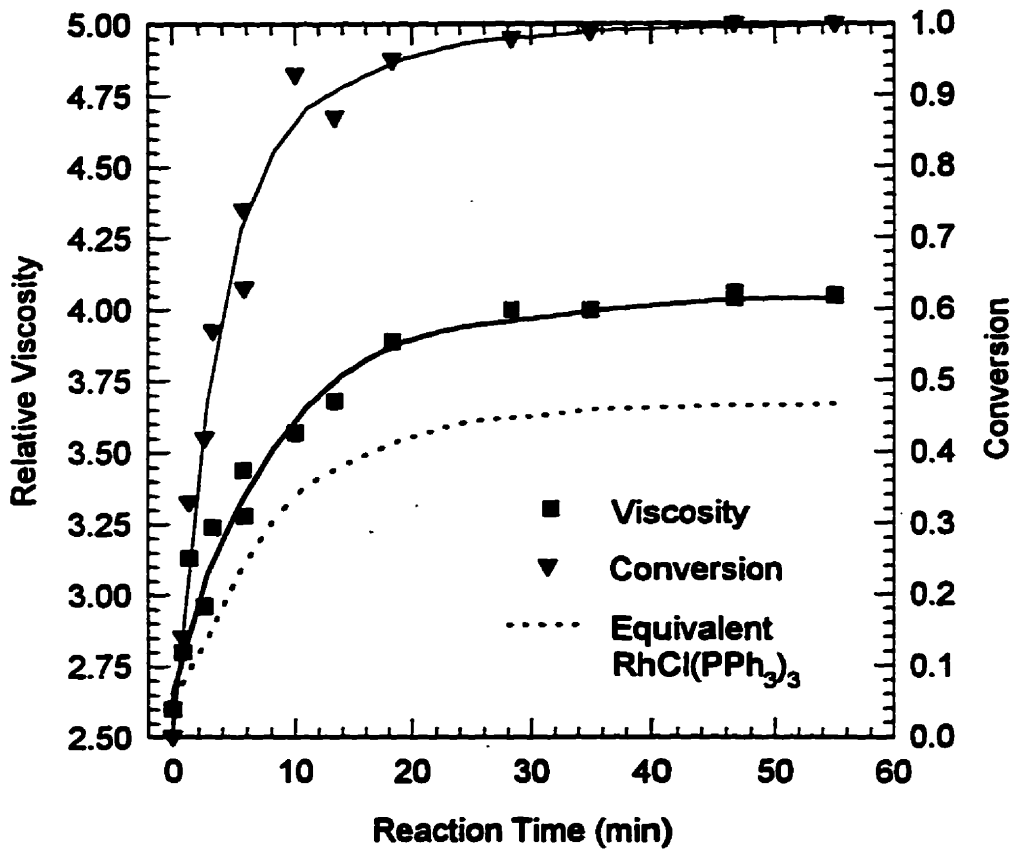

Figure 6.7: Conversion, η_{rel} versus time profiles; [7]=80 μM, P_{H2}=41 bar, [RCN]=249 mM, T=160°C

6.3.3 Efficacy of Viscosity Modifying Additives

Despite the remarkable activity of the osmium technology, its poor selectivity is likely to prevent its commercial acceptance without the advent of selectivity enhancing additives. McManus and Rempel (1991) have proven the efficacy of C_1-C_{20} primary amines to

enhance the performance of the ruthenium analogue. They suggested amine loadings below 1wt% relative to polymer were capable of significant viscosity reductions. Therefore, the impact of 1% octylamine on the selectivity of **2a** has been assessed. The results are presented in Figure 6.8.

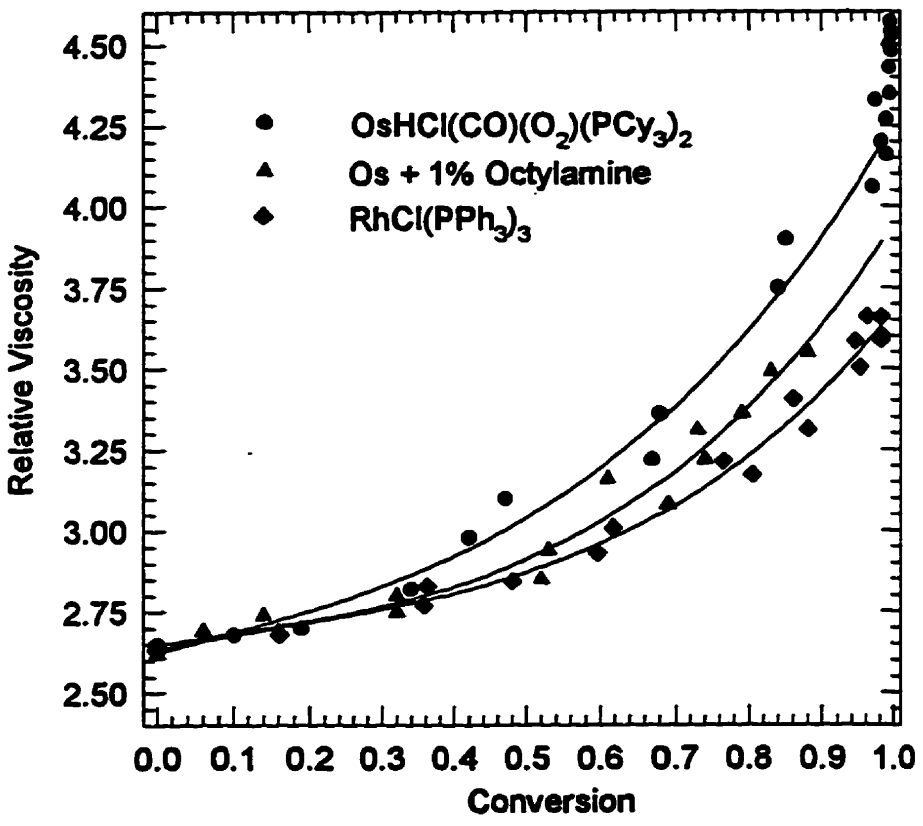

Figure 6.8: Influence of octylamine on HNBR viscosity

It is apparent that the primary amine reduced η_{rel} over the entire range of olefin conversion but could not produce HNBR of the quality created by $RhCl(PPh_3)_3$. Furthermore, the amine treatment was observed to inhibit the hydrogenation activity of the osmium system by nearly 50%. Subsequent work has confirmed the necessity of having the amine present during the hydrogenation, as its addition after 99.5% conversion was ineffective.

6.4 Interpretation of the Crosslinking Results

It is quite clear that the von Braun mechanism for secondary amine formation cannot account for the viscosity data presented in Figures 6.6 and 6.7. Nevertheless, it has provided a useful framework for the development of effective additives such as octylamine. Having acquired new information, it is necessary to propose a revised interpretation of the crosslinking process which will hopefully be equally serviceable. The ultimate objective is to understand the problem while designing a cost effective solution.

An alternate mechanism involves the nucleophilic addition of a primary amine to an activated olefin (Figure 6.9). As both of these reagents are lacking in the starting material, they must be produced by catalytic means. With respect to primary amine, there is no evidence to support á large-scale reduction of nitrile. However, there is a precedent for positional isomerization of olefins by $OsHCl(CO)(PiPr_3)_2$. Esteruelas et al. (1989) have reported the migration of olefin within 1,4-cyclohexadiene to the 1,3 position under either an N_2 or an H_2 atmosphere. Martin (1991) has direct evidence for the $RuHCl(CO)(Sty)(PCy_3)_2$ catalyzed migration of the residual olefin of NBR to a nitrile conjugated position.

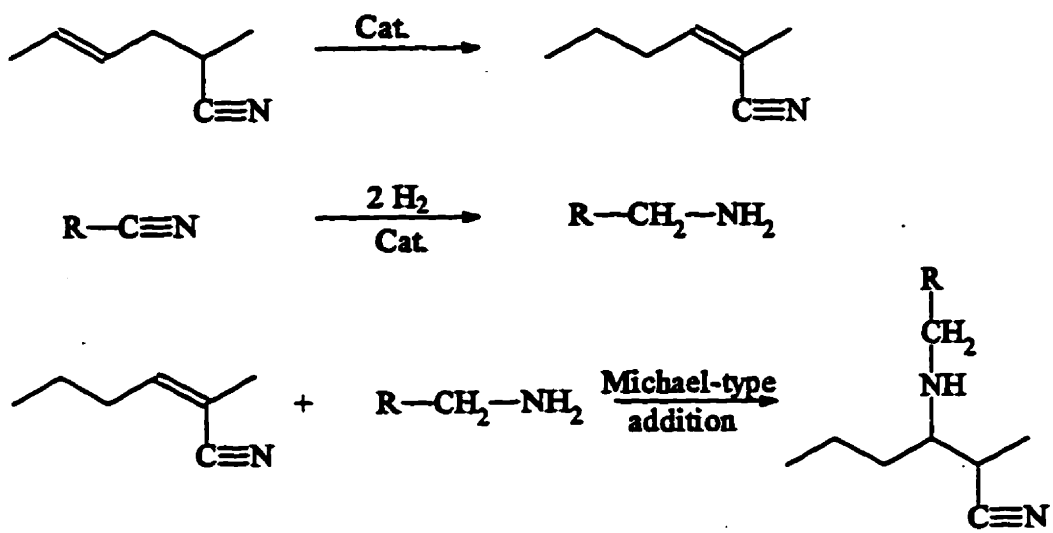

Figure 6.9: Michael-type addition mechanism for NBR crosslinking

The conjugated NBR system has a distinctive IR stretch at 2214 cm^{-1} that is 21 cm^{-1} lower in frequency than that of the standard nitrile. This has provided a means of monitoring its development by the ruthenium analogue. Figure 6.10 demonstrates the catalytic migration process observed at low hydrogen pressures. The conjugated system is not developed to an amount detectable by infra-red when more severe pressures are used.

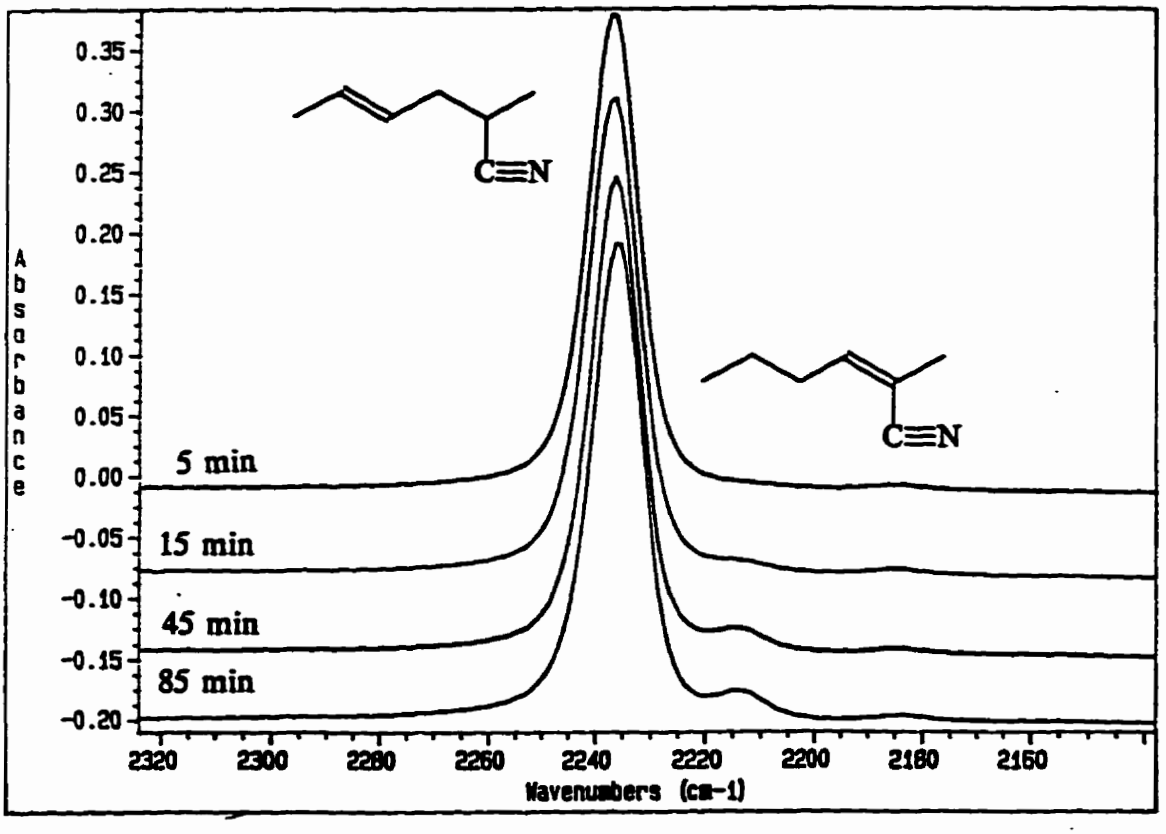

Figure 6.10: IR evidence for olefin migration within NBR
[7]=200μM, P_{H2}=7 bar, [RCN]=172 mM, T=160°C.

The Michael-type addition mechanism can account for the observations noted in this crosslinking study. The selectivity data of Section 6.3.1 demonstrated that elevated catalyst loadings compromised selectivity despite improving the hydrogenation rate. This suggests that the crosslinking process contains a catalytic component which, by the Michael-type addition mechanism, would involve both the reduction of nitrile to amine and the isomerization of olefin to a conjugated position. The efficacy of amine and acid additives may be rationalized in much the same manner as was assumed for the von Braun process.

Final verification of the model requires a demonstration of the ability of a primary amine to add to the activated olefin that may be created within HNBR.

Two approaches were taken to explore the addition process. In the first trial, the experimental conditions used to produce Figure 6.10 were repeated with 1% octylamine present. While the rate of hydrogenation was diminished, IR spectra of samples were comparable to those shown in Figure 6.10. That is, no significant loss of conjugated olefin could be detected. The second attempt involved charging a large excess of amine once all unactivated olefin had been hydrogenated. Once again, no evidence to support the addition of amine to the activated olefin was observed in the IR. These results contradict a Michael-type addition process for crosslinking.

It is conceivable that crosslinking could proceed by a free-radical process. If so, the addition of a temperature-stable free radical trap would be expected to improve the product viscosity. Depending upon the particular trap employed, this selectivity improvement could potentially be gained without a loss in the hydrogenation activity that is associated with the amine additives. Therefore, an experiment was run in the presence of 1 wt% of Tempo relative to the amount of olefin charged to the system (Figure 6.11). The resulting viscosity and conversion profiles are analogous to those derived in the absence of the additives, indicating that while Tempo did not inhibit the activity of **2a**, it did not improve the process selectivity.

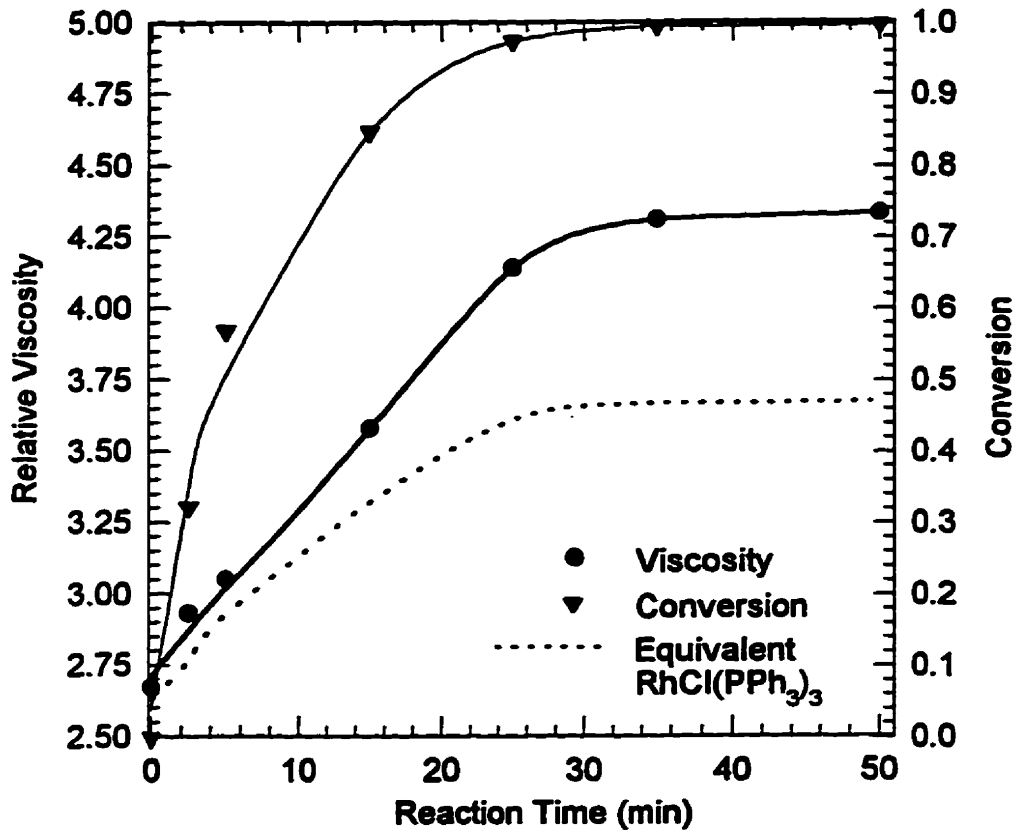

Figure 6.11: Conversion, η_{rel} versus time profile with added Tempo; [2a]=80 μM, P_{H2}=23.7 bar, [RCN]=249 mM, T=130°C.

Chapter 7

Development of a Continuous HNBR Process

As the demand for HNBR rises, the batch production strategy currently employed by commercial producers may become untenable. While batch processing is capable of achieving high olefin conversions, it is disadvantaged in terms of throughput, as the hydrogenation reaction is but one component of the overall production cycle. Furthermore, batch methods can be labour intensive and may be demanding from a reactor control standpoint. Nevertheless, it has yet to be demonstrated that a continuous HNBR process can offer an economic advantage. In this chapter, an efficient continuous process is defined within the context of reactor design. These concepts are then demonstrated on a bench-scale prototype.

The considerations taken in developing a continuous HNBR process are detailed in Section 7.1 along with the criteria used to assess its performance. Section 7.2 describes the bench-scale unit and the procedures developed for its operation. An example of the residence time distribution and NBR hydrogenation efficiency produced by the unit is presented in Section 7.3.

7.1 Process Design Considerations

There are two definitive requirements of a prospective HNBR process. In the first place, catalyst consumption must be minimized due to the cost of preparing and handling sensitive organometallic complexes. Secondly, it must be capable of attaining olefin conversions in excess of 98%. Given that the osmium technology requires a fraction of the metal loading demanded by the rhodium catalysts, a high-pressure process employing **2a** has been adopted. The conversion requirement precludes a CSTR approach as the capital and operating costs of a series of high-pressure autoclaves are prohibitively high. However, a plug flow reactor (PFR) configuration is capable of yielding high conversions in a single, low maintenance vessel. It is for this reason that a PFR system has been selected.

While the standard gas-liquid contactors used for industrial hydrogenations are trickle beds, a concurrent upflow process is believed to be most capable of meeting the design criteria (Figure 7.1). At a given set of operating conditions, concurrent upflow has proven to yield superior gas-liquid mass transfer rates and greater flexibility in terms of throughput (Hofmann, 1978). Unlike trickle bed processes which must avoid a flooded condition, upflow PFR's can accommodate a large liquid holdup and, consequently, can support longer residence times.

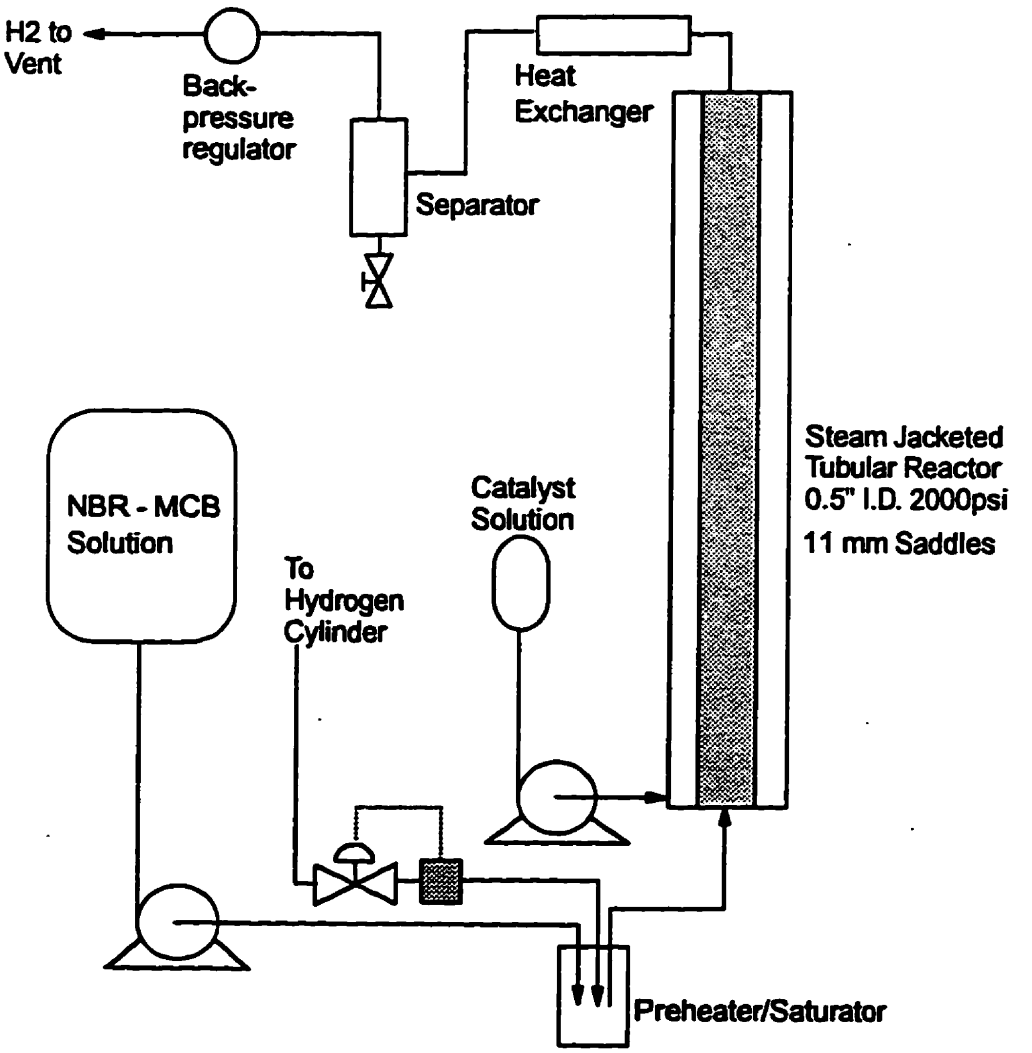

Figure 7.1: Concurrent upflow operation of a PFR

The decision to develop an upflow PFR was based as much on limitations to its physical scale as on mass transfer and holdup concerns. The dimensions of the packing relative to the reactor diameter influences the gas-liquid contacting efficiency of all continuous units (Satterfield, 1975). In order to restrict the output of the bench-scale process, a small diameter PFR was required. Operation of such a unit under trickle bed conditions is inconceivable, as channelling and wall effects would dominate the liquid phase flow. Concurrent upflow is known to promote a more effective phase distribution in small reactors, thereby minimizing the impact of its dimensions (Illuita et al., 1996).

The ideal operating conditions for an upflow PFR produce sufficient gas-liquid mixing to limit the influence of mass transfer on the hydrogenation rate. A failure in this respect creates a condition where the amount of catalyst employed is excessive given the rate of interfacial H_2 transport (Danckwerts, 1970). On the other hand, factors promoting H_2 transport in an upflow PFR are known to increase the amount of backmixing (See sections 7.1.1 and 7.1.2). By reducing the concentration of olefin at each point in the reactor, excessive backmixing, or dispersion, lowers the local hydrogenation rate and the overall conversion (Shaw et al., 1978). The relationships of concurrent upflow reactor conditions to axial dispersion and interfacial mass transfer form the content of Sections 7.1.1 and 7.1.2 respectively. Section 7.1.3 discusses the third variable of interest, the liquid holdup.

7.1.1 Residence Time Distribution (RTD) and Axial Dispersion

In an ideal HNBR process all fluid elements charged to the reactor would have the same "age" and identical residence times (Danckwerts, 1953). In reality, axial dispersion and stagnant liquid holdup effects broaden the residence time distribution (RTD) from a perfect plug flow condition. Inferences on the impact of these effects are usually based on measurements of the response of the reactor to a step change in the concentration of an inert tracer (Bischoff and McCracken, 1966). The time resolved evolution of the tracer signal is directly related to the cumulative age distribution, I(t). The RTD, E(t), may be derived by differentiation of this function with respect to time. It follows that,

$$I(t) = \int_0^t E(t)\, dt$$

$$t_m = \int_0^\infty t\, E(t)\, dt$$

$$\sigma^2 = \int_0^\infty (t-t_m)^2\, E(t)\, dt.$$

where t_m represents the mean and σ the standard deviation of the distribution.

Within the RTD is information regarding the degree of dispersion and liquid stagnation as well as the conversion that may be obtained for a given reaction. In the case of a first-order reaction, the overall conversion is related to the RTD by

$$\bar{X} = \int_0^\infty X(t)\, E(t)\, dt\ .$$

A great deal of research has focused on rationalizing RTD data in terms of a conceptual model. While differing in complexity (and number of parameters) all such models attempt to quantify the influence of process conditions on the mean, variance and overall form of the RTD. The most popular concept used to correlate RTD measurements is the axial dispersion or plug-dispersion (PD) model. This model accounts for backmixing using a Fick's Law diffusion term superimposed on ideal plug flow. A simple, one-dimensional equation results from a material balance over a differential element of the reactor, dz.

$$\frac{\partial C}{\partial t} + v_l \frac{\partial C}{\partial z} = D_a \frac{\partial^2 C}{\partial z^2}$$

which in dimensionless form yields

$$\frac{\partial C}{\partial \theta} + \frac{\partial C}{\partial l} = \frac{1}{Pe} \frac{\partial^2 C}{\partial l^2}$$

where C = concentration of tracer, mole/m^3
v_l = the superficial liquid velocity, m/s
D_a = dispersion coefficient, m^2/s
Θ = dimensionless time, tv_l/L
l = z/L = z/reactor length
Pe = Peclet number = v_l*L/D_a .

Note that as the Peclet number approaches zero, the model reduces to plug flow. The underlying assumption of the approach is that backmixing may be represented by diffusive and convective mixing of fluid elements. No stagnant zones or gross bypassing may contribute to RTD broadening.

The boundary conditions appropriate to a number of experimental circumstances have been discussed by Bischoff and Levenspeil (1962). Solving the partial differential equation yields the concentration of the tracer as function of time and Pe at the reactor exit. The RTD may be expressed in terms of this solution using the distribution's moments or by a technique involving the Laplace transform of the axial dispersion equation (Michelsen and Ostergaard, 1970). The Peclet number has been expressed in terms of the moments of the RTD by Levenspeil and Smith (1957);

$$\frac{\sigma^2}{t_m^2} = \frac{2}{Pe} + \frac{8}{Pe^2} .$$

Studies of the RTD produced by packed-bed, upflow reactors are scarce in comparison to the abundance of literature devoted to trickle beds. Hofmann (1961) and Heilmann and Hofmann (1971) have measured the dispersion produced in an upflow PFR as function of superficial gas and liquid velocity (v_g and v_l, respectively). Over a different range of packing size and fluid velocities, Steigel and Shaw (1977) have also assessed liquid phase dispersion. While the results differ in terms of magnitude, these reports have demonstrated that an increase in v_g and a reduction of v_l encourages liquid backmixing. Under the conditions studied by Carleton et al. (1967), inferior performance was observed when the PFR was operated without packing to distribute the two phases.

All of these studies have examined the air-water system at ambient temperature and pressure. Moreover, they have employed relatively large diameter reactors at gas flow rates that are more relevant to absorption processes than to hydrogenation reactions. Given that the current application involves a small diameter PFR operating upon a viscous liquid, only qualitative information may be derived from these literature reports.

Montagna and Shaw (1975) describe a more closely related application of an upflow PFR in a study of the hydrodesulfurization of heavy oil. Due to the larger liquid holdups accommodated by an upflow process, they observed a superior conversion relative to that found under trickle bed conditions. Inferences on the degree of axial dispersion were made from the progress of a hydrodesulfurization reaction carried out at 138 bar and 400°C. The conversion measurements linked high superficial gas velocities to an increase in liquid dispersion and a smaller liquid holdup.

The axial dispersion approach is appropriate for cases where backmixing is small. Residence time distributions affected by zones of relatively stagnant flow are therefore inadequately described by the one parameter model. An alternate treatment of the RTD assumes that liquid moves through the dynamic holdup as perfect plug flow. Backmixing is attributed not to dispersion, but the exchange of fluid between the dynamic and stagnant holdups (Sicardi et al., 1980). More recently, a composite model utilizing dispersion and static holdup exchange concepts has been applied to upflow PFR systems. The piston-diffusion-exchange (PDE) approach assumes a dispersion-type transport of liquid through the dynamic holdup along with a static holdup exchange process (Illuita et al., 1996). Two additional parameters, the ratio of the dynamic to the static liquid holdup and the mass transfer rate between them, are combined with the diffusion coefficient to correlate RTD data.

The development of the PDE model has created a debate regarding the significance of dispersion relative to stagnant holdup. Mazzarino et al. (1987) and Skomorokov and Krillov (1986) suggest axial dispersion effects are marginal in upflow operation, attributing broadening of the RTD to static holdup exchange. Illuita et al. (1996) report a more equitable balance between dispersion and holdup effects while the data of Yang et al. (1990) was inconclusive. Parameter estimation may account for some of the discrepancies, as three constants were fitted to the RTD data without regard for confidence intervals or possible parameter correlation. As few examples of the measured RTD's were provided in these reports, it is unknown whether the raw data differed greatly in each study.

7.1.2 Interfacial H_2 Transport

Gas-liquid mixing is generated by the difference in the velocities of the two phases as well as the turbulence produced by the reactor packing. In the present application, H_2 must be transferred across the gas-liquid interface at a rate that is sufficiently higher than the intrinsic hydrogenation rate. However, excessive mixing has been shown to be detrimental to the degree of backmixing. Past research has not centred on achieving an appropriate balance but has identified the factors that influence mass transfer rates alone.

The efficiency of interfacial mass transfer in an upflow PFR depends on the flow regime under which it is operated. Turpin and Huntington (1967) have visually identified three such flow regimes depending on the superficial velocities of the two phases. At low gas flow rates, liquid constitutes the continuous phase with the gas distributed in small bubbles. Increasing v_g generates a non-homogeneous flow regime wherein two gas-liquid mixtures of differing density appear alternately. This marks the transition from bubble flow regime to a pulse or slug flow regime. At extreme velocities, gas may become the continuous phase with the liquid entrained as a heavy mist or residing as a thin film about the packing. Transitions between the domains are not abrupt and depend upon the physical properties of the fluid as well as the reactor geometry and packing. As indicated by Alexander and Shaw (1976), the liquid and gas velocities applied in pilot scale hydroprocessing nearly always produce a bubble flow condition.

The flux of H_2 into the bulk liquid phase, N_{H2}, is governed by the mass transfer coefficient, k_lA/V (See Chapter 3.2.1).

$$N_{H_2} = \frac{k_l A}{V} (c^*_{H2} - c_{H2})$$

Whereas for a stirred tank reactor k_lA/V is a function of the fluid properties, the impeller design and the agitation speed, mass transfer in an upflow PFR is governed by the packing and the gas and liquid flow rates. The energy required for mixing is abstracted from the fluid and may be quantified by the pressure drop across the packed bed (Turpin and

Huntington, 1967) in accordance with the discussion of Calderbank and Moo Young (1961). Correlations of k_lA/V against the pressure drop ($\Delta P/\Delta Z$) have demonstrated the relationship between mass transfer rates and the intensity of gas-liquid mixing within the bed (Specchia et al., 1974).

A more direct approach deals directly with the gas and liquid superficial velocities, correlating k_lA/V against v_g and v_l or their corresponding Reynold's numbers (Sahay and Sharma, 1973; Tukashima and Kasuka, 1979). Under bubble flow conditions, k_lA/V was found to be greatly enhanced by an increase in v_g and more moderately by an increase in v_l. These results were dependent on the packing employed and apply to the air-water system. Empty columns have been shown to perform much less efficiently (Mashelar, 1970). This is attributed to a reduction in the degree of bubble coalescence by flow-induced shear about the packing. Voyer and Miller (1968) have demonstrated this principle using a screen packing of very high void fraction. At the high gas velocities studied by Sahay and Sharma (1973) the gas-liquid distributor at the PFR entrance was unimportant to mass transfer rates, presumably due to a rapid establishment of the two-phase flow by the reactor packing.

Alexander and Shaw (1976) provide k_lA/V data and pressure drop measurements for an upflow PFR operated in the range of gas and liquid flow rates that are relevant to pilot scale hydroprocessing. The PFR was a 6 cm diameter column packed to a height of 1.22 m with a variety of packings. Water velocities ranging from 0.9 mm/s to 6.0 mm/s and gas velocities from 1.5 mm/s to 31 mm/s were studied. Over this range of conditions, mass transfer coefficients from 0.02 s^{-1} to 0.1 s^{-1} were derived and correlated according to

$$k_lA = \alpha\, v_l^b\, v_g^c$$

$$b = 0.30 - 1.03$$
$$c = 0.44 - 1.69\ .$$

The exact values depended upon the size and geometry of the packing employed. Limited pressure drop data demonstrated a strong relationship between $\Delta P/\Delta Z$ and the $k_l A/V$ over this range of fluid velocities. Inefficient gas-liquid contacting was observed at low fluid velocities, resulting in poor interfacial transport rates and unusually low pressure drops.

7.1.3 Total Liquid Holdup

The liquid holdup represents the volume of liquid occupying the packed bed. For a given volumetric flow rate of liquid, the holdup therefore defines the time which an average fluid element must spend in the reactor. In a study of an air-water system, Steigel and Shaw (1977) correlated the total liquid holdup against the phase Reynold's numbers according to

$$H_{tl} = a\, Re_l^{0.11}\, Re_g^{-0.14} .$$

The parameter estimates are likely to be dependent on the apparatus and fluid properties and therefore do not apply to the present application. However, it is clear that high gas velocities and low liquid flow rates produced a low total liquid holdup. Their influence on the amount of static holdup may be equally important, but has yet to be investigated.

7.2 Experimental

A bench-scale prototype has been designed and constructed to demonstrate the principles of a continuous, upflow PFR process. Capable of handling pressures up to 86 bar and temperatures between 110°C and 170°C, the system may be used to study NBR hydrogenation at the conditions explored in Chapters 3 and 5. Detailed in this section are the process components and the procedures developed for its operation.

7.2.1 Apparatus

A schematic of the prototype is provided in Figure 7.2 while a list of the component models and part numbers are supplied in Appendix V. Solutions of NBR in chlorobenzene are prepared and stored in a 12 litre, polyethylene carboy (A) under a continuous flow of oxygen-free N_2. A high-pressure, positive displacement pump (B) meters a precise flow of

the polymer solution to a 300 cm^3 Parr autoclave (E) where it is contacted with the H_2 stream. Hydrogen is supplied via a Brooks mass flow controller (C). A high agitation rate is used to disperse the two phases while pre-heating them to about 15°C above the PFR temperature. Over the distance required to reach the reactor the mixture approaches the 130°C set point.

Solutions of catalyst are prepared and transferred to a 1 litre stainless steel bomb (F) under an N_2 atmosphere. The bomb is pressurized to 5 bar with H_2 to accommodate the volume increase created as the solution is metered into the PFR by a second, high pressure pump (G). Both pumps are driven by the same motor and cannot operate independently. Therefore, a three-way valve permits NBR solution to be pumped in the place of catalyst during times where zero catalyst flow is required.

The catalyst solution contacts the H_2/NBR mixture at the entrance of the reactor. From the PFR the reactants pass through a water-cooled heat exchanger (J) before reaching the distributing valve (H). Two 500 cm^3, high-pressure sight glasses operate in parallel to separate the gas and liquid phases. While the hydrogenated polymer solution is retained in the sight glass, H_2 proceeds through a check valve (D). This parallel system allows for collection in one unit while draining the other into a polyethylene collection flask (L).

The system pressure is maintained by the back pressure regulator (N) and measured by a Bourdon gauge (M). On the low pressure side of the regulator is a second separation stage (P) which protects the gas rotameter (O) in the event of a process upset. The H_2 is vented to the walk-in fumehood output ducts.

Steam is supplied at 40 psia to the top of the PFR jacket by a pressure regulating valve. Condensate expulsion from the bottom of the steam jacket is actuated by a thermostatic steam trap. This system delivers uniform heat to the reactor at a consistent temperature. The catalyst and NBR solution pumps provide an output of 30-580 cm^3/hour and 46 to 980 cm^3/hour respectively. Hydrogen may be delivered by the mass flow controller up to 2

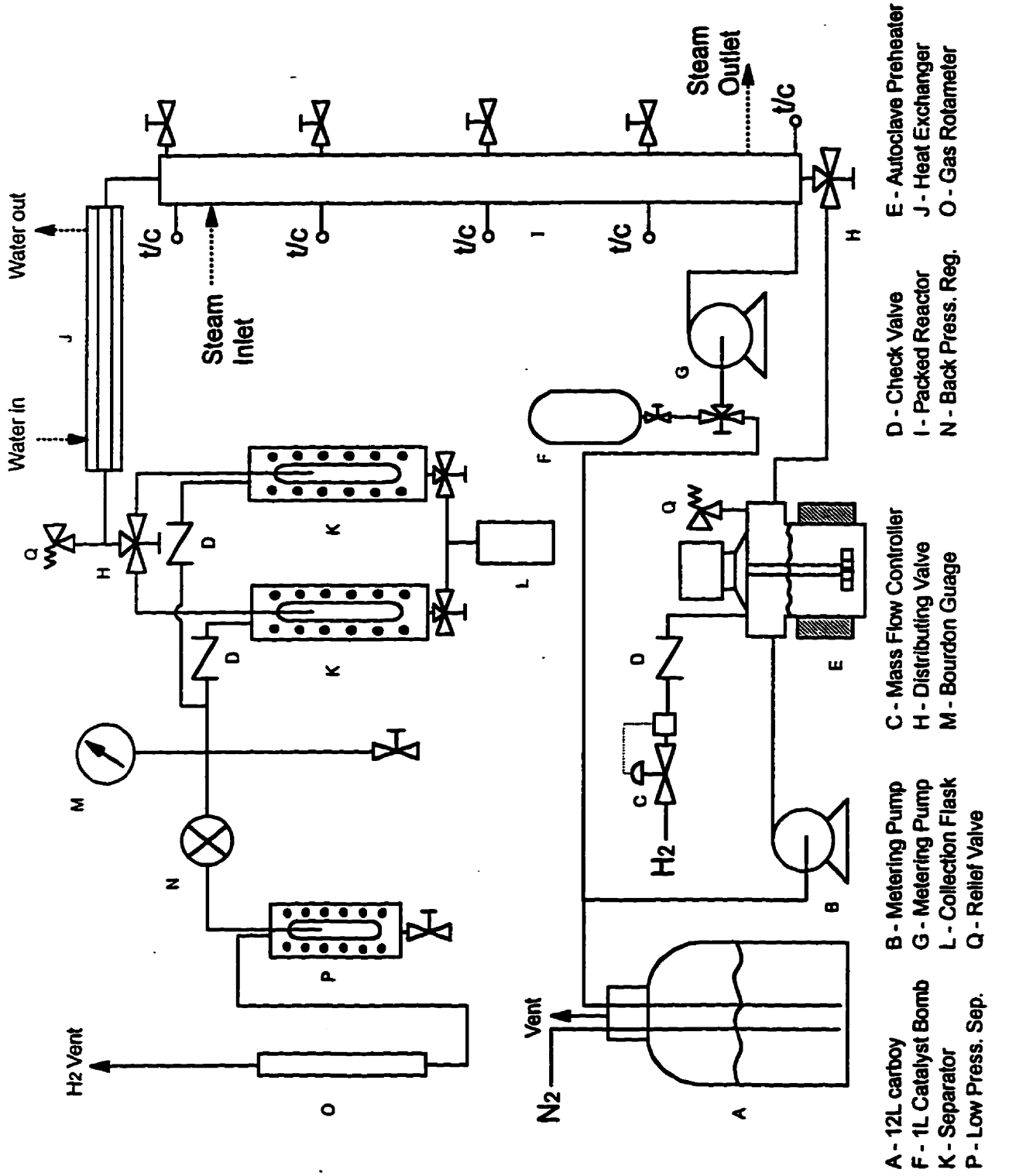

Figure 7.2: Schematic of the continuous process prototype

SLPM after which the flow must be manually adjusted. In either case the flow is measured by the gas rotameter that is calibrated for H_2 at STP.

The PFR is a 48" long, 1/2" schedule 80 stainless steel pipe having a 1.387 cm internal diameter. It has been pressure tested to 2000 psi at 23°C. The inner volume is accessed at five points along its length by pairs of opposing 3/32" holes, each tapped with a 1/8" pipe thread. These ports are used for sampling the reactor contents or monitoring its temperature. A 2" schedule 40 stainless steel pipe serves as a steam jacket and is rated for 100 psi steam.

A continuous pumping of liquid into a closed system may overpressurize the unit. This may occur should the system become blocked or if a distributing valve (H) is inadvertently closed. Therefore, a relief valve set at 1500 psi has been installed following the heat exchanger and a rupture disk with a 2000 psi burst rating has been placed on the preheater. Both components vent behind the reactor panel, away from the equipment operator. The entire apparatus is situated within a continuously purged, walk-in enclosure to vent H_2 and solvent fumes. A hydrostatic test of the equipment at 1000 psi and 130°C was undertaken before the experimental program was commenced.

7.2.2 General Operating Procedures

The solvents, polymer and reagents used were identical to those described in Chapter 5. Solutions of NBR in chlorobenzene were prepared in a 12 litre carboy and purged of atmospheric gases by bubbling with 99.99% pure N_2 for 2 hours. A slow stream of nitrogen through the carboy was maintained during the hydrogenation experiments to retain an inert atmosphere. Catalyst and salt solutions were prepared under N_2 using degassed chlorobenzene. Standard schlenk techniques were used to charge the solution to the catalyst bomb which was subsequently pressurized to about 5 bar with hydrogen.

With the NBR and catalyst solution vessels in place the positive displacement pumps were primed and the entire reactor system degassed by successive pressurization and venting of

10 bar H_2 for a total of three cycles. The steam lines were then bled and a steam pressure of 40 psia established in order to produce a temperature of 130°C. The reactor pressure was raised by adjusting the back-pressure regulator while hydrogen flowed into the system. Liquid and gas flows were initiated and the preheater temperature set to 150°C. Once the rotameter and reactor thermocouples recorded a steady state condition, the experiment was commenced by switching the catalyst pump to feed off of the 1 litre catalyst bomb.

7.2.3 Residence Time Distribution (RTD) Measurements

The liquid phase RTD was derived from the response of the system to a step change in the concentration of an inert tracer. A stable and organic-soluble salt, (n-Bu_3HNOAc), was introduced to the reactor using the catalyst addition system. Its concentration at the reactor exit was determined from measurements of the solution conductivity. Both the thermocouple and the sampling valve at the top of the reactor were replaced with conductivity probes made from 1/16" stainless steel wire. The dielectric fittings used to isolate the probes from the reactor were designed for high-pressure operation, allowing the RTD measurements to be made at the severe reaction conditions employed in the hydrogenation trials.

7.2.4 Liquid Holdup Measurements

A simple means of assessing the volume of the gas phase within the PFR required slight modifications to the system. Firstly, a valve was installed at the PFR outlet to provide a means of isolating the reactor volume. To the top sampling valve an 8.282 cm^3 bomb was fixed at ambient pressure and a known temperature. A calibrated differential pressure cell was attached to the second sample valve to measure the isolated reactor pressure.

To estimate the gas phase volume within the reactor the system was isolated using the inlet and outlet valves. The liquid phase pumps were quickly shut off after arresting the flow through the reactor. The closed system pressure was recorded. The sampling valve to the external bomb was then opened, expanding the system by 8.282 cm^3. The resulting pressure drop was used to calculate the gas phase volume using the following function;

$$V_{PFR} = V_b \frac{T_{PFR}}{T_b} \frac{(P_{b,2} - P_{b,1})}{(P_{PFR,2} - P_{PFR,1})}$$

$$V_{PFR} = (8.282\ cm^3) \frac{T_{PFR}}{T_b} \frac{P_2}{(P_2 - P_1)}$$

where, V_{PFR} = gas phase volume, cm^3
V_b = bomb volume = 8.282, cm^3
T_{PFR} = reactor temp, K
T_b = bomb temp, K
P_1, P_2 = initial and final gauge pressures

The technique assumes the liquid to be incompressible and the change in the solubility of H_2 in the liquid phase created by the small drop in pressure to be negligible. The use of an ideal gas approximation is valid for hydrogen at the conditions employed.

7.3 Results and Discussion

In this section the PFR system is demonstrated along with the techniques used to assess its performance. While the study is not comprehensive, it does establish a foundation for further work while advancing the thesis objective of assessing concepts that have been developed around the osmium technology.

7.3.1 Visual observations on a transparent PFR

Prior to operating the high-pressure PFR, a transparent reactor of equal dimension was installed to observe the two-phase flow characteristics. Material limitations dictated that an air-water system be studied at ambient pressure and temperature. While the observations are therefore of qualitative value, gross flow distribution problems that are otherwise difficult to diagnose may be identified.

Glass beads of 1.5 mm diameter were originally chosen due to their well defined packing structure and void fraction. When employed in the transparent reactor, the packing proved

to be incapable of providing adequate gas-liquid mixing. Unacceptable levels of bubble coalescence were detected as the helical packing structure of the beads produced a corresponding flow of the gas phase through their interstitial voids. This observation led to the adoption of an 11 mm, non-porous, ceramic saddle packing.

The void fraction produced by the saddles when packed into the transparent reactor was 0.671, meaning that the packing occupied nearly 33% of the PFR volume. The greater shear created at the surface of this packing limited the amount of bubble coalescence, resulting in a visibly greater gas-liquid interfacial area. Furthermore, turbulent flow conditions were established as opposed to the helical flow structure developed by the spherical packing. Both these factors are expected to enhance the rates of H_2 transfer across the gas-liquid interface.

7.3.2 Residence time distribution

Preliminary holdup measurements provided estimates of the liquid phase residence time over a range of gas and liquid flow rates. Based on the activity of **2a** at the central reaction conditions employed in Chapter 5 ([**2a**]=80 μM, [RCN]=172 mM, P_{H2}=24.2 bar, T=130°C) a 20 minute residence time within an ideal PFR would fully hydrogenate the material. Therefore, an average residence time of approximately 20 minutes was targeted. This corresponded to liquid and gas volumetric flow rates of V_l=4.92 cm^3/min and V_g=1.3 SLPM respectively. At 24.2 bar and 130°C, these flow rates develop superficial velocities of v_l=0.0543 cm/sec and v_g=0.676 cm/sec. Under these conditions the response of the exit solution conductivity to a step change in the concentration of *n*-Bu_3HNOAc was monitored. The acquired concentration versus time profile is illustrated in Figure 7.3.

Zero time in the tracer concentration profile marks the arrival of the step change at the reactor entrance. Note that the conductivity of organic salts may not be linearly proportional to their solution concentration. Furthermore, the conductivity baseline is affected by fluid flow rates as the measurement is sensitive to the average amount of liquid

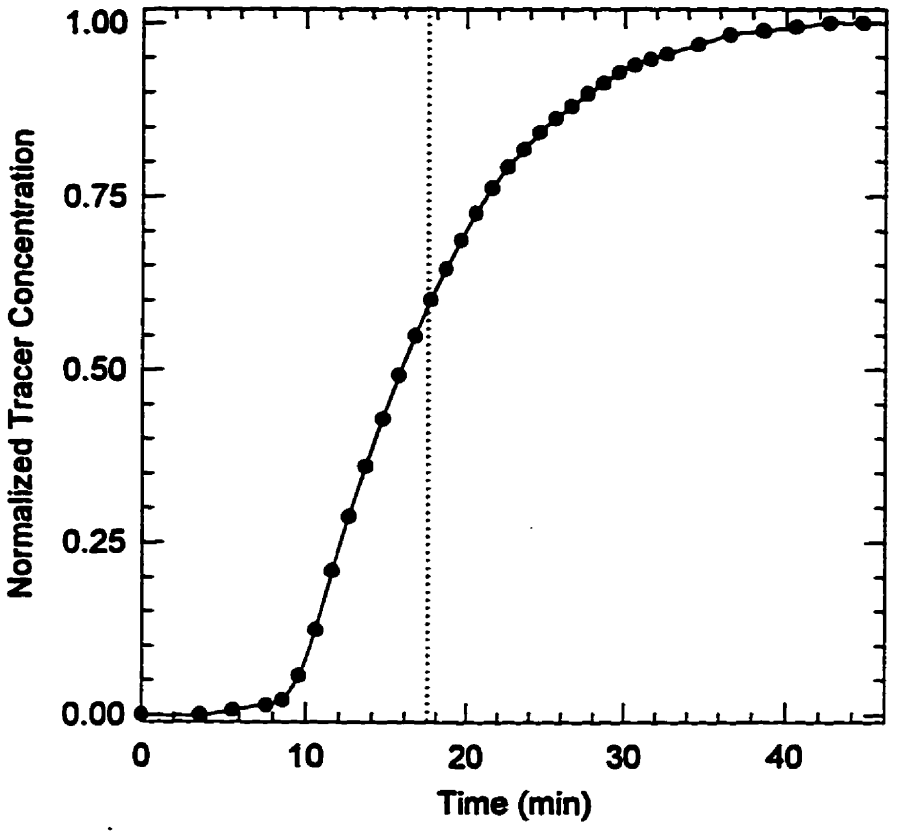

Figure 7.3: Conductivity versus time response to a step change input; T=130°C, v_l=0.0543 cm/s, v_g=0.676 cm/s, [RCN]=172 mM, P_{H2}=24.2 bar

which passes between the probes. Therefore, a RTD trial comprised three step changes, each plateau providing a point for a conductivity versus concentration calibration.

The derivative of the concentration profile, normalized with respect to the full scale concentration of the salt, yielded the RTD shown in Figure 7.4. The moments of this distribution provided a mean residence time, t_m, of 17.5 minutes and a standard deviation, σ, equal to 6.4 minutes. Using the axial dispersion model for an open-open boundary condition (Levenspeil and Smith, 1957) a Peclet number of 18.2 is derived, which is indicative of a "moderate" degree of dispersion. The RTD shows no evidence of liquid phase channelling but the tracer elution is characteristic of a static liquid holdup. These are zones within the PFR in which the flow rates are substantially less than those of the bulk liquid. To date, there are no reports of the influence of gas and liquid flow rates on the

distribution between the static and dynamic holdups in spite of their importance to upflow reactor performance.

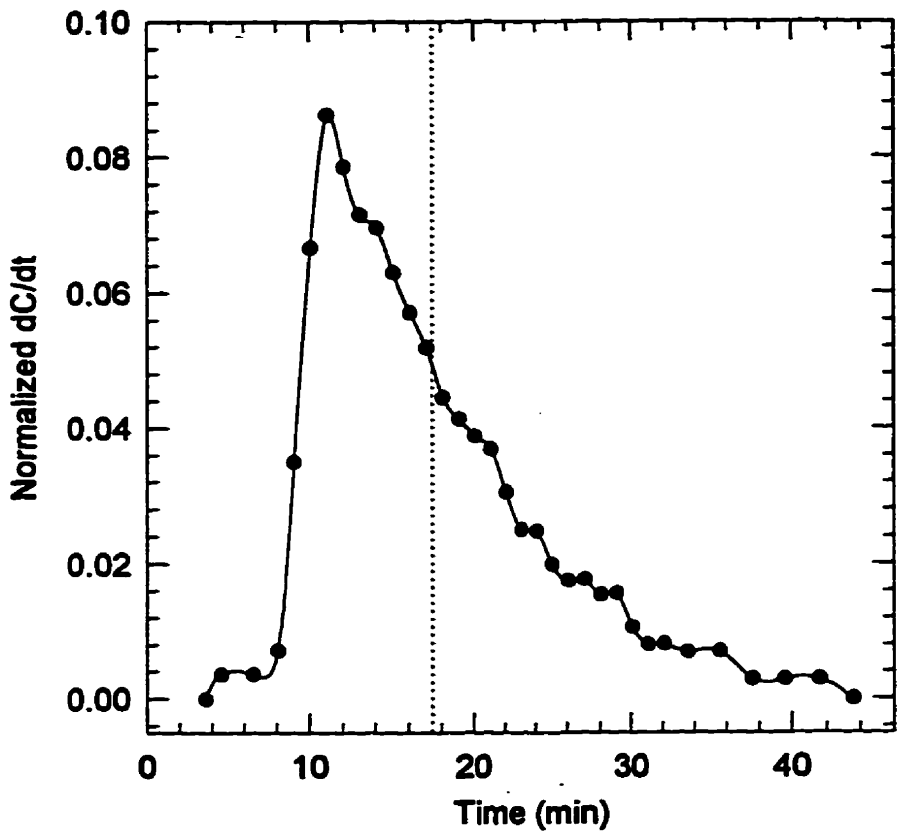

Figure 7.4: Calculated residence time distribution, T=130°C, v_l=0.0543 cm/s, v_g=0.676 cm/s, [RCN]=172 mM, P_{H2}=24.2 bar

7.3.3 Continuous hydrogenation of NBR

To demonstrate the ability of the concurrent upflow PFR process to produce HNBR, an hydrogenation trial has been performed using the flow conditions examined in the RTD study. Due to concerns of the stability of **2a** in solution over prolonged periods, its five coordinate analogue, **1a**, was employed. A batch hydrogenation carried out using [**1a**]=80 μM, [RCN]=172 mM, P_{H2}=24.2 bar and T=130°C yielded an apparent first-order rate constant of $1.38*10^{-3}$ s^{-1}. Over a 17.5 minute residence time, a perfect plug flow reactor would therefore produce an overall conversion of 76.5%. The actual conversion versus length profile observed in the continuous unit is illustrated in Figure 7.5.

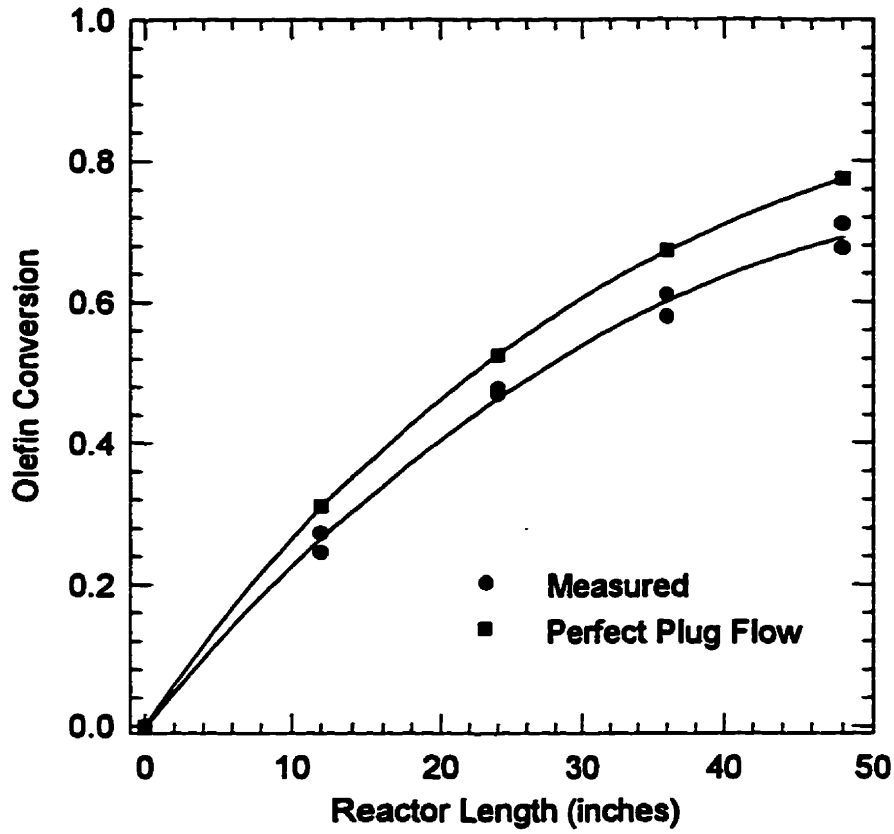

Figure 7.5: Conversion versus length profile, v_l=0.0543 cm/s, v_g=0.676 cm/s, [1a]=80 μM, [RCN]=172 mM, P_{H2}=24.2 bar, T=130°C

The impact of axial dispersion on the attainable conversion profile is evident from the difference between the ideal plug flow case and the measured data. Using the residence time distribution acquired under these flow conditions, the overall conversion of the system has been calculated according to:

$$\bar{X} = \int_0^\infty X(t)\ E(t)dt\ .$$

An overall conversion at the reactor outlet of 72.7% was derived, which is in fair agreement with the observed result.

The holdup, RTD and olefin conversion data are self-consistent, indicating that the theory and practice upon which the project is based are sound. The preliminary data suggest that the upflow approach, employing the osmium catalyst technology, is capable of efficiently

hydrogenating Krynac 38.50. Presently, an estimate of the H_2 interfacial transport rates that are supported by the PFR are lacking. However, the olefin hydrogenation profile does not appear to have been influenced by a mass transfer limitation. Therefore, optimization of the reactor flow conditions with respect to backmixing and mass transfer promises to improve the operating efficiency of the system while further characterizing its performance.

Chapter 8

Conclusions and Recommendations for Further Research

8.1 Conclusions

8.1.1 Solubility of H_2 in Chlorobenzene

Reliable estimates of the solubility of H_2 in pure monochlorobenzene have been acquired over the temperature range of 273.2 K to 443.2 K and pressures to 67 bar. The influence of acrylonitrile-butadiene copolymer on the solubility of H_2 is negligible for 4.04 wt% and 8.08 wt% solutions.

8.1.2 Catalytic Hydrogenation of NBR by $RhCl(PPh_3)_3$ and $RhH(PPh_3)_4$

Operating under extreme conditions, the rhodium(I) complexes are more active for the hydrogenation of NBR than previously reported. The catalytic chemistry observed at high temperatures and pressures is consistent with that derived at conditions near ambient. However, dissociative equilibria are favoured by an increase of temperature, resulting in the less severe inhibition of the hydrogenation rate by PPh_3 and nitrile.

A preferential hydrogenation of the *cis* isomer relative to the *trans* moiety within NBR that has been reported at 65°C and 1 bar H_2 is not detected at 145°C and an H_2 pressure of 24 bar. Based on NMR spectra of HNBR produced by $RhCl(PPh_3)_3$ and $RhH(PPh_3)_4$, these catalysts are wholly selective for the hydrogenation of olefin in the presence of nitrile. Dilute solution viscosity measurements confirm that neither catalyst promotes crosslinking of the material.

8.1.3 Nuclear Magnetic Resonance Studies

Under hydrogenation conditions, **2a** is activated by the dissociation of O_2 to form its 5-coordinate analogue, **1a**. Over a prolonged period, solutions of **2a** decompose, initially producing $OPCy_3$ and an uncharacterized complex.

The complexes which predominate during the hydrogenation of NBR are the nitrile and H_2 adducts, **6a** and **3a** respectively. Both H_2 and RCN compete for coordination to **1a** at exchange rates which are rapid relative to the NMR timescale. Olefin has a limited capacity to coordinate with the metal centre. No evidence to support the association of a third PR_3 to **1a,b** has been discovered, nor has any direct proof been acquired for the dissociation of PR_3 from either **1a,b** or **3a,b**.

8.1.4 NBR Hydrogenation Catalyzed by $OsHCl(CO)(O_2)(PCy_3)_2$, **2a**

2a is the most active catalyst for the selective hydrogenation of NBR at commercial reaction conditions. The system appears to preferentially saturate the *cis* olefin isomer within the copolymer. NMR spectra of HNBR produced by **2a** reveal no signs of nitrile reduction to amine.

A comprehensive kinetic study of *trans* olefin hydrogenation has defined the relationship between the reaction rate and the concentrations of **2a**, H_2 and nitrile as well as the temperature. The hydrogenation rate supported by **2a** is linearly proportional to its solution concentration, indicating that the active complex is mononuclear. The nitrile functionality within the copolymer has an inhibitory influence that is rationalized by a competitive coordination of RCN to **1a**. At pressures up to 40 bar, the hydrogenation rate abides by an apparent first order expression with respect to the concentration of olefin in solution.

NBR hydrogenations carried out at pressures below approximately 40 bar yield an apparent second order dependence with respect to $[H_2]$. The order shifts towards zero as the pressure approaches 80 bar, while systems lacking nitrile (SBR, 1-decene) demonstrate this zero order condition irrespective of the pressure employed. Both the second and zero order observations are likely to be limiting cases of the overall catalytic chemistry of the **2a** system.

An unconventional reaction mechanism in which two molecules of hydrogen are required to facilitate the rate determining step is capable of explaining all of the kinetic observations. This proposed mechanism attributes the second order H_2 dependence as a result of the strong coordination of nitrile. In the absence of RCN, it is suggested that hydrogen coordination equilibria dominate the reaction mechanism, resulting in the indifference of SBR hydrogenations to the system pressure. According to this scheme, the active complex is a monophosphine system which coordinates up to five hydrogen either as traditional hydrides or as fluxional hydride\dihydrogen ligands.

8.1.5 Selectivity of the **2a** System

While **2a** does not reduce nitrile in detectable amounts, it does promote the crosslinking of polymer molecules that is not encountered for the Rh(I) catalysts. Increasing H_2 pressures and minimizing the concentration of **2a** enhance the selectivity of the process, as does the use of additives such as octylamine.

The solution viscosity of HNBR produced by **2a** increases with time as long as olefin is present within the system, indicating that crosslinking involves residual olefin. It is not likely to be a free radical process. A proposal based on a Michael-type addition of reduced nitrile to activated olefin has not been substantiated.

8.1.6 Continuous HNBR Process

The demands for a high conversion, continuous process which makes efficient use of catalyst are best met by a concurrent, upflow PFR configuration. The ideal operating conditions of such a system generate sufficient gas-liquid mixing to eliminate mass transfer limitation while minimizing the amount of axial dispersion.

Preliminary residence time distribution (RTD) and hydrogenation data acquired from a bench-scale prototype have demonstrated the feasibility of the PFR approach. RTD measurements may be integrated with batch kinetic data to predict the overall conversion produced by the unit.

8.2 Recommendations for Further Research

8.2.1 Phosphine Exchange Studies

The observed inhibition of the hydrogenation activity by the addition of trace quantities of PCy_3 is a cornerstone of the reaction mechanism, in spite of an incomplete knowledge of phosphine lability. There is no direct evidence of an association of a third phosphine to **1a** or the loss of PCy_3 from either **1a** or **3a** to generate a monophosphine intermediate.

It is proposed that future research be directed towards characterizing the lability of phosphine. Exchange rates measured for a broader range of phosphines may advance this objective. However, the phosphine exchange procedure developed in the course of this study is cumbersome, and expensive and an alternative method should be developed.

8.2.2 Hydrogenation Kinetic Studies of 2a

Further knowledge of the influence of phosphine on the hydrogenation kinetics may be derived from kinetic studies of the analogues of **2a**. This work has demonstrated the superior activity of the PCy_3 system relative to the $PiPr_3$ analogue. By examining the activity of a series of bulky, alkyl phosphine complexes (PCp_3, $PMetBu_2$, etc), a relationship between the cone angle and basicity of phosphine may lead to insights into its role within the hydrogenation process. Only phosphines which produce a bis complex are likely to be relevant to such a discussion.

The proposed mechanism suggests that the influence of PCy_3 on the hydrogenation rate may not be as severe for SBR than has been observed for NBR. As the derived rate expression suggests that $K_{CN}[P][RCN]$ is the dominant term for NBR, a lack of nitrile in the system may act to diminish the magnitude of the phosphine inhibition. Additional testing of the model may involve charging a nitrile such as octylcyanide to an SBR hydrogenation. Under such conditions, the dependence of k' on the hydrogen pressure should be second order.

8.2.3 Selectivity of the **2a** System

Although the viscosity measurements have contributed to our knowledge of the crosslinking process, they cannot provide the structure of a crosslinked moiety. It is suggested that an attempt be made to ascertain, either by NMR or other spectroscopic means, the chemical structure of a highly gelled HNBR material.

One further recommendation centres on the need for nitrile hydrogenation to facilitate the crosslinking process. As most mechanisms suppose that nitrile reduction is required, it is proposed that an efficient nitrile hydrogenation catalyst such as $RhH(P\textit{i}Pr_3)_4$ be screened for potential crosslinking activity.

8.2.4 Continuous NBR Processing

Having demonstrated the operation of the bench-scale PFR, it remains to characterize its performance over a range of process conditions. Measurements of the liquid holdup and RTD as a function of the superficial velocities of the gas and liquid phases can quantify axial dispersion. Estimates of k_lA may be obtained by carrying out hydrogenation reactions under mass transfer limitation. By characterizing backmixing and interfacial H_2 transport, the optimal processing conditions for NBR hydrogenation by be predicted and tested experimentally.

Literature Cited

Ahmad, N., J.J. Levison, S.D. Robinson and M.F. Uttley; **Triphenylphosphine Complexes - Hydridotetrakis(triphenylphosphine)rhodium(I)**, *Inorganic Syntheses*, 58-59 (1974).

Alexander, B.F. and Y.T. Shah; **Gas-Liquid Mass Transfer Coefficients for Cocurrent Upflow in Packed Beds**, *Can. J. Chem. Eng.*, **54**, 556-559 (1976).

Andriollo, A., M.A. Esteruelas, U. Meyer, L.A. Oro, R.A. Sanchez-Delgado, E. Sola, C. Valero and H. Werner; **Kinetic and Mechanistic Investigation of the Sequential Hydrogenation of Phenylacetylene Catalyzed by $OsHCl(CO)(PR_3)_2$ [PR_3 = $PMetBu_2$ and $PiPr$]**, *J. Am. Chem. Soc.*, **111**, 7431-7437 (1989).

Baird, M.C., D.N. Lawson, J.T. Mague, J.A. Osborn and G. Wilkinson; **Novel Addition Reactions of Chlorotris(triphenyl phosphine)rhodium(I)**, *J. Chem. Soc., Chem. Commun.*, 129-130 (1966).

Bakhmutov, V.I., J. Bertran, M.A. Esteruelas, A. Lledos, F. Maseras, J. Modrego, L.A. Oro and E. Sola; **Dynamic Behaviour in Solution of the *trans*-Hydridodihydrogen Complex $OsHCl(\eta^2\text{-}H_2)(CO)(PiPr_3)_2$**, *Chem. Eur. J.*, **2**, 815-825 (1996).

Bhattacharjee, S., A.K. Bhowmick and B.N. Avasthi; **High Pressure Hydrogenation of Nitrile Rubber: Thermodynamics and Kinetics**, *Ind. Eng. Chem. Res.*, **30**, 1086-1092 (1991).

Bischoff, K.B. and O. Levenspiel; **Fluid Dispersion and Comparison of Mathematical Models**, *Chem. Eng. Sci.*, **17**, 245-255 (1962).

Bischoff, K.B. and E.A. McCracken; **Tracer Tests in Flow Systems**, *Ind. Eng. Chem.*, **58(7)**, 18-31 (1966).

Booth, B.L., R.N. Haszeldine and R.G.G Holmes; **Transition Metal Complexes Containing the Bis(trifluoromethyl)nitroxy Ligand**, *J. Chem. Soc., Chem. Commun.*, **13**, 489-490 (1976).

Box, G.E., W.G. Hunter and J.S. Hunter; **Statistics for Experimenters**; Wiley: New York, 1978.

Buding, H., J. Thoermer, W. Nolte, J. Fiedler, C. Paul and T. Himmler; European Patent EP 405,266 (1991).

Calderbank, P.H. and M. B. Moo-Young; **The Continuous Phase Heat and Mass Transfer Properties of Dispersion**, *Chem. Eng. Sci.*, **16**, 39-54 (1961).

Carleton, A.J., R.J. Flain, J. Rennie and F.H.H. Valentin; **Some Properties of a Packed Bubble Column**, *Chem. Eng. Sci.*, **22**, 1839-1845 (1967).

Danckwerts, P.V.; **Continuous Flow Systems**, *Chem. Eng. Sci.*, **2(1)**, 1-13 (1953).

Danckwerts, P.V.; *Gas-Liquid Reactions*, McGraw-Hill, New York (1970).

Esteruelas, M.A. and H. Werner; **Five and Six Coordinate Hydrido(Carbonyl)-Ruthenium(III) and -Osmium(II) Complexes Containing Triisopropylphoshine as a Ligand**, *J. Organometallic Chem.*, **303**, 221-231 (1986).

Esteruelas, M.A., L.A. Oro and C. Valero; **Hydrogenation of Benzilideneacetone Catalyzed by $OsHCl(CO)(PR_3)_2$ [PR_3 = $PiPr_3$ and $PMetBu_2$]**, *Organometallics*, **11(10)**, 3362-3369 (1992).

Esteruelas, M.A., E. Sola, L.A. Oro, U. Meyer and H. Werner; **Coordination of H_2 and O_2 to $[OsHCl(CO)(PiPr_3)_2]$: A catalytically Active $M(\eta^2\text{-}H_2)$ Complex**, *Angew. Chem. Int. Ed. Engl.*, **27**, 1563-1564 (1988).

Farnetti, E., M. Graziani, A. Mezzetti and A. Del Zotto; **Effect of Bulky Ligands on the Hydrogenation of Olefins Catalyzed by cis-$[MH_2(dcpe)_2]$ (M=Ru,Os)**, *J. Mol. Catal.*, **73**, 147-155 (1992).

Fogg, P.G.T. and W. Gerrard; *The Solubility of Gases in Liquids*, Wiley: Chichester, 309 (1991).

Fukushima, S. and K. Kusaka; **Gas-Liquid Mass Transfer and Hydrodynamic Flow Region in Packed Columns with Cocurrent Upward Flow**, J. Chem. Eng. Japan, **12(4)**, 296-301 (1979).

Gilbert, J.D. and G. Wilkinson; **New Complexes of Ruthenium(II) with Triphenylphosphine and other Ligands**, *J. Chem. Soc. (A)*, 1749-1753 (1969).

Halpern, J.; **Hydrogenation of Tris(triphenylphosphine)chlororhodium(I)**, *J. Chem. Soc., Chem. Commun.*, 629-630 (1973).

Hashimoto, K., N. Watanabe and A. Yoshioka; **Highly Saturated Nitrile - A New High Temperature, Chemical Resistant Elastomer**, *Rubber World*, **190(2)**, 32-47 (1984).

Heilmann, W. and H. Hofmann; **Zur Hydrodynamik Zweiphasig Durchstomter Schuttschichten**, *Proceedings of the 4th European Symposium on Chemical Reaction Engineering*, Pergamon Press, London, 169-181 (1971).

Hertz, D.L. and H. Bussem; **Nitrile Rubber-Past, Present and Future,** *Rubber Chem. Technol.*, **68**, 540-546 (1995).

Hjortkjaer, J.; **The Hydrogenation of 1-Hexene Catalyzed by Solutions of Hydridotetrakis(Triphenylphosphine)Rhodium(I),** *Adv. Chem Series*, **132**, 133-144 (1974).

Hofmann, H.P.; **Multiphase Catalytic Packed-bed Reactors,** *Catal. Rev.- Sci. Eng.*, **17(1)**, 71-177 (1978).

Hofmann, H.P.; **Der derzeitig Stand be der Vorausberechnung der Verweilzeitverteilung in technischen Reaktoren,** *Chem. Eng. Sci.*, **14**, 193 (1961).

Horiuti, J.; **The Solubility of Gas and Coefficient of Dialation by Absorption,** *Sci. Pap. Inst. Phys. Chem. Res. (Tokyo)*, **17**, 125-256 (1931).

Iluita, I., F.C. Thyrion, O. Muntean and M. Giot; **Residence Time Distribution of the Liquid in Gas Liquid Cocurrent Upflow Fixed-bed Reactors,** *Chem. Eng. Sci.*, **51(20)**, 4579-4593 (1996).

James, B.R.; *Homogeneous Hydrogenation*, Wiley: New York, 1973.

Jardine, F.; **Chlorotris(triphenylphosphine)rhodium(I): Its Chemical and Catalytic Reactions,** *Prog. Inorg. Chem*, **29**, 63-202 (1981).

Jessop, P.G. and R.H. Morris; **Reactions of Transition Metal Dihydrogen Complexes,** *Coord. Chem. Rev.*, **121**, 155-284 (1992).

Klingender, R.C and W.G. Bradford; **HNBR Exhibits Dynamic Properties Well-suited for Timing Belt Use,** *Elastomerics*, (8), 10-17 (1991).

Kubo, Y. and T. Khotaki; US Patent 4,510,393 (1985).

Kubo, Y. and K. Ohura; US Patent 4,337,329 (1982).

Lee, J.I. and A.E. Mather; **Solubility of Hydrogen Sulfide in Water,** *Ber. Bunsen-Gesellschaft*, **81**, 1020-1023 (1977).

Levenspiel, O. and W.K. Smith; **Notes on the Diffusion-type Model for the Longitudinal Mixing of Fluids in Flow,** *Chem. Eng. Sci.*, **6**, 227-233 (1957).

Linn, D.E. and J. Halpern; **Roles of Neutral and Anionic Ruthenium Polyhydrides in the Catalytic Hydrogenation of Ketones and Arenes,** *J. Am. Chem. Soc.*, **109**, 2969-2974 (1987).

Marshall, A.J., I.R. Jobe; T. Dee and C. Taylor; **Determination of the Degree of Hydrogenation in Hydrogenated Nitrile-Butadiene Rubber (HNBR)**, *Rubber Chem. and Tech.*, **63**, 244-255 (1990).

Martin, P.; M.A.Sc. Thesis, University of Waterloo (1991).

Martin, P., N.T. McManus and G.L. Rempel; **Hydrogenation of Nitrile-butadiene Rubber Catalyzed by Ru(II) Complexes**, *Stud. Surf. Sci. Catal.*, **73**, 161-168 (1992).

Mashelkar, R.A.; **Bubble Columns**, *Brit. Chem. Eng.*, **15(10)**, 1297-1304 (1970).

Mazzarino, I., S. Sicardi and G. Baldi; **Hydrodyamics and Solid-Liquid Contacting Effectiveness in an Upflow Multiphase Reactor**, *Chem. Engng. J.*, **36**, 151-160 (1987).

McGrath, M.P., E.D. Sall and S.J. Tremont; **Functionalization of Polymers by Metal-Mediated Processes**, *Chem. Rev.*, **95**, 381-398 (1995).

McManus, N.T. and G.L. Rempel; **Chemical Modification of Polymers. Catalytic Hydrogenation and Related Reactions**, *J. Macromol. Sci., Rev. Macromol. Chem. Phys.*, C35, 239-285 (1995).

McManus, N.T., J.S. Parent and G.L. Rempel; US Patent 5,561,197 (1996).

McManus, N.T. and G.L. Rempel; US Patent 5,075,388 (1991).

Mezzeti, A., E. Zangrando, A. Del Zotto and P. Rigo; **Dioxygen Addition to Five-Coordinate Osmium(II) Complexes**, *J. Chem. Soc., Chem. Commun.*, 1597-1598 (1994).

Michelsen, M.L. and K. Ostergaard; **The Use of Residence Time Distribution Data for Estimation of Parameters in the Axial Dispersion Model**, *Chem. Eng. Sci.*, **25**, 583-592 (1970).

Mitchell, T.R.B.; **Stereochemistry of Hydrogenation of 4-t-Butlymethylenecyclohexane**, *J. Chem. Soc.(B)*, 823-825 (1970).

Moers, F.G.; **Ruthenium(II) and Osmium(II) Complexes of Tricylcohexylphosphine**, *J. Coord. Chem.*, **13**, 215-219 (1984).

Moers, F.G.; **A New Hydridocarbonyl Complex of Osmium(II)**, *J. Chem. Soc., Chem. Commun.*, 79 (1971).

Moers, F.G., R.W.M. ten Hoedt and J.P. Langhout; **Sulfur Dioxide and Carbon Disulfide Complexes of Osmium(II)**, *Inorg. Chem.*, **12**, 2196-2198 (1973).

Moers, F.G., R.W.M. ten Hoedt and J.P. Langhout; **New Carbonyl Tricyclohexylphosphine Complexes of Ruthenium(II) and Osmium(II)**, *J. Organometallic. Chem.*, **65**, 93-98 (1974).

Moers, F.G., R.W.M. ten Hoedt and J.P. Langhout; **Activation of Small Molecules by Osmium(II) and Ruthenium(II) Complexes**, *J. Inorg. Nucl. Chem.*, **36**, 2279-2282 (1974b).

Moers, F.G. and J.P. Langhout; **Cyanoolefin Complexes of Osmium(II) and Ruthenium(II)**, *J. Inorg. Nucl. Chem.*, **39**, 591-593 (1977).

Mohammadi, N.A. and G.L. Rempel; **Homogeneous Selective Catalytic Hydrogenation of C=C in Acrylonitrile-Butadiene Rubber**, *Macromolecules*, **20**, 2362-2368 (1987).

Mohammadi, N.A. and G.L. Rempel; **Control, Data Acquisition and Analysis of Catalytic Gas-Liquid Mini Slurry Reactors using a Personal Computer**, *Comput. Chem. Engng.*, **11**, 27-35 (1987).

Montagna, A. and Y.T. Shaw; **Backmixing in an Upflow Cocurrent Hydrodesulfurization Reactor**, *Chem. Engng. J.*, **10**, 99-105 (1975).

Ohshima, S., T. Takematsu, Y. Kuriki, K. Shimada, M. Suzuki and J. Kato; **Liquid-Phase Mass Transfer Coefficient and Gas Holdup in a Packed-Bed Cocurrent Upflow Column**, *J. Chem. Eng. Japan*, **9(1)**, 29-34 (1976).

Ohtani, Y., A. Yamagishi and M. Fujimoto; **Substitution Reactions of (Acetonitrile)chlorobis(triphenylphosphine)rhodium(I) in Benzene**, *Bull. Chem. Soc. Jpn.*, **52**, 2149-2150 (1979).

Oppelt, D., H. Schuster, J. Thormer and R. Braden; British Patent 1 558 491 (1976).

Osborn, J.A., F.H. Jardine, J.F. Young and G. Wilkinson; **The Preparation and Properties of Tris(triphenylphosphine)halogenorhodium(I)**, *J. Chem. Soc. (A) Inorg. Phys. Theor.*, 1711-1732 (1966).

Peng, D.Y. and D.B. Robinson; **A New Two-Constant Equation of State**, *I & EC Fundmentals* **15(1)**, 59-64 (1976).

Pimblett, B., C.D. Garner and W. Clegg; **Isolation and Crystal Structure of $[Rh(PPh_3)_3(MeCN)][BF_4]$, Acetonitriletris(triphenyl phosphine)rhodium(I) Tetrafluoroborate.**, *J. Chem. Soc., Dalton Trans.*, 1977-1980 (1985).

Rempel, G.L., N.T. McManus and X.Y. Guo; US Patent 5,258,467 (1993a).

Rempel, G.L., N.T. McManus and X.Y. Guo; US Patent 5,241,013 (1993b).

Rempel, G.L., N.T. McManus and N.A. Mohammadi; US Patent 5,057,581 (1991).

Rempel, G.L., N.A. Mohammadi and R. Farwaha; US Patent 4,816,525 (1989).

Rempel, G.L. and H. Azizian; US Patent 4,464,515 (1984).

Roe, D.C.; **Sapphire Tube for High-Resolution Studies at Elevated Pressure**, *J. Magn. Reson.*, **63**, 388-391 (1985).

Sahay, B.N. and M.M. Sharma; **Absorption in Packed Bubble Columns**, *Chem. Eng. Sci.*, **28**, 2245-2255 (1973).

Sanchez-Delagado, R.A., A. Andriollo, E. Gonzalez and N. Valencia; **The Chemistry and Catalytic Properities of Ruthenium and Osmium Complexes**, *J. Chem. Soc., Dalton Trans.*, 1859-1863 (1985).

Sanchez-Delgado, R.A., M. Rosales, M.A. Esteruelas and L. Oro; **Homogeneous Catalysis by Osmium Complexes. A Review**, *J. Mol. Catal.*, **96**, 231-243 (1995).

Sanchez-Delgado, R.A., A. Andriollo and N. Valencia; **Bromocarbonylhydrido tris(triphenylphosphine)osmium(II): A Versatile Catalyst for Homogeneous Organic Reactions**, *J. Chem. Soc., Chem. Commun.*, 444-445 (1983).

Satterfield, C.N.; **Trickle-Bed Reactors**, *AIChE J.*, **21(2)**, 209-228 (1975).

Schlaf, M., A.J. Lough, P.A. Maltby and R.H. Morris; **Synthesis, Structure and Properities of the Stable and Highly Acidic Dihydrogen Complex trans-[Os(η^2-H_2)(CH_3CN)(dppe)$_2$](BF_4)$_2$**, *Organometallics*, **15**, 2270-2278 (1996).

Schrock, R.R. and J.A. Osborn; **Catalytic Hydrogenation Using Cationic Rhodium Complexes. I. Evolution of the Catalytic System and the Hydrogenation of Olefins**, *J. Am. Chem. Soc.*, **98:8**, 2134-2143 (1976).

Schultz, D.N.; **Chemical Modification of Synthetic Elastomers** in *Handbook of Elastomers*, Marcel Dekker, New York, 75-100 (1988).

Shaw, Y.T., G.J. Steigel and M.M. Sharma; **Backmixing in Gas-Liquid Reactors**, *AIChE J.*, 24(3), 369-400 (1978).

Sicardi, J., G. Baldi, V. Specchia and I. Mazzarino; *Ind. Chim. Ital.*, **20**, 66 (1984).

Simnick, J.J., H.M. Sebastian, H.M. Lin and K.C. Chao; **Gas-Liquid Equilibrium in Mixtures of Hydrogen + m-xylene and + m-cresol**, *J. Chem. Thermodyn.* **11**, 531-537 (1979).

Skomorokov, V.B., V.A. Kirillov and G. Baldi; **Simulation of Liquid Hydrodynamics in a Cocurrent Two-Phase Upward Flow through a Packed Bed**, *Chem. Engng. J.*, **33**, 169-173 (1986).

Sokolov, B.I. and A.A. Polyakov; **Solubility of Hydrogen in n-decane, n-tetradecane, 1-hexene, 1-heptene, 1-octene, isopropylbenzene, 1-methylnaphthalene and decalin**, *Zh. Prikl. Khim.*, **50(6)**, 1403-1405 (1977).

Specchia, V., S. Sicardi and A. Gianetto; **Absorption in Packed Towers with Concurrent Upward Flow**, *AIChE J.*, **20(4)**, 646-653 (1974).

Steigel, G.J. and Y.T. Shah; **Backmixing and Liquid Holdup in a Gas-Liquid Cocurrent Upflow Packed Column**, *Ind. Eng. Chem., Proc. Des. Dev.*, **16(1)**, 37-43 (1977).

Strohmeier, W., E. Hitzel and B. Kraft; **Comparison Between Homogeneous Catalysts and their Heterogenised Counterparts**, *J. Mol. Catal.*, **3**, 61-69 (1977).

Turpin, J.L. and R.L. Huntington; **Prediction of Pressure Drop for Two-Phase, Two-Component Concurrent Flow in Packed Beds**, *AIChE J.*, **13(6)**, 1196-1202 (1967).

Vaska, L.; **Hydridocarbonyl Complexes of Osmium by Reaction with Alcohols**, *J. Am. Chem. Soc.*, **86**, 1943 (1964).

Vaska, L.; **Homogeneous Catalysis by Five and Six Coordinated Metal Hydride Complexes**, *Inorg. Nucl. Chem. Lett.*, **1**, 89-95 (1965).

von Braun, J., G. Blessing and F. Zobel; **Catalytic Hydrogenations Under Pressure in the Presence of Nickel Salts VI. Nitriles**, *Berichte*, **56b**, 1988 (1923).

Voyer, R.D. and A.I. Miller; **Improved Gas-liquid Contacting in Cocurrent Flow**, *Can. J. Chem. Eng.*, **46**, 335-341 (1968).

Watanabe, N. and K. Hashimoto; **HSN Compound for Power Steering Hose**, *Kaut. Gummi Kunstst.*, **10**, 912-916 (1989).

Weinstein, A.H.; **Elastomeric Tetramethylene-Ethylethylene-Acrylonitrile Copolymers**, *Rubber Chem. Technol.*, **57**, 203-215 (1984).

Yang, X.L., J.P. Euzen and G. Wild; **Residence Time Distribution of the Liquid in Gas-Liquid Cocurrent Upflow Fixed-bed Reactors with Porous Particles,** *Chem. Eng. Sci.*, 45, 3311-3317 (1990).

Yoshida, T, T. Okano and S. Otsuka; **Catalytic Hydrogenation of Nitriles and Dehydrogenation of Amines with the Rhodium(I) Hydrido Compounds [RhH(P*i*Pr$_3$)$_3$] and [Rh$_2$H$_2$(μ-N$_2$){P(cyclohexyl)$_3$}$_4$],** *J. Chem. Soc., Chem. Commun.*, 870-871 (1979).

Young, C.L. (ed); *Solubility Data Series Volumes 5/6, Hydrogen and Deuterium,* Pergamon Press, Oxford **1981.**

Appendix I

Solubility of Hydrogen in Chlorobenzene

Table AI: Solublity of H_2 in chlorobenzene

T = 273.2 K		T = 296.2 K		T = 328.2 K	
P/bar	10^2x_{H2}	P/bar	10^2x_{H2}	P/bar	10^2x_{H2}
6.1	0.15	14.1	0.40	13.2	0.44
25.1	0.56	19.2	0.52	23.3	0.76
33.4	0.67	25.2	0.70	28.6	0.92
40.3	0.89	28.8	0.74	34.1	1.08
47.7	0.94	32.2	0.85	39.4	1.23
53.8	1.13	35.7	0.90	44.3	1.34
59.9	1.29	39.2	1.04	50.9	1.58
65.6	1.38	43.0	1.11	56.7	1.74
---	---	47.8	1.19	64.4	1.93
---	---	52.5	1.38	---	---
---	---	56.3	1.44	---	---
T = 363.2 K		T = 403.2 K		T = 443.2 K	
P/bar	10^2x_{H2}	P/bar	10^2x_{H2}	P/bar	10^2x_{H2}
11.7	0.47	8.4	0.41	13.2	0.66
15.1	0.61	13.1	0.72	16.5	0.88
18.6	0.77	18.6	0.89	20.1	1.05
25.4	0.98	22.1	1.06	23.2	1.19
29.2	1.11	24.0	1.17	25.4	1.31
31.4	1.23	26.3	1.22	27.4	1.47
34.9	1.36	28.9	1.36	29.9	1.58
39.6	1.50	33.6	1.54	35.9	1.81
44.0	1.62	39.1	1.87	41.1	2.20
49.0	1.85	44.3	2.06	46.3	2.42
55.2	2.06	49.4	2.34	50.8	2.72
62.3	2.36	54.3	2.51	56.6	3.06
---	---	60.3	2.89	61.4	3.26
---	---	66.3	3.10	67.1	3.61

Appendix II

Raw Kinetic and Viscosity Data:

$RhCl(PPh_3)_3$ and $RhH(PPh_4)_4$

Table AII-A: Kinetic Results on the $RhCl(PPh_3)_3$/NBR System

Expt. #	$[Rh]_T$ μM	[RCN] mM	$[PPh_3]$ mM	P_{H2} bar	$[H_2]$ mM	Temp K	$k'*10^3$ s^{-1}	η_{rel}
1	200.4	150.6	7.60	54.5	190	373.2	0.95	-----
2	19.6	171.8	1.00	23.7	101	418.2	0.79	-----
3	49.9	172.1	2.50	23.7	101	418.2	2.42	3.54
4	110.4	171.2	5.51	23.7	101	418.2	5.14	3.71
5	140.2	171.6	7.01	23.7	101	418.2	6.67	3.66
6	80.3	47.6	4.00	23.7	101	418.2	7.92	-----
7	79.6	85.8	4.00	23.7	101	418.2	6.03	-----
8	80.4	116.0	4.00	23.7	101	418.2	4.87	3.74
9	80.2	190.0	4.00	23.7	101	418.2	3.42	3.75
10	79.9	255.4	4.00	23.7	101	418.2	2.64	3.57
11	80.4	172.0	0.02	23.7	101	418.2	4.29	-----
12	80.6	171.6	0.94	23.7	101	418.2	4.44	3.93
13	80.0	171.4	1.60	23.7	101	418.2	4.17	3.61
14	80.5	171.8	2.40	23.7	101	418.2	4.11	3.82
15	80.3	171.6	5.60	23.7	101	418.2	3.47	3.67
16	79.8	85.7	2.41	23.7	101	418.2	7.12	-----
17	80.5	85.7	5.59	23.7	101	418.2	6.07	-----
18	80.4	172.1	3.98	4.85	20.6	418.2	1.05	3.54
19	80.2	172.0	4.02	8.28	35.2	418.2	1.87	3.35
20	80.5	172.0	4.00	13.4	57.1	418.2	2.96	3.59
21	79.8	171.5	4.00	33.9	144	418.2	4.75	3.48
22	79.7	171.4	4.01	46.9	199	418.2	5.78	3.67
23	80.4	171.8	4.01	76.2	324	418.2	6.34	3.52
24	80.3	171.8	4.01	23.7	101	418.2	3.59	3.65
25	80.0	171.4	4.00	23.7	101	418.2	3.85	-----
26	79.6	171.8	4.01	23.7	101	418.2	3.56	-----
27	80.4	171.8	4.00	23.7	98.7	403.2	1.38	-----
28	80.2	171.8	4.07	23.7	102	423.2	4.95	-----
29	80.4	171.8	4.00	23.7	103	433.2	7.31	-----
30	80.1	171.7	4.00	23.7	105	443.2	10.2	-----

Continued.

Table AII-A: Kinetic Results on the $RhCl(PPh_3)_3$/NBR System Continued

Expt. #	$[Rh]_T$ μM	[RCN] mM	$[PPh_3]$ mM	P_{H2} bar	$[H_2]$ mM	Temp K	$k'*10^3$ s^{-1}	η_{rel}
31	80.2	131.0	2.81	15.1	64.4	418.2	3.58	-----
32	80.1	212.3	5.21	15.1	64.4	418.2	2.49	-----
33	79.9	212.4	5.19	15.1	64.4	418.2	2.37	-----
34	79.9	131.0	5.22	15.1	64.4	418.2	3.32	-----
35	80.5	212.3	2.81	15.1	64.4	418.2	2.67	-----
36	80.2	130.9	2.81	32.3	137	418.2	6.03	-----
37	80.5	130.9	5.21	32.3	137	418.2	5.38	-----
38	80.0	131.2	5.20	32.3	137	418.2	5.29	-----
39	79.9	212.2	2.80	32.3	137	418.2	4.30	-----
40	80.4	212.5	5.20	32.3	137	418.2	3.96	-----
SBR[a]	80.0	------	4.02	23.7	101	418.2	4.96	-----
SBR[b]	80.1	------	4.01	23.7	101	418.2	4.93	-----

a: 28.3 g /l ; b: 14.2 g/l

Table AII-B: Kinetic Results on the $RhH(PPh_3)_4$/NBR System

Expt. #	$[Rh]_T$ μM	[RCN] mM	$[PPh_3]$ mM	P_{H2} bar	$[H_2]$ mM	Temp K	$k'*10^3$ s^{-1}	η_{rel}
1	50.4	172.0	2.51	23.7	101	418.2	1.81	----
2	110.0	171.9	5.49	23.7	101	418.2	4.04	3.52
3	139.4	171.5	7.01	23.7	101	418.2	5.27	3.67
4	80.3	172.0	4.00	4.90	20.6	418.2	1.01	3.65
5	79.9	171.6	4.01	11.7	49.8	418.2	2.27	----
6	79.8	171.5	4.01	40.8	174	418.2	4.49	3.52
7	80.3	191.9	4.01	68.9	293	418.2	4.95	3.63
8	80.0	172.0	0.80	23.7	101	418.2	3.53	3.48
9	79.9	172.0	2.41	23.7	101	418.2	3.41	----
10	80.2	172.0	5.61	23.7	101	418.2	2.85	3.63
11	80.4	47.7	4.01	23.7	101	418.2	4.66	3.56
12	79.7	85.5	4.00	23.7	101	418.2	3.46	3.36
13	80.3	249.2	4.01	23.7	101	418.2	2.21	3.59
14	79.9	171.9	4.01	23.7	101	418.2	3.06	3.48
15	79.6	171.8	4.00	23.7	101	418.2	2.81	3.64
16	80.0	171.5	4.00	23.7	101	418.2	2.93	----
17	80.4	171.6	4.00	23.7	96.4	388.2	0.74	----
18	80.3	171.7	4.01	23.7	98.7	403.2	1.86	----
19	80.4	172.0	4.01	23.7	103	433.2	4.92	----

Appendix III

Spectroscopic Data - Phosphine Exchange Studies

Table AIII - Spectroscopic data

Complex	^{1}H NMR[a] δ ppm	J(PH) Hz	^{31}P{^{1}H}[a] δ ppm	ν(CO) cm^{-1}	ν(CN) cm^{-1}
$OsHCl(CO)(PCy_3)_2$ [b]	-32.6, t	----	36.7	1886	----
$OsHCl(CO)(O_2)(PCy_3)_2$ [c]	-2.5, t	30.4	13.7	1948	----
$OsH(H_2)Cl(CO)(PCy_3)_2$	-6.5, t	19	27.4	----	----
$OsHCl(CO)(PhCN)(PCy_3)_2$ [b]	-12.3, t	19.0	14.5	1883	2230
$OsHCl(CO)(PiPr_3)_2$ [b]	-32.1, t	----	48.0	1889	----
$OsHCl(CO)(O_2)(PiPr_3)_2$ [c]	-2.43, t	30.1	23.4	1945	----
$OsH(H_2)Cl(CO)(PiPr_3)_2$	-6.8, t	18.9	36.1	----	----
$OsHCl(CO)(RCN)(PiPr_3)_2$ [b]	-12.6, t	18.5	24.3	1885	2232

[a] All NMR spectra recorded in benzene-d^6
[b] IR spectrum recorded in benzene
[c] IR spectrum recorded in nujol

Table AIII-A: $OsH(H_2)Cl(CO)(Pi\text{-}Pr_3)_2$ / PCy_3 Exchange[a]

Reaction Time[b],hr	$Os(PiPr_3)_2$ mole/L	$Os(PCy_3)_2$ mole/L	$Os(PiPr_3)(PCy_3)$ mole/L	$PiPr_3$ mole/L	PCy_3 mole/L
2	0.0423	0.0000	0.0109	0.0104	0.1041
4	0.0355	0.0029	0.0149	0.0152	0.0812
6	0.0304	0.0038	0.0191	0.0173	0.0682
8	0.0279	0.0045	0.0209	0.0186	0.0638
10	0.0261	0.0052	0.0219	0.0192	0.0574
12	0.0248	0.0060	0.0225	0.0197	0.0566
14	0.0220	0.0072	0.0240	0.0211	0.0518
16	0.0211	0.0073	0.0249	0.0224	0.0503
18	0.0201	0.0074	0.0258	0.0246	0.0471
20	0.0186	0.0083	0.0264	0.0267	0.0470
22	0.0182	0.0089	0.0262	0.0284	0.0461
24	0.0177	0.0088	0.0268	0.0293	0.0452

a: P_{H2} = 24.2 bar, T = 71°C
b: Time measured from insertion into probe

Table AIII-B: $OsH(H_2)Cl(CO)(Pi\text{-}Pr_3)_2$ / PCy_3 Exchange

Time hr	$Os(PiPr_3)_2$ mole/L	$Os(PCy_3)_2$ mole/L	$Os(PiPr_3)(PCy_3)$ mole/L	$PiPr_3$ mole/L	PCy_3 mole/L
0	0.0499	0.0000	0.0000	0.0000	0.3159
2	0.0290	0.0028	0.0180	0.0211	0.2370
4	0.0200	0.0074	0.0225	0.0285	0.2081
6	0.0155	0.0100	0.0244	0.0321	0.1756
8	0.0117	0.0131	0.0251	0.0343	0.1608
10	0.0099	0.0149	0.0252	0.0358	0.1497
12	0.0092	0.0163	0.0244	0.0374	0.1430
14	0.0082	0.0175	0.0241	0.0384	0.1372
16	0.0072	0.0190	0.0237	0.0397	0.1369
18	0.0067	0.0195	0.0237	0.0396	0.1340

Table AIII-C: $OsH(H_2)Cl(CO)(Pi\text{-}Pr_3)_2$ / PCy_3 Exchange

Time hr	$Os(PiPr_3)_2$ mole/L	$Os(PCy_3)_2$ mole/L	$Os(PiPr_3)(PCy_3)$ mole/L	$PiPr_3$ mole/L	PCy_3 mole/L
0	0.0494	0.0000	0.0000	0.0000	0.1092
2	0.0432	0.0000	0.0061	0.0080	0.0951
4	0.0359	0.0000	0.0134	0.0105	0.0723
6	0.0312	0.0025	0.0156	0.0136	0.0593
8	0.0286	0.0037	0.0171	0.0152	0.0546
10	0.0258	0.0035	0.0200	0.0146	0.0512
12	0.0257	0.0040	0.0197	0.0168	0.0512
14	0.0240	0.0046	0.0208	0.0180	0.0471
16	0.0223	0.0060	0.0211	0.0190	0.0441
18	0.0219	0.0057	0.0217	0.0205	0.0423
20	0.0208	0.0058	0.0228	0.0224	0.0446

Table AIII-D: $OsH(H_2)Cl(CO)(Pi\text{-}Pr_3)_2$ / PCy_3 Exchange

Time hr	$Os(PiPr_3)_2$ mole/L	$Os(PCy_3)_2$ mole/L	$Os(PiPr_3)(PCy_3)$ mole/L	$PiPr_3$ mole/L	PCy_3 mole/L
2	0.0593	0.0000	0.0080	0.1145	0.0662
4	0.0545	0.0000	0.0166	0.1130	0.0601
6	0.0509	0.0000	0.0216	0.1153	0.0548
8	0.0490	0.0021	0.0209	0.1173	0.0539
10	0.0481	0.0023	0.0216	0.1188	0.0524
12	0.0474	0.0028	0.0207	0.1226	0.0509
14	0.0453	0.0029	0.0235	0.1222	0.0497
16	0.0448	0.0034	0.0228	0.1245	0.0486
18	0.0443	0.0031	0.0249	0.1235	0.0473
20	0.0429	0.0034	0.0251	0.1254	0.0471
22	0.0424	0.0042	0.0254	0.1244	0.0467

Table AIII-E: $OsH(H_2)Cl(CO)(Pi\text{-}Pr_3)_2$ / PCp_3 Exchange

Time hr	$Os(PiPr_3)_2$ mole/L	$Os(PCp_3)_2$ mole/L	$Os(PiPr_3)(PCp_3)$ mole/L	$PiPr_3$ mole/L	PCp_3 mole/L
0.1	0.0411	0.0000	0.0000	0.0069	0.1148
2.1	0.0219	0.0066	0.0182	0.0292	0.0883
4.1	0.0128	0.0104	0.0186	0.0320	0.0571
6.1	0.0116	0.0150	0.0222	0.0423	0.0592
8.1	0.0084	0.0149	0.0189	0.0392	0.0475
10.1	0.0077	0.0162	0.0187	0.0433	0.0461
12.1	0.0070	0.0165	0.0177	0.0446	0.0428
14.1	0.0070	0.0195	0.0204	0.0541	0.0496
16.1	0.0064	0.0178	0.0197	0.0503	0.0456
18.1	0.0056	0.0165	0.0176	0.0457	0.0404
20.1	0.0052	0.0176	0.0184	0.0516	0.0439

Table AIII-F: $OsH(H_2)Cl(CO)(Pi\text{-}Pr_3)_2$ / $PMet\text{-}Bu_2$ Exchange

Time hr	$Os(PiPr_3)_2$ mole/L	$Os(PR_3)_2$ mole/L	$Os(PiPr_3)(PR_3)$ mole/L	$PiPr_3$ mole/L	PR_3 mole/L
0.0	0.0514	0.0000	0.0000	0.0000	0.1303
2.2	0.0447	0.0000	0.0067	0.0076	0.0771
4.4	0.0405	0.0000	0.0109	0.0087	0.0675
6.4	0.0393	0.0000	0.0122	0.0077	0.0655
8.4	0.0396	0.0000	0.0119	0.0081	0.0662
10.4	0.0397	0.0000	0.0117	0.0090	0.0660
12.4	0.0386	0.0000	0.0129	0.0079	0.0643
14.4	0.0420	0.0000	0.0094	0.0086	0.0686
16.4	0.0397	0.0000	0.0117	0.0079	0.0651
18.4	0.0385	0.0000	0.0129	0.0083	0.0627
20.4	0.0409	0.0000	0.0106	0.0088	0.0669

Appendix IV

$OsHCl(CO)(O_2)(PCy_3)_2$ Hydrogenation:

Data and Rate Expression Derivation

Table AIV: First order rate constants derived from **2a**

Expt. #	[Os] mM	[RCN] mM	P_{H2} bar	$[H_2]$ mM	$k'*10^5$ s^{-1}
1	0.0498	171	24.2	98.2	1.80
2	0.0523	172	24.2	98.2	2.53
3	0.0633	172	24.2	98.2	3.39
4	0.0635	172	24.2	98.2	3.13
5	0.1083	172	24.2	98.2	5.51
6	0.1104	171	24.2	98.2	6.26
7	0.1302	171	24.2	98.4	6.87
8	0.1602	172	24.1	97.9	9.51
9	0.2004	171	24.2	98.4	13.40
10	0.0200	172	34.5	140.2	2.17
11	0.0498	172	34.4	139.9	5.17
12	0.1103	171	34.5	140.2	11.80
13	0.1301	171	34.8	141.3	13.10
14	0.0505	171	13.8	56.1	0.50
15	0.1102	172	14.0	57.0	1.27
16	0.1604	172	13.9	56.4	1.69
17	0.2504	171	13.8	56.1	3.32
18	0.2506	172	13.9	56.4	2.97
19	0.0802	86	24.3	98.7	9.74
20	0.0802	86	24.2	98.4	9.47
21	0.0802	107	24.2	98.2	7.16
22	0.0805	138	24.2	98.2	4.52
23	0.0798	198	24.2	98.2	3.31
24	0.0800	225	24.1	97.9	2.29
25	0.0800	258	24.0	97.6	2.04
26	0.0797	172	10.4	42.1	0.42
27	0.0795	171	13.8	55.9	0.64
28	0.0801	172	33.9	137.6	8.60
29	0.0798	171	34.4	139.6	8.43
30	0.0805	171	38.0	154.2	11.00
31	0.0802	171	41.4	168.2	12.90
32	0.0796	172	41.4	168.2	14.50
33	0.2005	170	2.8	11.3	0.90
34	0.1998	171	2.9	11.6	0.98
35	0.2000	171	5.9	23.9	4.29

Continued.

Table AIV: Continued.

Expt. #	[Os] mM	[RCN] mM	P_{H2} bar	$[H_2]$ mM	$k'*10^3$ s^{-1}
36	0.2002	171	10.4	42.1	1.64
37	0.1995	171	13.1	53.3	3.07
38	0.2001	171	15.9	64.5	6.01
39	0.2002	172	18.3	74.4	8.03
40	0.2002	171	21.4	87.0	11.20
41	0.0298	171	13.8	56.1	0.16
42	0.0303	171	20.8	84.4	0.55
43	0.0301	172	31.3	127.0	2.17
44	0.0294	171	34.4	139.9	2.70
45	0.0302	172	34.6	140.4	2.89
46	0.0301	171	41.9	170.1	3.84
47	0.0802	172	24.2	98.2	3.75
48	0.0802	172	24.2	98.2	3.73
49	0.0808	171	24.2	98.2	3.72
50	0.0799	171	24.2	98.2	3.41
51	0.0806	171	24.2	98.2	3.57
52	0.0701	188	20.7	84.2	1.81
53	0.0699	188	20.7	84.2	1.80
54	0.0897	156	20.7	84.2	3.39
55	0.0703	157	27.6	112.2	5.69
56	0.0904	157	20.7	84.2	3.37
57	0.0702	188	27.6	112.2	4.20
58	0.0699	188	27.6	112.2	4.39
59	0.0905	188	20.7	84.2	2.43
60	0.0701	156	20.7	84.2	2.63
61	0.0902	156	27.6	112.2	6.96
62	0.0903	188	27.6	112.2	5.61
63	0.0899	188	27.6	112.2	5.19
64	0.0910	189	20.7	84.2	2.29
65	0.0702	156	20.7	84.2	2.33
66	0.0906	156	27.6	112.2	6.97
67	0.0698	156	27.6	112.2	5.13
68	0.0905	156	20.7	84.2	3.22
69	0.0698	156	27.6	112.2	5.43
70	0.0896	188	27.6	112.2	5.02

Derivation of the expression from the proposed Kinetic model.

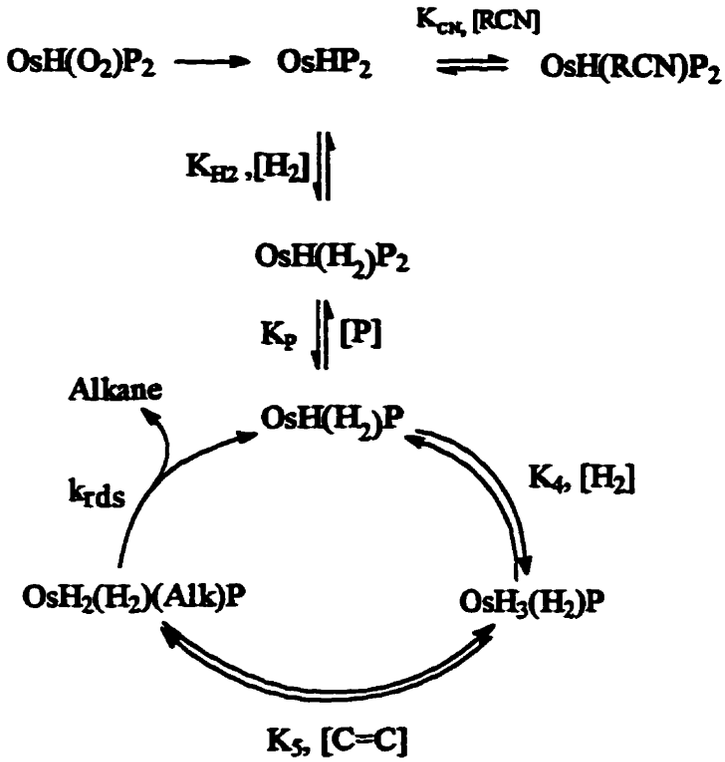

Proposed catalytic cycle, Os = OsCl(CO).

Using the steady state assumption for reaction intermediates, the following equilibria define the concentrations of each may be related to the rate determining step according to:

$$K_5 = \frac{[OsH_2(H_2)(Alk)P]}{[OsH_3(H_2)P][C=C]} \rightarrow [OsH_3(H_2)P] = \frac{1}{K_5[C=C]}[OsH_2(H_2)(Alk)P] \qquad \text{(A1)}$$

$$K_4 = \frac{[OsH_3(H_2)P]}{[OsH(H_2)P][H_2]} \rightarrow [OsH(H_2)P] = \frac{1}{K_4K_5[C=C][H_2]}[OsH_2(H_2)(Alk)P] \qquad \text{(A2)}$$

$$K_P = \frac{[OsH(H_2)P][P]}{[OsH(H_2)P_2]} \rightarrow [OsH(H_2)P_2] = \frac{[P]}{K_PK_3K_5[C=C][H_2]}[OsH_2(H_2)(Alk)P] \qquad \text{(A3)}$$

$$K_{H2} = \frac{[OsH(H_2)P_2]}{[OsHP_2][H_2]} \rightarrow [OsHP_2] = \frac{[P]}{K_{H2}K_PK_3K_5[C=C][H_2]^2}[OsH_2(H_2)(Alk)P] \qquad (A4)$$

$$K_{CN} = \frac{[OsH(RCN)P_2]}{[OsHP_2][RCN]} \rightarrow [OsH(RCN)P_2] = \frac{K_{CN}[P][RCN]}{K_{H2}K_PK_3K_5[C=C][H_2]^2}[OsH_2(H_2)(Alk)P] \qquad (A5)$$

A material balance on the osmium charged to the system yields;

$$[Os]_T = [OsH_2(H_2)(Alk)P] + [OsH_3(H_2)P] + [OsH(H_2)P] + [OsH(H_2)P_2] + [OsHP_2] + [OsH(RCN)P_2] \qquad A(6)$$

Which, using equations A(1)-A(5) is transformed to;

$$[Os]_T = [OsH_2(H_2)(Alk)P] * \left(1 + \frac{1}{K_5[C=C]} + \frac{1}{K_4K_5[C=C][H_2]} + \frac{[P]}{K_PK_4K_5[C=C][H_2]} + \frac{[P]}{K_{H2}K_PK_4K_5[C=C][H_2]^2} + \frac{[K_{CN}[P][RCN]}{K_{H2}K_PK_4K_5[C=C][H_2]^2}\right) \qquad A(7)$$

Rearranging A(7) yields;

$$[OsH_2(H_2)(Alk)P] = \frac{[Os]_TK_{H2}K_PK_4K_5[C=C][H_2]^2}{[P] + K_{CN}[P][RCN] + KH2[P][H_2] + K_{H2}K_P[H_2] + K_{H2}K_PK_4[H_2]^2(1+K_5[C=C])} \qquad A(8)$$

Given that the rate determining step of the process is,

$$-\frac{d[C{=}C]}{dt} = k_{rds}\,[OsH_2(H_2)(Alk)P] \qquad \text{A(9)}$$

the relationship of the hydrogenation rate to the operating conditions may be derived by the substitution of equation A(8) into A(9).

$$-\frac{d[C{=}C]}{dt} = \frac{[Os]_T K_{H2} K_P K_4 K_5 [C{=}C][H_2]^2}{[P]+K_{CN}[P][RCN]+KH2[P][H_2]+K_{H2}K_P[H_2] + K_{H2}K_P K_4[H_2]^2(1+K_5[C{=}C])}$$

Appendix V

Continous HNBR Process Components

Table AV: Prototype components

Component	Supplier	Specifications
A. 12 litre carboy	Nalgene	Polyethylene
B. High-pressure metering pump	Milton Roy	Model# 2396-57 6000 psi, 580 cm^3/hour max.
C. Mass flow control valve Mass flow controller	Brooks Brooks	Model# 5850, 1250 psi max. Model# 5896
D. Check Valves	Whitey	Kal-rez sealing seat
E. Preheating Autoclave	Parr	Model # 561M 300 cm^3 capacity, 3000 psi max
F. Catalyst Bomb	Whitey	1 litre stainless steel bomb
G. High-pressure metering pump	Milton Roy	Model# 2396-89 6000 psi, 920 cm^3/hour max.
J. Shell and tube heat exchange	Custom	Coaxial 12" long stainless steel tubing - 1/2" and 1/4" diameters
K. Separators	Penberthy	Model# IRM8-316SS 500 cm^3, 2300 psi max.
M. Bourdon guage	Weksler	0-3000 psi range
N. Back-pressure regulator	Tescom	Model# 26-1725-24 0-1500 psi range
O. Gas rotameter	Brooks	Model# R-25-B-MM
Steam pressure regulator	Watts	Model# 141M1 30-140 psi range
Steam trap	Spirax Sarco	Model# T-250, 250 psi max.